CONTROLLING FRINGE SENSITIVITY OF ELECTRO-OPTIC HOLOGRAPHY SYSTEMS USING LASER DIODE CURRENT MODULATION

by

Shannon J. Bybee

A thesis submitted in partial fulfillment of the

Requirements for the degree of

MASTER OF SCIENCE

IN

MEASUREMENT AND CONTROL ENGINEERING

IDAHO STATE UNIVERSITY

JANUARY, 2001

To the Graduate Faculty:

The members of the committee appointed to examine the thesis of SHANNON J. BYBEE find it satisfactory and recommend that it be accepted.

Dr. Jonathan Blotter, Major Advisor

Dr. Habib Sadid, Committee Member

Gary A. Fleming, Committee Member

Dr. Ron Hatzenbuler, GFR

ACKNOWLEDGMENTS

This project was funded in part by the National Aeronautics and Space Administration (NASA), Advanced Measurements and Diagnostics Branch at the Langley Research Center in Hampton, Virginia.

I would like to extend a special thanks to my major advisor, Dr. Jonathan Blotter for his assistance and guidance in completing this thesis study and to my Co-Advisor and committee member Mr. Gary A. Fleming of the National Aeronautics and Space Administration whose direction helped to guide me to a better understanding of science, optics and a solution to my query.

I also wish to express appreciation to Mr. James F. Myers of the National Aeronautics and Space Administration whose introduction to general research and computer science helped to guide and encourage me to continue my education.

TABLE OF CONTENTS

LIST OF FIGURES vii

LIST OF TABLES xi

ABSTRACT xii

CHAPTER 1 INTRODUCTION 1

1.1 NOMENCLATURE 1

1.2 PROBLEM STATEMENT 2

1.3 THESIS GOALS 6

1.4 INTRODUCTION TO LIGHT 7

1.5 INTRODUCTION TO HOLOGRAPHY 14

CHAPTER 2 ELECTRO-OPTIC HOLOGRAPHY 18

2.1 NOMENCLATURE 18

2.2 INTRODUCTION TO EOH 21

2.2.1 EOH THEORY, THE DYNAMIC CASE 23

2.2.2 VERIFICATION OF THE BESSEL FUNCTION INTENSITY DISTRIBUTION 27

2.3 FRINGE LOCUS AND THE SENSITIVITY VECTOR 31

2.4 STATIC MEASUREMENTS 37

2.4.1 STATIC EOH THEORY 37

2.5 DYNAMIC MEASUREMENTS 45

2.5.1 DYNAMIC EOH THEORY 45

CHAPTER 3 FRINGE CONTROL 54

3.1 NOMENCLATURE 55

3.2 INTRODUCTION TO FTEOH 58

3.3 FTEOH THEORY 61

3.3.1 FTEOH REFERENCE AND OBJECT BEAMS 61
3.3.2 THEORY OF MODULATION EFFECTS 63
3.3.3 BESSEL FUNCTIONS AND THE INTENSITY DISTRIBUTION . . . 68
3.3.4 MORE BESSEL FUNCTION EXAMPLES. 72
3.3.5 LOOK-UP TABLES 76
3.3.4.1 LOOK-UP TABLE FOR FTEOH 78
3.4 ESTIMATING THE FRINGE DENSITY 84
3.4.1 THE "EVERY THIRD ORDER" RULE 85
3.4.2 ESTIMATING THE DISPLACEMENT 89
3.4.3 THEORY SUMMARY 93
3.5 APPLIED FTEOH 95
3.5.1 SCATTERING OF THE OBJECT LIGHT 99
3.5.2 SERRODYNING 101
3.5.2.1 SERRODYNING AT THE SOURCE 102
3.5.3 WAVEFORMS, VERIFYING THE SAWTOOTH THEORY 105
CHAPTER 4 EXPERIMENTAL SETUP AND PROCEDURE 107
4.1 THE EXPERIMENTAL SETUP 107
4.1.1 TELESCOPE ASSEMBLY 109
4.1.2 THE FARADAY ISOLATOR 112
4.1.3 BEAM SPLITTER 113
4.1.4 FIBER OPTIC COUPLERS AND CABLE 114
4.1.5 PHASE STEPPER 117
4.1.6 CCD CAMERA 118
4.2 PROCEDURE 119

CHAPTER 5 RESULTS AND DISCUSSION **121**

5.1 LIST OF EQUIPMENT **121**

5.2 THE EXPERIMENT AND DATA CAPTURE **123**

5.3 FTEOH DATA CAPTURE PROCEDURE **127**

5.4 DETERMINING DISPLACEMENTS **128**

5.5 FUTURE WORK **133**

5.6 CONCLUSION **133**

CHAPTER 6 REFERENCES **134**

LIST OF FIGURES

Figure 1.1: An EOH image for an object under dynamic loading, too many fringes for clear resolution 3
Figure 1.2: An optimal EOH image with resolvable fringes. 3
Figure 1.3 Thesis contributions to the field of EOH 5
Figure 1.4: Construction and Destruction of Light waves as described by Young 9
Figure 1.5: Young's Double Slit Experiment [6]. (A) Light traveling through a large diameter hole does not experience diffraction. (B) Light traveling through a small diameter hole with respect to the wavelength is diffracted upon reaching exit of the hole. 10
Figure 1.6: Light waves in phase 12
Figure 1.7: (A) Young's Double Slit experiment and the (B) interference pattern produced [6]. 13
Figure 1.8: (A) The light from the two holes travels equal distance and reach the screen in phase. (B) The light from the top hole travels one wavelength further than the light from the bottom hole, light is in phase. (C) The light from the top hole travels one half of a wavelength further than the light from the bottom hole, the light is out of phase [6]. 14
Figure 1.9: The basic set up for creating a hologram. 16
Figure 2.1: Optical set-up [18] 22
Figure 2.2: EOH image of a dynamically loaded structure. The large bright fringe is denoted as the zero order fringe. 29
Figure 2.3: Zero order and square of the zero order Bessel function 29
Figure 2.4: Second mode shape and corresponding hologram [3] 30
Figure 2.5: Third mode shape and corresponding hologram [3] 30
Figure 2.6: Normal deformation of a cantilever beam: (A) Side view of the beam with displacement in the *z* direction and illumination in the -*z* direction. (B) Interference pattern observed on the front of the beam [13]. 31
Figure 2.7: Nomenclature for fringe analysis. (A) Schematic diagram of the system. (B) Position and propagation vectors [22]. 33
Figure 2.8: Bessel function vs. Cosine Function 51

Figure 2.9: EOH wrapped phase map [4]. 52

Figure 2.10: Unwrapped phase map with corresponding wrapped phase map [4]. 53

Figure 3.1: Typical EOH image of a cantilever beam 59

Figure 3.2: The desired result of modulation. The density of the fringes from Fig. 3.1 have been reduced to a more resolvable level. 59

Figure 3.3: The initial maximum of the 10^{th} order Bessel function occurs at a larger argument with respect to the initial maximum of the zero order Bessel 68

Figure 3.4: No modulation with an excitation amplitude of 2 volts and a total of 7 fringes 69

Figure 3.5: Results of using the FTEOH method on a cantilever beam with sinusoidal excitation. The left image is of the unmodulated case while the right is the modulated case. Note the making of the low order fringes for the modulated case 70

Figure 3.6: J_0 vs. J_5 70

Figure 3.7: Fifth order Bessel function 70

Figure 3.8: EOH image and its corresponding FTEOH image. Here a 4^{th} order modulation was used to mask two fringes from the FTEOH image.. 72

Figure 3.9: Cantilever beam shown as first the EOH image and then with corresponding FTEOH images. It can be seen that by increasing the modulation order the interference fringes are in fact masked by a dark null.. 73

Figure 3.10: More FTEOH images. The images here show a greater number of fringes, yet as the order of modulation is increased the fringes become more resolvable 74

Figure 3.11: A cantilever beam excited at a frequency which has induced a torsion mode. Once again, as the modulation order is increased the interference fringes become more resolvable. Note that the zero order fringe is still visible, this effect may be corrected by controlling the shuttering of the CCD camera. 75

Figure 3.12: Exact fringe locus function vs. the approximate fringe locus function for the zero order Bessel function case, i.e. no modulation. Axes are shown in units of π radians. 80

Figure 3.13: Exact fringe locus function vs. the approximate fringe locus function for the fifth order Bessel function case. Axes are shown in units of π radians. 80

Figure 3.14: The exact fringe locus function vs. the approximate fringe locus function for the zero order and fifth order Bessel function cases, respectively. Axes are shown in units of π radians. 81

Figure 3.15: Plot of $J_5^2(\Omega_t)$ and Ω_{ll}. The horizontal axis is shown in units of π radians, the vertical is the normalized intensity 81

Figure 3.16: The exact fringe locus function vs. the approximate solution for the zero order and fifth order (+ Ω_{ll}) cases. Axes are shown in units of π radians. 82

Figure 3.17: The overlay for $J_{15}^2(\Omega)$, $J_{10}^2(\Omega)$, $J_5^2(\Omega)$, and $J_0^2(\Omega)$ look up tables. For this figure $\Omega_{unwrapFT}$ indicates all look up tables where FT varies in value from 0 to 15 in steps of 5. Note that the $J_0^2(\Omega)$ look up table is an approximation for the higher order look up tables. Axes are shown in units of π rads. 82

Figure 3.18: J_{13}^2 vs. J_0^2. The 1st dark fringe of J_{13}^2 is the 5th dark fringe of J_0^2. 85

Figure 3.19: J_{16}^2 vs. J_0^2. The 1st dark fringe of J_{16}^2 aligns with the 7th dark fringe of J_0^2. 87

Figure 3.20: J_{19}^2 vs. J_0^2. The 1st dark fringe of J_{19}^2 aligns with the 1st dark fringe of J_0^2. 87

Figure 3.21: J_{22}^2 vs. J_0^2. The 1st dark fringe of J_{22}^2 aligns with the 8th dark fringe of J_0^2. 88

Figure 3.22: J_{18}^2 vs. J_0^2. the 1st dark fringe of J_{18}^2 sits 2/3 of the way between the 6th and the 7th fringe of J_0^2 which introduces error into the unwrapped measurement. 88

Figure 3.23: 0 modulation 7 total fringes. 89

Figure 3.24: 3rd modulation order 5 remaining fringes. 90

Figure 3.25: 4th modulation order 5 remaining fringes. 90

Figure 3.26: 5th modulation order 5 remaining fringes. 90

Figure 3.27: 6th modulation order 4 remaining fringes. 91

Figure 3.28: 7th modulation order 4 remaining fringes. 91

Figure 3.29: 8th modulation order 3 remaining fringes. 91

Figure 3.30: 9th modulation order 3 remaining fringes. 92

Figure 3.31: 10th modulation order 3 remaining fringes. 92

Figure 3.32: J_{13}^2 vs. J_0^2. The 1st dark fringe of J_{13}^2 is the 5th dark fringe of J_0^2. 93

Figure 3.33: 0 modulation 7 total fringes. 94
Figure 3.34: 10^{th} modulation order 3 remaining fringes. 94
Figure 3.35: Frequency content and physical signal processing that occurs in the FTEOH technique. 97
Figure 3.36: Fourier Transform of the phase modulated spectrum of reflected light off of a sinusoidally moving object [33]. 100
Figure 3.37: The modulated spectral composition of the scattered object wave . 101
Figure 3.38: Frequency shift of the laser diode. The dotted frequency spike represents the original lasing frequency. The solid line is the frequency shift $\Delta\upsilon$. which oscillates about the lasing frequency and is expressed as $\Delta\upsilon \sin(\omega t)$, the modulating frequency. Where the modulating frequency = the test structure excitation. However, the mean frequency over the period of oscillation for the frequency is still the lasing frequency υ 102
Figure 3.39: Forth order modulation obtained with ramp waveform fringe resolution is clean and distinguishable 106
Figure 3.40: Forth order modulation obtained by using a sine waveform fringe resolution has been greatly reduced 106
Figure 3.41: Forth order modulation obtained with square waveform. The image shows no signs of fringe reduction 106
Figure 3.42: Fourth order modulation obtained with a triangular waveform, fringe resolution is degraded 106
Figure 4.1: FTEOH Optical set up 108
Figure 4.2: FTEOH optical path 109
Figure 4.3: Telescope assembly and Faraday isolator 110
Figure 4.4: Cut-away of the telescope assembly. 111
Figure 4.5: Cross-section of the anamorphic prism pair [1]. 111
Figure 4.6: Ray trace of the contracted beam 111
Figure 4.7: The three major components of the Faraday isolator. In this figure the light is traveling through the isolator in the forward direction [42] 112
Figure 4.8: The polarization of back reflected light, traveling in the reverse direction through the isolator. Light traveling in this direction will not be able to pass through the input polarizer and will be prevented from re-entering the laser diode cavity [38]. 113
Figure 4.9: Front of reference leg fiber coupler 114

Figure 4.10: Back of reference leg fiber coupler 114

Figure 4.11: Propagation of light through a fiber optic cable. The cladding refractive index is n_c, and the core refractive index is n_o [43] 115

Figure 4.12: Test object 116

Figure 4.13: Top view of the phase stepper 117

Figure 4.14: Side view of the phase stepper 117

Figure 4.15: Reference light directed into the CCD 118

Figure 5.1: Cantilever beam used to obtain EOH and FTEOH data analysis... 122

Figure 5.2: Shaded area represents the area used to obtain the interference pattern for FTEOH analysis 122

Figure 5.3: Typical EOH image of a cantilever beam in a bending mode..... 126

Figure 5.4: FTEOH image using a fifth order modulation. Note how the zero fringe and the 1st order fringe have been masked..... 126

Figure 5.5: Zero order Bessel function..... 127

Figure 5.6: 3-D plot of displacement for the interference pattern of Figure 5.3, i.e no modulation..... 129

Figure 5.7: 3-D plot of displaced beam and interference pattern of Figure 5.4.. 130

Figure 5.8: Average omega value for each row within the unwrapped omega image vs. the actual displacement of the test structure..... 131

List of Tables

Table 3.1: The n^{th} order Bessel function and the location of the maximum of the first initial peak..... 83

Table 3.2: J_n Zeros and the corresponding J_0 zeros..... 86

Table 5.1: Data capture procedure for both the EOH and FTEOH techniques.. 124

Table 5.2: Setting the amplitude of the laser diode current source..... 127

Table 5.3: Zeros of the Bessel function J_0^2..... 132

Controlling Fringe Sensitivity of Electro-Optic Holography Systems Using Laser Diode Current Modulation

ABSTRACT

Electro-Optic Holography (EOH) is a non-intrusive, laser-based, displacement measurement technique capable of static and dynamic displacement measurements. EOH is an optical interference technique in which fringe patterns that represent displacement contour maps are generated. At excessively large displacements the fringe density may be so great that individual fringes are not resolvable using typical EOH techniques. This thesis focuses on the development and implementation of a method for controlling the sensitivity of the EOH system. This method is known as Frequency Translated Electro-Optic Holography (FTEOH). It was determined that by modulating the current source of the laser diode at integer multiples of the object vibration, the fringe pattern is governed by higher order Bessel function of the first kind and the number of fringes that represent a given displacement can be controlled. The reduction of fringes is theoretically unlimited but physically limited by the frequency bandwidth of the signal generator, providing modulation to the laser diode. Although this research technique has been verified theoretically and experimentally in this thesis, due to the current laser diode capabilities it is a tedious and time consuming process to acquire data using the FTEOH technique.

CHAPTER 1.0

INTRODUCTION

Holographic interferometry has been used as a method for determining surface displacements for small amplitude vibrations for a number of years. This laser-based technique is extremely sensitive and is capable of measuring displacements as small as $\frac{\lambda}{100}$ where λ is the laser wavelength. The interferometric method uses the principles of light interference to create a fringe pattern to measure structural displacement [1]. Using this method for out-of-plane measurements one complete (black to white) interference fringe is approximately equal to one-half laser wavelength of light [2]. The fringe patterns are captured and analyzed producing displacement information at a sensitivity level that would otherwise be unattainable.

The goals undertaken by the author of this work are laid out in Section 1.3 and include the method for controlling EOH fringe density and conversion of the current mirror based system to a fiber optic based system. In Section 1.4 and 1.5 background information on the physics and behavior of light as well as an introduction to holography is presented.

1.1 NOMENCLATURE

CCD	Charged Couple Device camera
EOH	Electro-Optic Holography
FTEOH	Frequency Translated Electro-Optic Holography
k	Wave number, equal to $2\pi / \lambda$
λ	Wavelength of the laser light used to produce interference
θ	The angle between the illumination and reflection beams

1.2 PROBLEM STATEMENT

Conventional interferometry, although sensitive and relatively accurate, has many difficulties which hinder the rate of data acquisition. Conventional holography requires a photographic recording and development process preventing real-time measurements. It is this limitation which instigated the development of a more advanced method for performing holographic interferometry. Using this method interference patterns are formed and recorded with a charged coupled device (CCD) camera and processed by a computer acquisition system. The technique is known as Electro-Optic Holography (EOH). This method is used to generate fringe patterns in a near real time fashion with the same sensitivity as typical holographic interferometry [3].

The major drawback of EOH is that the measurement range is limited. For example, a typical laser diode with a wavelength of 852 nm has an upper measurement limit of approximately 20 microns. With increased displacement, the number of fringes that appear in the interference pattern increase causing the EOH image to become saturated with fringes. When the fringe density becomes too high it is impossible to clearly identify individual fringes, which prevents counting fringes accurately. This lack

of resolution is the physical mechanism limiting the upper measurement range of the EOH system. In order for large amplitude displacements to be measured the sensitivity of the EOH system must be reduced such that each fringe represents a displacement greater than $\frac{\lambda}{2}$.

C.C. Aleksoff [5] discussed a conventional holographic interferometry technique, which involved modulation of the reference beam as means of controlling fringe characteristics. He stated that by modulating the reference wave at higher harmonics any number of fringes corresponding to the smaller amplitude displacements could be eliminated, thereby alleviating the image of high fringe density. This method, however, has yet to be established with EOH technology. This thesis describes the method for controlling fringe density for EOH measurements, thereby allowing larger displacement measurements to be acquired. The goal is to take an image like that of Fig. 1.1 and reduce the number of fringes so that resulting the image will look like that of Fig 1.2.

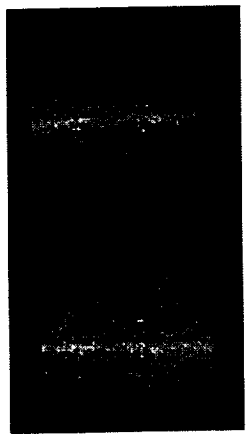

Figure 1.1: An EOH image for an object under dynamic loading, too many fringes for clear resolution.

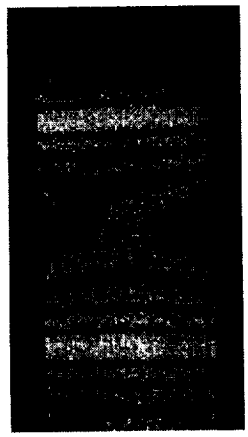

Figure 1.2: An optimal EOH image, with resolvable fringes.

A simple flow chart showing the modern methods for determining structural displacements is shown in Figure 1.3. The figure illustrates where FTEOH will be placed within the discipline of current metrology. The flow chart is broken down into two general categories: theoretical/numerical methods and experimental methods for

determining structural displacements. EOH can be described as a subset of holography under the experimental methods category. EOH itself can be broken down into two additional sub-categories, Typical EOH and FTEOH, which is the contribution this thesis work will add to the arena of structural displacement measurement methods.

In Chapter 2 the EOH theory is presented in detail and mathematical models for the intensity and phase distribution for both the static and dynamic cases are examined. Finally, Chapter 3 includes the method for controlling fringe density for the EOH system by means of laser diode current modulation and the results are verified.

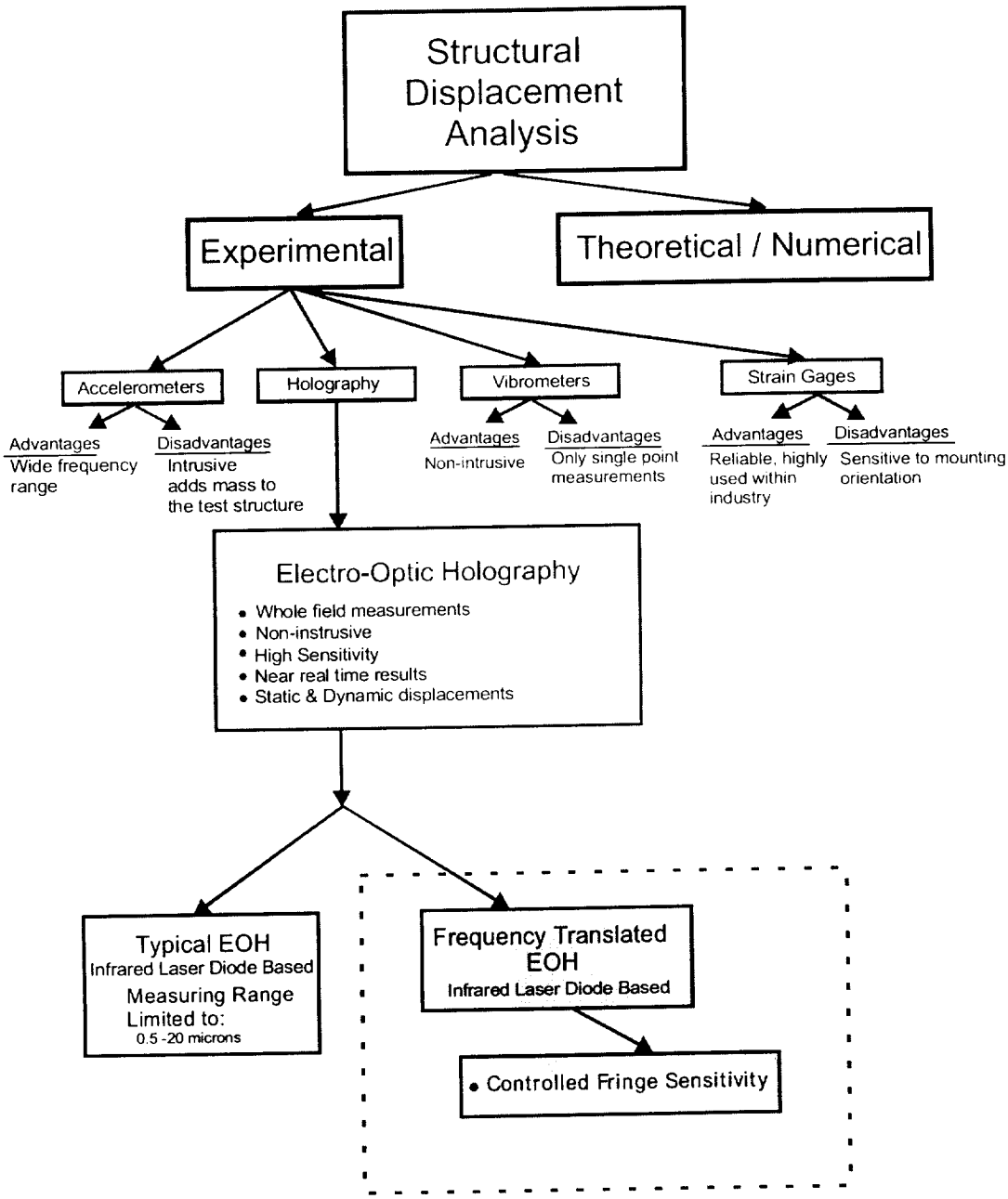

Figure 1.3 Thesis contributions to the field of EOH.

1.3 THESIS GOALS

- Develop a method for controlling EOH fringe density using laser diode current modulation.
- Convert the existing optical setup from a mirror-based setup to an optical fiber based setup.
- Modification of the computer software to allow for FTEOH data analysis.

1.4 INTRODUCTION TO LIGHT

Light has proven to be of major interest by many great scholars. Newton, Huygens, Young, and Rayleigh, rather than shown light could behave dually, attempted to prove that light was either a particle or a wave [6]. In the seventeenth century Isaac Newton was the most prominent advocate of the particle theory. Newton had proclaimed that rays of light were streams of particles, which were emitted from a source and traveled in a straight line. His supporting argument stated that light from a source casts a sharp shadow of objects in its path, in contrast to water and sound waves, which bend around obstacles [7], therefore light must be a particle.

In contradiction to Newton and also a contemporary of the same time was Dutch physicist Christian Huygens who favored the opposite theory that light was a wave. Huygens' discussed the wave behavior of light by explaining that light spreads out from a light source in all directions not just in a straight path. Thomas Young, an Englishman in support of Huygens, performed an experiment in which he passed light through two small slits and produced a complex interference pattern of light and dark bands a phenomenon that could only be explained by the fact that light must be a wave.

The beginning of the nineteenth century served to show strong support for the wave theory but as the century came to a close so too did this support [7]. Such physicists as Planck, Einstein, Bohr, and Compton once again proved that light must be a particle by examining blackbody radiation, the photoelectric effect and the scattering of X-rays from electrons [7].

In 1924, Luis de Broglie began to look at light with a new approach when he began to look at the dichotomy of light. He suggested that a particle with momentum had

associated wave properties. This new idea brought the argument of light full circle but now under the pretense of duality. James Clerk Maxwell was able to combine these concepts and determined that light is merely electromagnetic energy, which he described as electromagnetic waves [8]. Maxwell determined that the complete spectrum of electromagnetic energy includes radio, infrared, visible, ultraviolet, x-ray and gamma radiation. His theory also encompassed the quantum theory, as revealed by Planck, Einstein, Bohr, and Compton, who stated that electromagnetic energy is 'quantized,' and can be taken from the electromagnetic field in discrete amounts known as photons. Thus, the modern concept of light was born [8].

Although light does have a dual nature, the wave behavior holds the greatest interest in the study and research of Electro-Optic Holography, which is the focus of this thesis. Therefore, a general understanding of wave properties as applied to EOH will be examined in detail. The inquiry will be inclusive to Young's double slit experiment, diffraction, wave interference, and superposition, which are the foundations of the EOH technique.

Thomas Young provided the first demonstration of the wave characteristic of light in 1801, by demonstrating that light exhibits an interference behavior. He established that light waves coming from a single source arriving at a point by two different paths can combine and cancel each other by destructive interference to produce an interference pattern as shown in Fig. 1.4. Constructive interference occurs when the slopes of the two interfering waves carrying the same sign add together to create a band of light in the interference pattern. Conversely, destructive interference occurs when the

slopes of the two waves are opposite in sign and when added together cancel one another out to create a band of dark in the interference pattern.

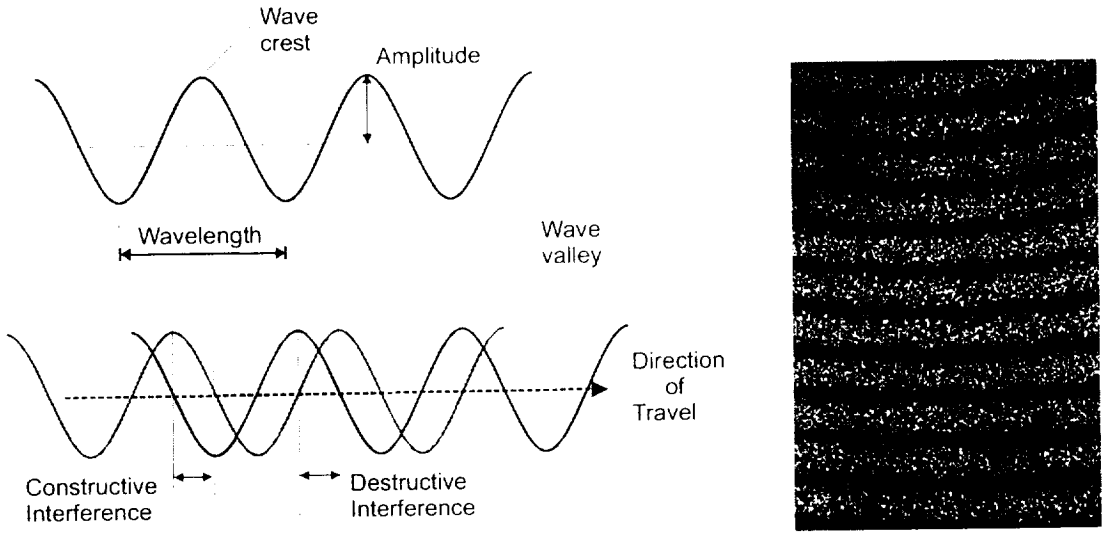

Figure 1.4: Construction and Destruction of Light waves as described by Young.

At the time the interference phenomenon was discovered, it was not explainable by means of the particle theory. It was thought that two or more particles could not come together and cancel one another out in such an orderly pattern. Therefore, the phenomenon had to be the result of wave interaction.

Consequently, the wave theory was not immediately accepted among scholars. There were those who understood that waves, such as sound, traveled through some type of medium. Their argument was based on the fact that light from the sun arrives at the surface of the earth through a vacuum of empty space, without a medium. Therefore, light must be a particle because waves need a medium for propagation [6]. In the mid-nineteenth century, British physicist James Clerk Maxwell suggested that a medium, which he called the ether, must exist everywhere, even in the empty vacuum of space and

it was this substance, he proclaimed, that light, as a wave was able to propagate. However, in 1887, Albert Michelson and Edward Morley at the Case school of Applied Science in Cleveland, Ohio, disproved the existence of ether. Dutch physicist Hendric Lawerence and Albert Einstein [9] later disproved the existence of ether thereby leaving the wave theory in limbo.

Nevertheless, the argument proceeded on with one of the most intriguing questions of the time: If the nature of light were to be wave-like, then light would be able to bend around objects like water and sound waves thus allowing one to see around corners. Of course we know that we cannot actually see around corners, but in fact light does bend around them. For example, if an object is held up against a light so that a shadow is cast, one should notice that the edges of the shadow are not as sharp as one might expect. These soft edges are a result of light bending around the object. This type of bending is known as diffraction. Diffraction is the modulation of waves in response to an obstacle or grating in the path of propagation. Figure 1.5 is an illustration of Young's double slit experiment, which demonstrates diffraction

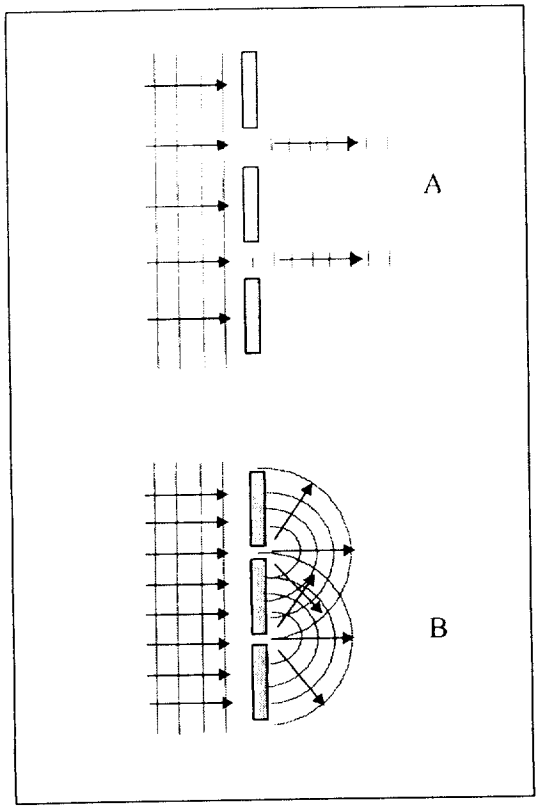

Figure 1.5: Young's Double Slit Experiment [6]. (A) Light traveling through a large diameter hole does not experience diffraction. (B) Light traveling through a small diameter hole with respect to the wavelength is diffracted upon reaching exit of the hole.

on slit openings of different sizes. Diffraction of light will occur regardless of the size of object, but in Fig. 1.5 (A) the effect of diffraction is less apparent because the size of the slit opening is relatively large with respect to the wavelength of the illuminating light. Therefore, the light rays that meet the wall of Fig. 1.5 (A) will continue to move through the opening in a straight line. On the other hand, if the diameter of the hole is small with respect to the wavelength of light, like it is shown in Fig. 1.5 (B), the effect of diffraction is more apparent. The light passing through the relatively small aperture will spread out in all directions as a result of diffraction.

When coherent light waves pass through a small aperture like that of Fig. 1.5 (B), an interference pattern, rather than a sharp spot of light is seen on the second screen [6]. Because there are two slits in Young's experiment, the light from the two slits interfere with each other in both a constructive and destructive manner, which is dependent on path length. Therefore, diffraction can be regarded as a consequence of interference from many coherent wave sources. In other words, diffraction and interference are basically equivalent [6].

The short wavelengths of visible light make interference patterns difficult to see, and in order to observe this phenomenon the following conditions must exist:

1. The light sources must be coherent and of identical wavelength.
2. The superposition principle must apply.

The first condition states that the two interfering waves must be coherent, by definition, longitudinal coherence is a function of laser frequency stability and emission linewidth, not phase. However, one can argue that two incoherent beams cannot maintain a constant phase relationship since they will be of different frequencies. Two waves are

said to be in phase with one another when the wave crests and valleys of both waves coincide. If all three waves of Fig. 1.6 coincide, then they are in phase with one another regardless of amplitude. However, two waves are said to be out of phase when the wave crests and valleys do not coincide but instead intersect elsewhere along the wave. Thus the frequency along the wave must be maintained, otherwise, the wave is said to be incoherent [6].

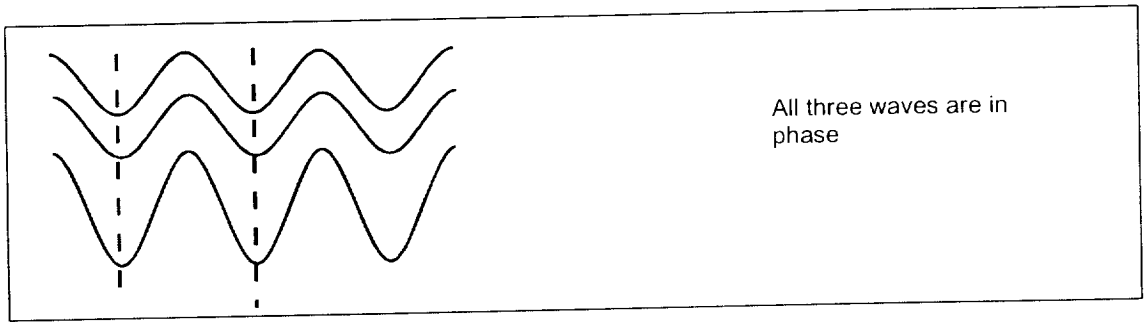

Figure 1.6: Light waves in phase .

The second condition states that the superposition principle must apply, which is simply the arithmetic addition of the two interfering waves. Two coherent waves originating from the same source only differ by the path length for which the two waves travel. The difference in path length causes the two waves to differ in optical phase. This difference, upon superposition, results in interference.

As mentioned previously, Thomas Young was the first to demonstrate the wave behavior of light through means of interference in his double slit experiment, as shown in Fig. 1.5. A drawing of the complete experiment is shown in Fig. 1.7 (A) with the resulting interference pattern Fig. 1.7 (B). In the experiment, the light is incident on a screen in which there is a small opening [6]. The light emerges from the opening in the screen and is incident on a second screen that contains two small openings. These two

openings serve as a pair of coherent light sources because the waves emerging from them are created by the same wavefront and, therefore, maintain a constant phase relationship. When the light reaches the third screen the interference pattern of Fig. 1.7 (B) can be seen [6]. The areas of constructive interference are described in Fig. 1.7 (A) as 'max' and result in a band of light in Fig. 1.7 (B). The opposite it true for destructive interference, which will produce both a bright fringe (constructive interference) and a dark fringe (destructive interference). This phenomenon is illustrated in Fig. 1.8. The two waves leaving the two small openings leave in phase and strike the third screen at a central point in Fig. 1.8 (A). At this point the two waves have traveled an equal distance. The waves are said to be in phase, thus resulting in constructive interference or a band of light in the interference pattern. In Fig. 1.8 (B) the path lengths are not equal because the top wave has to travel one wavelength further than the bottom wave. Since the path difference is one wavelength the two waves are still in phase and will again result in a band of light. Last, in Fig. 1.8 (C) the top wave has traveled one half wavelength farther than the bottom wave. Therefore, the wave valley of the top wave will add to the wave crest of the bottom wave causing destructive interference or a dark band in the optical interference pattern.

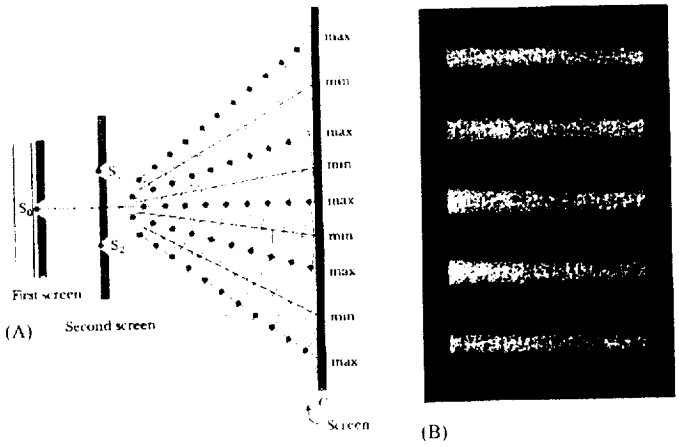

Figure 1.7: (A) Young's Double Slit experiment and the (B) interference pattern produced [6].

(A) (B) (C)

Figure 1.8: (A) The light from the two holes travels equal distance and reach the screen in phase. (B) The light from the top hole travels one wavelength further than the light from the bottom hole, light is in phase. (C) The light from the top hole travels one half of a wavelength further than the light from the bottom hole, the light is out of phase [6].

The light and dark bands in the interference pattern in Fig. 1.7 (B) appear to be speckled with light and dark spots throughout. This phenomenon is known as speckle noise and is a result of light scattering off of an optically rough surface. The roughness of the surface varies the optical path length causing constructive and destructive interference with the diffracted wave front, which results in a granular, speckle appearance throughout the interference pattern.

1.5 INTRODUCTION TO HOLOGRAPHY

Many optical measuring techniques take advantage of light interference using the fact that light and dark bands, fringes, represent approximately one wavelength of light. This technique is known as interferometry. One such interferometric method is known as holographic interferometry. The images produced from this method are known as holograms, which will now be discussed.

In 1948, British scientist Dennis Gabor invented a photographic technique known as holography. Holography produces a three-dimensional image that has all the depth and parallax of a real-life scene [7]. Gabor called his images holograms and explained their

three-dimensionality as a reconstruction of the coherent scattered light reflected off of a structure combined with a coherent reference light field [7-10]. Optical coherence, or the ability of a light source to maintain constant phase, is of vital importance in the development of holograms. In 1948, however, a coherent light source was not readily available, and the ability to produce holograms was at best difficult. The growth of holography stood at a virtual stand still until 1962, when coherent lasers became available. The advent of the laser brought back interest to holography, and Emmet Leith and Juris Upatnieks of the University of Michigan produced the first laser based holographic image [7]. Leith and Upatnieks' development resulted in a surge of activity with scientists world wide trying their hand at holography and the production of holograms [11].

A hologram is a three dimensional image of an object produced by recording the patterns of interference, on a special photographic film, formed by a split laser beam. The holographic image can only be viewed after "reconstruction." Reconstruction is the illumination the photographic plate with the same wavelength laser light, illuminated at the same "reference beam angle". In the case of a simple hologram the image is created by first splitting the beam of a coherent laser into two separate beams, the *object beam* and the *reference beam*. The object beam is used to illuminate the test object, and the second beam is maintained as a reference source. Upon illumination of the test object, the beam is phase modulated, with respect to the reference beam [12]. The modulated beam is recombined with the reference beam to yield an interference pattern. The interference pattern can then be seen on the special photographic film when illuminated

by the reference beam. Figure 1.9 illustrates a simple optical set up used for creating a holographic image.

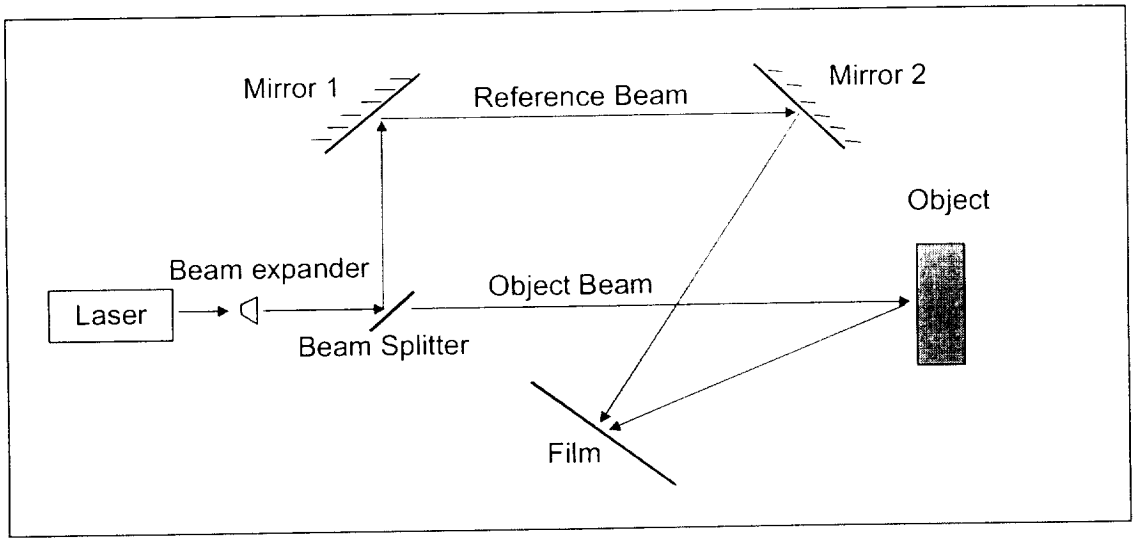

Figure 1.9: The basic set up for creating a hologram.

The resultant interference pattern or *fringe pattern* includes the phase relationships of each part of the light from the scene with the reference light and therefore with every other part [7]. The interferogram is essentially a coded contour map where the interference fringes are the lines of code that contain the information about the depth and displacement of the object. The displacement information can be decoded by counting the number of fringes which represent lines of constant displacement, multiplying the count by the quantity $\frac{\lambda}{2k\cos\theta}$, where θ is the angle between the illumination and reflection vectors and k is the wave number (Section 2.1 details these vectors and derives the above quantity in full). The method of determining displacement through the use of interference fringes is called *holographic interferometry*.

Holographic interferometry provides the means by which deformations and displacements can be analyzed through the use of a interferogram. Holograms have traditionally been recorded on light sensitive photographic film that operates much like diffraction gratings [13]. During interferometric applications a large number of holograms are needed in order to fully analyze the displacements of the object of interest. After the holographic images have been recorded on film, the interpretation and quantitative analysis of the interferograms begins. This process can be tedious and extremely lengthy, especially when dealing with interferograms of dynamically excited objects. More importantly this recording and development process inhibits real-time measurements.

Since the development of holographic interferometry a more advanced method for processing holographic images has arisen. This method records interference patterns with a charged coupled device (CCD) camera and analyzes the data with a computer acquisition system. The three-dimensionality of the images is lost using this new technique but the rate of computation is much faster. This technique is EOH and can generate interference patterns in a near real time fashion with the same sensitivity as typical holographic interferometry [3].

CHAPTER 2.0

ELECTRO-OPTIC HOLOGRAPHY

Holograms have traditionally been recorded on either photographic film or expensive cumbersome glass film [13]. When large numbers of holograms are required, inexpensive, flexible film is usually chosen. Regardless, film is difficult to work with. The development of EOH began in 1985, presenting a method to capture and store holograms electronically [13]. It was during this time that Karl Stetson [13] and others [14-16] came to develop EOH. This chapter discusses EOH in detail with a brief introduction in section 2.2 followed by a detailed description of both static EOH and dynamic EOH in sections 2.3 and 2.4 respectively. The chapter will conclude with a discussion of the sensitivity vector.

2.1 NOMENCLATURE

A_o	Amplitude of the object beam, the laser beam directed onto the test object.
A_r	Amplitude of the reference beam, the laser beam directed into the CCD camera.
B	Phasor bias, a phase change incurred by the reference beam to solve for Ω, the fringe locus function.
CCD	Charged Couple Device camera
e_o	The amplitude of vibration for the test structure

E_o	The time dependent displacement of a point on the vibrating structure.
EOH	Electro-Optic Holography.
e_r	The amplitude of the PZT.
E_r	The time dependent displacement of a point on the vibrating structure.
f	Emission frequency of the laser diode.
$F_{interference}$	The resulting light field of the scattered object and reference beams.
F_o	The object light field, the beam of light that illuminates the test object.
F_r	The reference light field, the beam of light that is directed into the CCD camera.
FTEOH	Frequency Translated Electro-Optic Holography.
F_{rec}	The digitally reconstructed light field.
F_v	The resulting object beam upon reflecting off of the test object.
g_o	A geometrical factor with $g_o = 2$ for displacements perpendicular to the object surface with normal incidence.
I	The light intensity of the laser beam.
I_{at}	The time averaged background intensity.
I_{mt}	The time dependent maximum intensity.
I_n	The intensity of the n^{th} sequential frame.
I'_n	The intensity of the n^{th} sequential frame with the object in its deformed state.
I_{nt}	The time dependent intensity of the n^{th} sequential frame.
I_o	The intensity of the object beam, the beam directed onto the test object.
I'_o	The intensity of the object beam while the object is in its deformed state.
I_{ot}	The time dependent intensity of the object beam.
I_r	The intensity of the reference beam, the beam directed into the CCD camera.
J_o	The zero order Bessel function of the first kind.

K	Sensitivity Vector, the vectorial difference between the propagation vectors.
k	The wave number whose value is given by $2\pi/\lambda$.
$\hat{k}_i$	Vector of propagation for both illumination and reflection, where i = 1 to 4.
L	Magnitude of displacement of the test object.
l_n	Distance the light travels.
$M(\Omega(t))$	The characteristic equation given by the zero order Bessel function of the first kind.
N	The fringe order.
O	The point location of the light source.
P	The point of interest on the test object.
P′	The point of interest on the test object while the object is in its displaced state.
PZT	Piezoelectric actuator.
Q	Point detector.
R	Direction vector from the point source O to the point detector Q.
r_i	Direction vectors where i = 1 to 4.
T	Exposure time of the CCD camera.
$Z(x)$	Displacement in the z-direction.
$\Delta\phi$	The optical phase difference between the scattered object beam and the reference beam. The magnitude is an unknown value.
$\Delta\phi_t$	The time dependent unknown phase difference between the scattered object beam and the reference beam.
$\Delta\theta_n$	90° sequential phase step used to determine the fringe locus function.
ε	Error between the estimated fringe locus function and the actual fringe locus function.

ϕ_a Arbitrary phase value assigned to the object and scattered object beams.

ϕ_o Optical phase of the object beam.

ϕ_r Optical phase of the reference beam.

ϕ_1 Optical phase of the illuminating object beam.

ϕ_2 Optical phase of the reflected object beam.

θ Angle between the illumination and reflection vectors.

λ The wavelength of the laser light used for interference.

$\Omega(t)$ The fringe locus function.

Ω_{approx} The approximated fringe locus function.

2.2 Introduction to EOH

EOH is a non-intrusive, laser-based, whole-field measurement technique that uses the basic physics of holographic interferometry to measure small surface displacements on statically or dynamically loaded structures. The fringe pattern that results from the optical interference of scattered object light combined with reference light are essentially contour maps of the object's displacement, where each fringe represents a line of constant displacement [17]. EOH differs from typical holography in that the images are not recorded on special photographic film and processed individually but instead are captured with a charged-coupled device (CCD) camera and processed with a computer acquisition system. The captured images are digitized and processed all within a matter of seconds to produce a near real time measurement [18]. This method allows the deformation of the object's surface to be directly perceived by the observation of the fringes [19], where a great number of fringes would indicate a relatively large displacement.

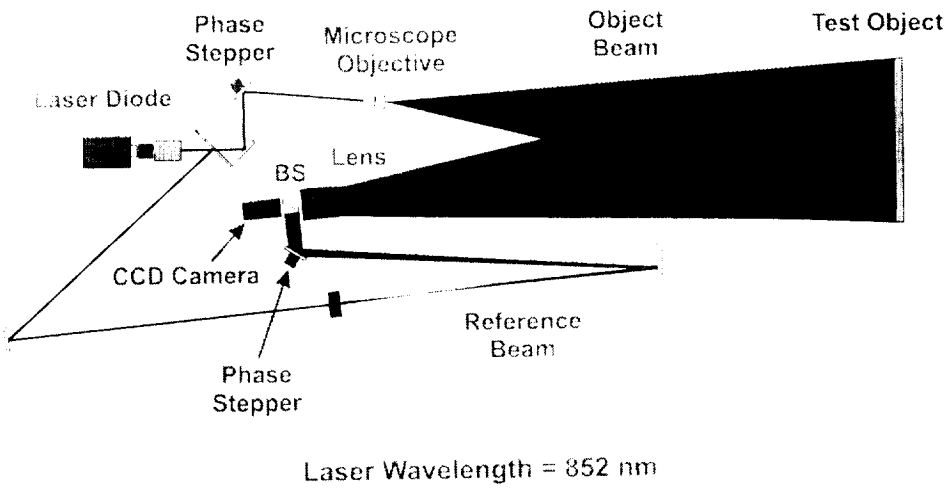

Figure 2.1: Optical set-up [18].

EOH interference patterns are generated by the combination of scattered light from the test object and non-scattered light from a reference source. This is accomplished by splitting the beam of a coherent, single frequency laser into *object* and *reference* beams. The object beam maintains most of the laser light energy, while the reference beam is typically of about 5% of the laser energy [4]. As shown in Fig. 2.1 a microscope objective is used to expand the object beam and project it onto the test specimen. A CCD camera lens focused on the test object collects a portion of the scattered light and directs it to a beam combiner, where it is recombined with the reference light. The collected scattered light has a random, unknown phase distribution, which cannot be measured directly by the CCD camera. However, constructive/destructive interference caused by relative phase differences between the collected scattered object light and reference light will result in a spatial intensity variation dependent upon the relative phase. The CCD camera records these spatial intensity variations in the form of an electronic hologram. Movement of the test object results in changes of the object beam optical path length, producing a change in the

collected scattered light/reference beam relative phase and observed pixel intensity [4]. For the case of static measurements EOH interference patterns, or *interferograms*, result when two electronic images of the object obtained under different states of stress are digitally subtracted. In this manner, differences in optical path length between the non-loaded and loaded conditions can be distinguished as intensity variations observed by the CCD camera [4]. The method of subtracting the non-stressed image with the stressed image is known as double exposure holography and is used to determine displacements for statically loaded structures.

2.2.1 EOH Theory, The Dynamic Case

For the case of dynamically loaded structures, which is the major focus of this thesis, the double exposure method is not sufficient in gathering all the information necessary to obtain displacement information [20]. To do so, a method known as continuous time averaged interferometry is used. This method requires that an interferogram of the moving object be recorded for an exposure time well in excess of the period of oscillation. By guaranteeing that the exposure time is greater than the period of oscillation, the interferogram will effectively record a continuous distribution of double exposure EOH images corresponding to the various points during the vibration cycle [20]. This interferogram represents the time-averaged displacement of the object as well as the intensity variations of the interference fringes, for the period of oscillation. Just as the displacement varies with the vibration cycle so does the intensity distribution of the interference fringes. It can be shown that the intensity of the interference fringes varies as the square of the zero order Bessel function of the first kind. This relation can be derived by first defining the light fields from both the object F_o, and reference F_r, beams as well

as the light field scattered from the vibrating object F_o. Next, by defining the interaction between these light fields, the Bessel function as it relates to the intensity distribution of a dynamically loaded object, can be derived as follows.

$$F_o(x,y,t) = A_o \exp\left[i\phi_o(x,y,t) + i\Omega(t) + 2\pi ft\right] \tag{2.1}$$

where A_o is the amplitude of the object beam, $\Omega(t)$ is the temporal phase change caused by reflection off the vibrating structure, f is the emission frequency of the laser diode and ϕ_o is the phase of the object beam given by Eq. 2.2

$$\phi_o(x,y,t) = \frac{2\pi g_o E_o(x,y,t)}{\lambda} \tag{2.2}$$

where g_o is a geometrical factor with $g_o = 2$ for displacements perpendicular to the object surface with normal incidence. E_o is the time dependent displacement of a point on the vibrating structure and can be expressed as

$$E_o(x,y,t) = e_o \sin(\omega t). \tag{2.3}$$

In Eq. 2.3 e_o is the amplitude of vibration for the test structure and ω is the frequency of vibration. The reference beam field can be expressed as Eq. 2.4

$$F_r(x,y,t) = A_r \exp\left[i\phi_o(x,y,t) + 2\pi ft\right] \tag{2.4}$$

where A_r is the amplitude of the reference beam and ϕ_r is the phase, which is given as Eq. 2.5

$$\phi_r(x,y,t) = \frac{2\pi g_r E_r(x,y,t)}{\lambda} \tag{2.5}$$

where g_r is a geometrical factor with $g_r = 2$ for displacements perpendicular to the object surface with normal incidence. E_r is the time dependent displacement of a point on the vibrating structure and can be expressed as

$$E_r(x,y,t) = e_r \sin(\omega t). \tag{2.6}$$

In Eq. 2.6 e_r is the amplitude of the PZT and ω is the frequency of vibration.

When the reflected object beam recombines with the reference beam, the phase difference between the two beams form a pattern of fringes. These fringes are described by the fringe locus function Ω(t), which is the major element for determining structural displacements. However, in order to solve for the fringe locus function, the intensity relation of the fringes must first be solved. Interference is the addition of the reference and the reflected object beams, which can be expressed as Eq. 2.7

$$F_{interference} = [A_o \exp(i(\phi_o + \Omega(t) + 2\pi ft) + A_r \exp(\phi_r + 2\pi ft)] \tag{2.7}$$

The intensity, or the energy delivered by the wave per unit area per unit time [6], is defined as the product of the interference beam (Eq. 2.7) and its complex conjugate, which can be rewritten as Eq. 2.8

$$I \propto [F_r + F_v][F_r + F_v]^* \tag{2.8}$$

where * represents a complex conjugate. Substitution of Eq 2.1 and 2.4 into Eq. 2.8 yields the intensity relation of the interference fringes as shown in Eq. 2. 9- 2.22.

$$\begin{aligned} I = &\left[A_o \exp(i\phi_o + i\Omega + 2\pi ft) + A_r \exp(i\phi_r + 2\pi ft)\right] \bullet \\ &\left[A_o \exp(-i(\phi_o + \Omega + 2\pi ft)) + A_r \exp -i(\phi_r + 2\pi ft)\right] \end{aligned} \tag{2.9}$$

Recognizing that $\exp(i\omega) = \cos\omega + \sin\omega$ and $\exp(-i\omega) = \cos\omega - \sin\omega$ and $\exp i(2\pi ft - 2\pi ft) = 1$, Eq. 2.9 can be expanded as shown in Eq. 2.10

$$\begin{aligned} I = &\left[A_o(\cos(\phi_o + \Omega) + i\sin(\phi_o + \Omega)) + A_r(\cos\phi_r + i\sin\phi_r)\right] \bullet \\ &\left[A_o(\cos\phi_o + \Omega) - i\sin(\phi_o + \Omega) + A_r\cos\phi_r - i\sin\phi_r\right] \end{aligned} \tag{2.10}$$

Multiplying the dot product of Eq. 2.10 and using the identity $\cos^2 x + \sin^2 x = 1$ and $i^2 = -1$ (complex variable) Eq. 2.10 expands to the following:

$$I = A_o^2 + A_r^2 + A_o A_r[\cos(\phi_o + \Omega)\cos\phi_r - i\sin\phi_r\cos(\phi_o + \Omega)]$$
$$+ A_o A_r[i\sin(\phi_o + \Omega)\cos\phi_r + \sin(\phi_o + \Omega)\sin\phi_r]$$
$$+ A_o A_r[\cos\phi_r\cos(\phi_o + \Omega) - i\sin(\phi_o + \Omega)\cos\phi_r]$$
$$+ A_o A_r[i\sin\phi_r\cos(\phi_o + \Omega) + \sin\phi_r\sin(\phi_o + \Omega)] \quad (2.11)$$

Eq. 2.11 can be reduced as shown by Eq. 2.12

$$I = A_o^2 A_r^2 + 2A_o A_r[\cos(\phi_o + \Omega)\cos\phi_r + \sin(\phi_o + \Omega)\sin\phi_r]. \quad (2.12)$$

Recognizing the trigonometric identity $\cos(x - y) = \cos x\cos y + \sin x\sin y$, Eq. 2.12 is reduced to the following

$$I = A_o^2 A_r^2 + 2A_o A_r\cos[(\phi_o + \Omega) - \phi_r]. \quad (2.13)$$

Where $F_v F_r^* = F_r F_v^*$ and is given by

$$F_v F_r^* = [A_o(\cos(\phi_o + \Omega) + i\sin(\phi_r))][A_r(\cos(\phi_r) - i\sin(\phi_r))]. \quad (2.14)$$

Multiplication of Eq. 2.14 yields

$$= A_o A_r\cos((\phi_o + \Omega) - \phi_r), \quad (2.15)$$

hence,

$$F_v F_r^* + F_r F_v^* = 2\cos((\phi_o + \Omega) - \phi_r). \quad (2.16)$$

The intensity relation can now be rewritten as Eq. 2.17

$$I = A_o^2 + A_r^2 + F_v F_r^* + F_r F_v^*. \quad (2.17)$$

The camera will only record the average energy over the duration of the exposure time. Thus, Eq. 2.17 must be integrated over time in order to obtain the correct intensity relation. This operation yields Eq. 2.18

$$\frac{1}{T}\int I dt = A_o^2 + A_r^2 + \frac{1}{T}F_r\int_0^T F_v^* dt + \frac{1}{T}F_r^*\int_0^T F_v dt. \quad (2.18)$$

The final term in Eq. 2.14 is of primary importance; it governs the form of the EOH interference fringes. Thus by evaluating this term it can be determined that the intensity of the fringes will be directly proportional to the zero order Bessel function as shown in Eq. 2.19-2.22.

$$\frac{1}{T}\int_0^T F_1 dt = \frac{1}{T}\int_0^T A_o \exp(i(\phi_o + \Omega(t)))dt \tag{2.19}$$

When the EOH image is digitally reconstructed, it follows that the reconstructed wavefront F_{rec} is given by Eq. 2.20.

$$F_{rec} = \frac{1}{T} A_o \exp(i\phi_o)\int_0^T \exp(i\Omega(t))dt \tag{2.20}$$

The integral of Eq. 2.20 is called the characteristic function and is denoted by M as shown in Eq. 2.21

$$\frac{1}{T}\int_0^T \exp(i\Omega(t))dt = M(\Omega(t)) \tag{2.21}$$

The time average integral of Eq. 2.21 can be evaluated as $J_0(\Omega)$. The zero order Bessel function of the first kind with argument $\Omega(t)$ and the intensity of the reconstructed wavefront will then be proportional to Eq. 2.22

$$I \propto F_{rec}F_{rec}^* = A_o^2 \exp(i2\phi_o)\left|\frac{1}{T}\int_0^T \exp(i\Omega)dt\right|^2 = qJ_0^2(\Omega(t)), \tag{2.22}$$

where, q is a constant. Thus, from the physics of two interfering beams off the surface of a vibrating object the intensity of the fringe is found to be proportional to the zero order Bessel function as shown in Eq. 2.22.

2.2.2 Verification of the Bessel Function Intensity Distribution

The zero order Bessel function and its square are shown in Fig. 2.3. As shown in Eq. 2.22, the EOH fringe spatial intensity distribution is proportional to the zero order Bessel function for vibrating structures. Nodal positions on the structure can be identified by what is termed the zero order fringe, which corresponds to the largest peak of J^2_0. The intensity distribution of this fringe is approximately 6 times brighter than all other fringes, providing easy visual identification. The zero order fringe is the brightest fringe because of the time integration properties of the camera and scattering statistics [4]. The zero-order fringe occurs at the nodal positions, where there is no object motion. Since there is no object motion at the nodes, pixel intensity is constant and does not vary with time. Integrating this over the exposure time of the CCD camera is simply integrating a constant and the result is the constant itself. Thus, when two holograms of a vibrating object are subtracted, the non-nodal pixels will not be as bright as the zero-order fringe [4]. When there is an optical phase difference the intensity of the fringes decreases until the two light fields are 180° out of phase. This event corresponds to the Bessel function's touching of the x-axis, which results in a dark fringe within the EOH interferogram.

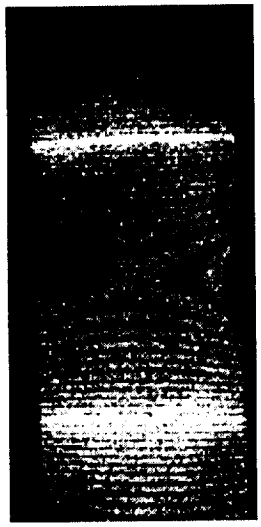

Figure 2.2: EOH image of a dynamically loaded structure. The large bright fringes are denoted as zero order fringes.

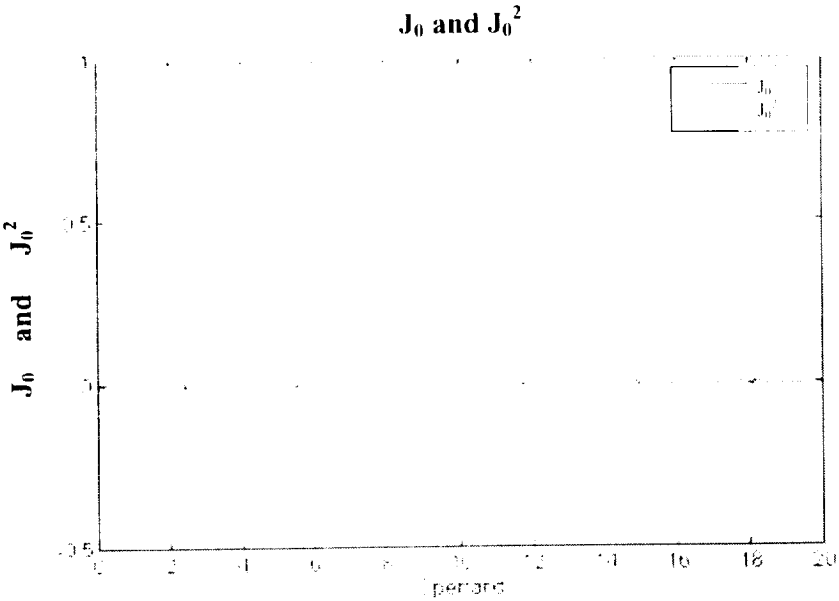

Figure 2.3: Zero order and square of the zero order Bessel function

Figures 2.4 and Fig. 2.5 illustrate a cantilever beam vibrating at different frequencies. In Fig. 2.4 the beam is vibrating such that two zero order fringes appear corresponding to the first and second flexural modes. Figure 2.5 illustrates a third flexural mode shape for this cantilever beam. These figures are shown as an example of how EOH images corresponds to object displacement and motion. Note how the intensity varies across the image, where high intensity relates to small displacements and low intensity relates to large displacements.

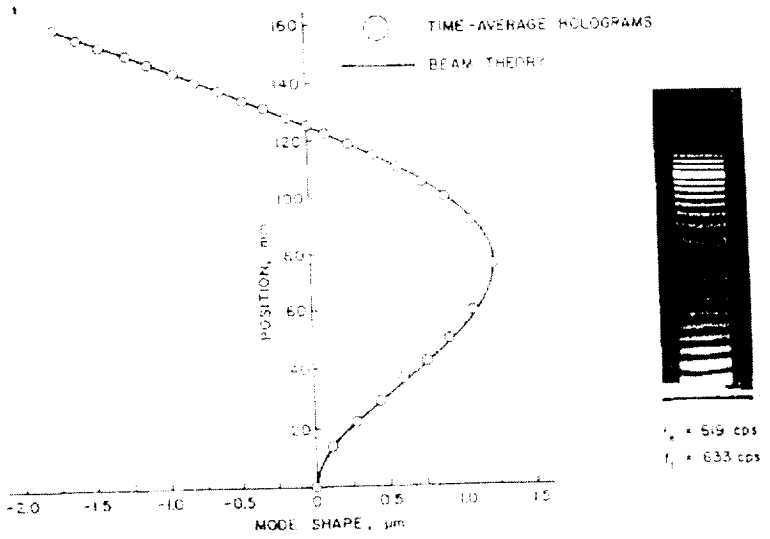

Figure 2.4: Second mode shape and corresponding hologram [3]

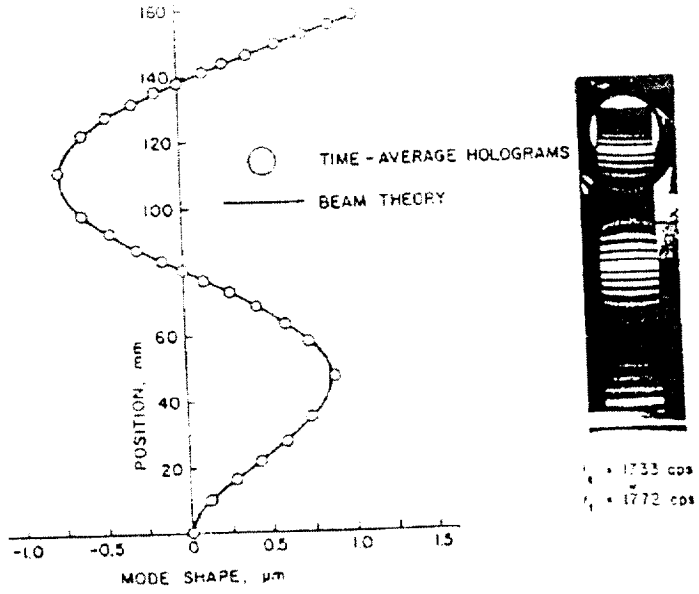

Figure 2.5: Third mode shape and corresponding hologram [3]

2.3 FRINGE LOCUS AND THE SENSITIVITY VECTOR

Electro-optic holographic numerical analysis, in particular the determination of the fringe locus function $\Omega(t)$, depends on knowledge of the illumination and the observation directions used while recording the EOH images. These directions are given by the illumination vector $\hat{k}_1$ and the observation vector $\hat{k}_2$, which describe the propagation of light from a point source to the structure, and from that point, to the CCD camera. The difference of these two vectors is known as the sensitivity vector and is denoted as $\overline{K} = (\hat{k}_2 - \hat{k}_1)$, where $\overline{K}$ is considered to be a vector corresponding to the measurement direction which bisects the illumination and observation vectors of a single point. The fringe locus function is related to the sensitivity vector as well as the displacement vector $\overline{L}$, as shown in Eq. 2.23.

$$\overline{K} \cdot \overline{L} = \Omega \qquad (2.23)$$

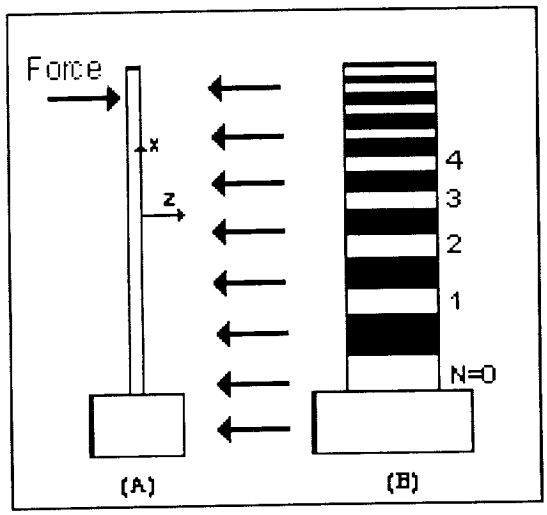

Figure 2.6: Normal deformation of a cantilever beam: (A) Side view of the beam with displacement in the z direction and illumination in the -z direction, arrows indicate direction of illumination. (B) Interference pattern observed on the front of the beam [13].

The derivation of the sensitivity vector can easily be determined by examining the static measurement case, however, the vector is the same for both static and dynamic cases. First assume the test object is a simple cantilever beam moving in the transverse direction as shown in Fig. 2.6 (a). A wave traveling normal to the plane of the

object illuminates its surface, as shown in Fig. 2.6, where the arrows normal to the surface indicate the direction of illumination [22]. For the static case, the light scattered by the test object is initially recorded while the object is in a no-load condition. Then a second capture is identically made with the object under loaded conditions. Interference patterns, like the one in Fig. 2.6 (B), are produced when the difference is taken between the light scattered from the no-load conditions and the loaded conditions. The figure shows what the virtual image of the reconstruction may look like. The force applied to the test object is small and displacement only occurs in the z direction, which is denoted as $z = Z(x)$. If the distance the light travels is l_0, then the distance it would travel after displacement is $l_0 - 2Z(x)$ and the corresponding optical phase shift is equal to $\Omega = \frac{2\pi}{\lambda} 2Z(x)$ [22]. The next step in determining displacements is to assign fringe order to the bright fringes. If the base of the test object is fixed, the zero order fringe will appear at the base of the structure and will be assigned the number $N = 0$. Sequential bright fringes are then assigned positive integers from N =1, 2, 3, . . . N. The N^{th} bright fringe will correspond to a phase change of $\Omega = 2\pi N = \frac{2\pi}{\lambda} 2Z(x)$. Thus solving for the displacement Z, one would arrive at Eq. 2.24

$$Z(x) = \frac{N\lambda}{2} \quad . \tag{2.24}$$

Displacements normal to the surface of the object are easily determined by counting the fringes. However, for structures that undergo more complex motion, (i.e., two and three dimensions) the method of determining displacement by simply counting the fringes is no longer valid. Vector displacements must be extracted from the interference pattern by a

careful point-by-point analysis. First, a model must be developed from which the derivation of fringe interpretation can be based. Consider the surface of the test object as a collection of point scatterers. When a point P is displaced by a distance of $\vec{L}$ to its new position P' the interference between the light scattered at P and the light scattered at P' contribute to the fringes in the interferogram. Figure 2.7 shows the important elements of the physical system [22].

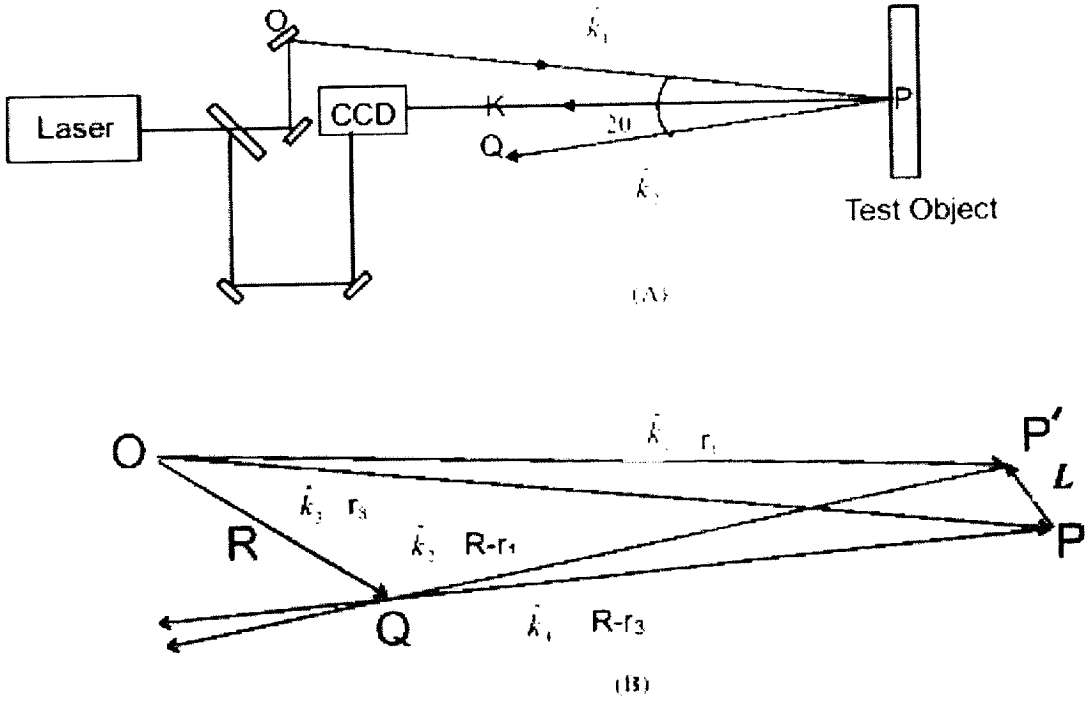

Figure 2.7: Nomenclature for fringe analysis. (A) Schematic diagram of the system. (B) Position and propagation vectors [22].

In Fig. 2.7 (B) several vectors are used to determine the relationship between the fringe locus function and the displacement vector. The vectors $\overline{R}$ and $\overline{r}_1$ lie in the same plane as the points O, P and Q. The vectors $\hat{k}_1$ and $\hat{k}_2$ are the propagation vectors of the light illuminating point P from point O and the light reflected point P to point Q respectively [22].

The phase of the illumination beam and the reflected scattered light beam would reach the detector at point Q and would have values as shown by Eqs. 2.25 and 2.26,

$$\phi_1 = \hat{k}_1 \cdot \overline{r}_1 + \hat{k}_2 \cdot (\overline{R} - \overline{r}_1) + \phi_a \tag{2.25}$$

and

$$\phi_2 = \hat{k}_3 \cdot \overline{r}_3 + \hat{k}_4 (\overline{R} - \overline{r}_3) + \phi_a \tag{2.26}$$

where ϕ_a is given as the arbitrary phase assigned to the beams from the point O and ϕ_1 is the phase of the scattered light before displacement. The variable ϕ_2 is the phase of the scattered light after displacement. The total phase of the scattered beam would then reach point Q with a value equal to Eq 2.27

$$\Omega = \phi_2 - \phi_1 . \tag{2.27}$$

After the test object is displaced, the illumination vector and reflected scattered light vector are $\hat{k}_3$ and $\hat{k}_4$ respectively. Combining these vectors into Eq. 2.27 the fringe locus function can now be expressed as Eq. 2.28

$$\Omega = (\hat{k}_2 - \hat{k}_1) \cdot (\overline{r}_1 - \overline{r}_3) + (\hat{k}_3 - \hat{k}_1) \cdot \overline{r}_3 + (\hat{k}_4 - \hat{k}_2) \cdot (\overline{R} - \overline{r}_3) . \tag{2.28}$$

In a real EOH system the magnitude of the vectors $\overline{r}_1$ and $\overline{r}_3$ are much larger the displacement vector $L = |\overline{r}_3 - \overline{r}_1|$, so for all practical purposes $(\hat{k}_3 - \hat{k}_1)$ is perpendicular to

$\bar{r}_3$ and $(\hat{k}_4 - \hat{k}_2)$ is perpendicular to $(\bar{R} - \bar{r}_3)$. This condition causes the dot product of these four terms to be identically equal to zero thus allowing the fringe locus function to become

$$\Omega = (\hat{k}_2 - \hat{k}_1) \cdot \bar{L} \tag{2.29}$$

The difference between these two vectors is known as the sensitivity vector, which is denoted by $\bar{K} = (\hat{k}_2 - \hat{k}_1)$. The fringe locus function can now be rewritten as

$$\Omega = \bar{K} \cdot \bar{L} . \tag{2.30}$$

In Fig. 2.7 (A) the angle between the propagation vectors is given as 2θ [22]. The magnitude of the sensitivity vector can be determined using vector algebra and the unit directional components of the propagation vectors as shown by Eqs. 2.31 and 2.32

$$\hat{k}_1 = |k_1| \sin(\theta) i + |k_1| \cos(\theta) j \tag{2.31}$$

and

$$\hat{k}_2 = |k_2| \sin(\theta) i - |k_2| \cos(\theta) j . \tag{2.32}$$

The sensitivity vector then becomes the difference of these two vectors given as

$$\bar{K} = 2k\left(\hat{k}_2 - \hat{k}_1\right)\cos(\theta) \tag{2.33}$$

where $k = 2\pi / \lambda$ is the wave number. A single point observation of the test object would yield a displacement shown by Eq. 2.34

$$\bar{L} = \frac{\Omega}{2k \cos(\theta)} . \tag{2.34}$$

The ideal EOH system is one where the propagation vectors lie normal to the plane of the test object's surface, and the angle between the vectors is $\theta = 0$. However, alignment of the equipment usually does not allow for such ideal conditions, and the vectors do have

some small angle. The angle is said to be small enough that it is approximately equal to zero, which allows the displacement vector to become

$$\overline{L} = \frac{\Omega}{2k}, \tag{2.35}$$

where $\cos(0) = 1$. The full three-dimensional displacement vector is given as

$$\overline{L} = L_x \hat{i} + L_y \hat{j} + L_z \hat{k}. \tag{2.36}$$

CCD cameras used in the EOH technique have a two-dimensional array of sensors, or pixels. Each pixel on the CCD array functions as an independent interferometer. The light within the speckle field has a particular amplitude and phase relative to the reference beam [19]. This amplitude and phase are encoded as intensity variations detected by the CCD. By recording and processing the values of the light intensity before and after the test object moves, an estimate of surface deformation can be calculated by subtraction of the phase measured before and after loading of the object [19]. Although each point will have a different intensity that varies sinusoidally according to its initial phase, the phase change at different points will be the same as long as the surface displacement is the same. The result of subtraction of the images at different times is the contour map representing areas of constant displacement by means of interference fringes [19].

Referring back to Eqs. 2.25 and 2.26, the phase variations of a single point are based on the fact that when coherent light illuminates the optically rough surface of a test object, variations in the roughness of the surface produce diffracted waves. These diffracted waves can interfere with each other when the optical path lengths between surface variations differ. These local fluctuations cause the image to have a granular appearance known as speckle. However, these variations in intensity are directly related

to variations in phase, which also vary accordingly across the rough surface [22]. If the alignment of the EOH system is correct, then the scattered object and reference beams will be coherent with one another and any small variation in optical path length will cause the speckle pattern to "sparkle." This indicates that the speckle pattern is moving in and out of phase, which allows one to know when the alignment of the EOH system is correct. If this phenomenon does not occur prior to data collection, fringes will not be formed because the conditions for interference will not have been met.

2.4 STATIC MEASUREMENTS

EOH can be broken down into two categories, static measurements and dynamic measurements. Static measurements are obtained by utilizing the double exposure method on stationary objects subject to static loading. Dynamic measurements employ the time-average holographic method and are used to obtain vibration amplitude data. The method of measuring a dynamically loaded object is of major interest for controlling fringe characteristics, the subject of this thesis. In order to completely understand the physics of the dynamic case, the technique for obtaining static measurements must first be understood.

2.4.1 STATIC EOH THEORY

Static measurements are made by capturing two sets of four sequential frames of EOH images. Each image varies from the other by introducing a 90° optical phase step induced on the reference beam. After the original laser beam has passed through the beam splitter, the reference beam phase is directed onto a piezoelectrically driven mirror. The PZT moves in such a manner that the reference beam phase is incremented by 90°

for each frame [3]. The first four images are of the object in its original position while the second four images are of the object in the displaced position. The following equations in this section and in Section 2.3 are used for the static and dynamic measurements respectively. The equations are used for the quantitative determination of the displacement vector and are a product of the work shown by R. Pryputniewicz in Holographic Numerical Analysis [3].

The image of the object in its original, unstressed (no displacement) state can be described by the illumination of the object in its original state of the *n*th sequential frame, as shown in Eq. 2.37.

$$I_n(x,y) = I_o + I_r - 2\, A_o\, A_r \cos[\Delta\varphi + \Delta\theta_n]. \tag{2.37}$$

The illumination or irradiance of the object in the displaced state can be described as

$$I_n'(x,y) = I_o' + I_r + 2\, A_o'\, A_r \cos[\Delta\varphi + \Omega + \Delta\theta_n]. \tag{2.38}$$

In the above equations, I_o is the intensity of the light scattered off of the object prior to deformation, I_o' is the intensity of the scattered light off of the object after deformation and I_r is the intensity of the reference beam. $\Delta\theta_n$ is the 90° sequential phase step, which is induced onto the reference beam between recordings of each individual frame. The addition of the phase step $\Delta\theta_n$ is used to eliminate the phase difference $\Delta\varphi$ between the object and reference beams, which is an unknown, from the intensity. These steps are used to solve for Ω, the fringe locus function, which is directly related to the displacement of the object. Therefore, adding in the sequential phase steps into Eqs. 2.37 and 2.38 the four sequential frames recorded by the CCD camera for both positions of the object become

$$I_1 = I_o + I_r + 2\, A_o\, A_r \cos[\Delta\varphi + 0°], \tag{2.39}$$

$$I_2 = I_o + I_r + 2\ A_o\ A_r \cos[\Delta\varphi + 90°], \tag{2.40}$$

$$I_3 = I_o + I_r + 2\ A_o\ A_r \cos[\Delta\varphi + 180°], \tag{2.41}$$

$$I_4 = I_o + I_r + 2\ A_o\ A_r \cos[\Delta\varphi + 270°], \tag{2.42}$$

and

$$I_1' = I_o' + I_r + 2\ A_o'\ A_r \cos[\Delta\varphi + \Omega + 0°], \tag{2.43}$$

$$I_2' = I_o' + I_r + 2\ A_o'\ A_r \cos[\Delta\varphi + \Omega + 90°], \tag{2.44}$$

$$I_3' = I_o' + I_r + 2\ A_o'\ A_r \cos[\Delta\varphi + \Omega + 180°], \tag{2.45}$$

$$I_4' = I_o' + I_r + 2\ A_o'\ A_r \cos[\Delta\varphi + \Omega + 270°]. \tag{2.46}$$

Using both sets of intensity equations, prior to deformation (Eqs. 2.39-2.42) and after deformation (Eqs. 2.43-2.46), there are four unknowns -- the irradiance I_o, I_o', the phase difference between the object light field and the reference light field $\Delta\varphi$, and the fringe locus function, Ω. By adding in the 90° phase step $\Delta\theta_n$, $\Delta\varphi$ can be eliminated from the intensity equations as shown in Eqs. 2.47 –2.55.

$$I_1 = I_o + I_r + 2\ A_o\ A_r \cos(\Delta\varphi + 0°), \tag{2.47}$$

$$I_2 = I_o + I_r + 2\ A_o\ A_r \sin(\Delta\varphi + 90°), \tag{2.48}$$

$$I_3 = I_o + I_r - 2\ A_o\ A_r \cos(\Delta\varphi + 180°), \tag{2.49}$$

$$I_4 = I_o + I_r - 2\ A_o\ A_r \sin(\Delta\varphi + 270°), \tag{2.50}$$

and

$$I_1' = I_o' + I_r' + 2\ A_o'\ A_r \cos(\Delta\varphi + \Omega + 0°), \tag{2.51}$$

$$I_2' = I_o' + I_r' + 2\ A_o'\ A_r \sin(\Delta\varphi + \Omega + 90°), \tag{2.52}$$

$$I_3' = I_o' + I_r' - 2\ A_o'\ A_r \cos(\Delta\varphi + \Omega + 180°), \tag{2.53}$$

$$I_4' = I_o' + I_r' - 2\ A_o'\ A_r \sin(\Delta\varphi + \Omega + 270°). \tag{2.54}$$

Using the trigonometric addition and subtraction formula of Eq. 2.55

$$\cos(x + y) = \cos x \cos y \quad \sin x \sin y \tag{2.55}$$

Eqs. 2.47-2.54 become

$$I_1 = I_o + I_r + 2 A_o A_r \cos(\Delta\varphi), \tag{2.56}$$

$$I_2 = I_o + I_r + 2 A_o A_r \sin(\Delta\varphi), \tag{2.57}$$

$$I_3 = I_o + I_r - 2 A_o A_r \cos(\Delta\varphi), \tag{2.58}$$

$$I_4 = I_o + I_r - 2 A_o A_r \sin(\Delta\varphi), \tag{2.59}$$

and

$$I_1' = I_o' + I_r' + 2 A_o' A_r \cos(\Delta\varphi + \Omega), \tag{2.60}$$

$$I_2' = I_o' + I_r' + 2 A_o' A_r \sin(\Delta\varphi + \Omega), \tag{2.61}$$

$$I_3' = I_o' + I_r' - 2 A_o' A_r \cos(\Delta\varphi + \Omega), \tag{2.62}$$

$$I_4' = I_o' + I_r' - 2 A_o' A_r \sin(\Delta\varphi + \Omega). \tag{2.63}$$

Subtracting Eqs. 2.56 and 2.58 as well as Eqs. 2.57 and 2.59 the following set of equations are obtained for the intensity difference image of the object in its undeformed state.

$$(I_1 - I_3) = 4 A_o A_r \cos \Delta\varphi \tag{2.64}$$

and

$$(I_2 - I_4) = 4 A_o A_r \sin \Delta\varphi \tag{2.65}$$

Performing the same procedure for Eqs. 2.60 and 2.61 as well as 2.61 and 2.63 the intensity difference images of the object in its deformed state are obtained as the following

$$(I_1' - I_3') = 4 A_o' A_r \cos \Delta\varphi \tag{2.66}$$

and

$$(I_2' - I_4') = 4\, A_o'\, A_r \sin \Delta\varphi \tag{2.67}$$

The addition of Eqs. 2.64 and 2.65 will yield Eq. 2.68

$$(I_1 - I_3) + (I_1' - I_3') = 4\, A_o\, A_r \cos \Delta\varphi + A_o'\, A_r \cos(\Delta\varphi + \Omega) \tag{2.68}$$

Using the trigonometric addition formula $\cos(\Delta\varphi + \Omega) = \cos\Delta\varphi \cos\Omega - \sin\Delta\varphi \sin\Omega$ and assuming that the amplitude of the original object beam is approximately equal to the amplitude of the displaced object beam, $A_o \approx A_o'$, and Eq. 2.68 can be rewritten as

$$(I_1 - I_3) + (I_1' - I_3') = 4\, A_o\, A_r [\cos \Delta\varphi + \cos \Delta\varphi \cos\Omega - \sin\Delta\varphi \sin\Omega] \tag{2.69}$$

and then simplified as Eq. 2.70

$$(I_1 - I_3) + (I_1' - I_3') = 4\, A_o\, A_r [(1+ \cos \Omega) \cos\Delta\varphi - \sin\Delta\varphi \sin \Omega]. \tag{2.70}$$

Equation 2.68 is the entire data image processed by the EOH computer. The remaining images are then processed in order to solve for Ω, the fringe locus function.

Similarly for Eqs. 2.66 and 2.67 the image of intensity can be given as Eq. 2.71

$$(I_2 - I_4) + (I_2' - I_4') = 4\, A_o\, A_r [(1+ \cos \Omega) \sin\Delta\varphi - \cos\Delta\varphi \sin \Omega]. \tag{2.71}$$

Finally, $\Delta\varphi$ is eliminated by adding the squares of Eqs. 2.70 and 2.71 together

$$[(I_1 - I_3) + (I_1' - I_3')]^2 + [(I_2 - I_4) + (I_2' - I_4')]^2 =$$

$$\{4\, A_o A_r[(1+ \cos \Omega)\cos\Delta\varphi - \sin\Delta\varphi \sin \Omega]\}^2$$

$$+ \{4\, A_o A_r[(1+ \cos \Omega) \sin\Delta\varphi - \cos\Delta\varphi \sin \Omega]\}^2 \tag{2.72}$$

Let $[(I_1 - I_3) + (I_1' - I_3')]^2 + [(I_2 - I_4) + (I_2' - I_4')]^2$ be denoted as $D_1^2 + D_2^2$, then solve to eliminate $\Delta\varphi$ as shown in the following equations

$$D_1^2 + D_2^2 = 16\, A_o^2\, A_r^2\, [(1+ \cos \Omega) \cos\Delta\varphi - \sin\Delta\varphi \sin \Omega]^2$$

$$+ 16\, A_o^2\, A_r^2\, [(1+ \cos \Omega) \sin\Delta - \cos\Delta\varphi \sin \Omega] \tag{2.73}$$

Expansion of Eq. 2.73 yields Eq. 2.74

$$D_1^2 + D_2^2 = 16\, A_o^2\, A_r^2\, [(\cos^2\Delta\varphi + \sin^2\Delta\varphi) + 2\cos\Omega(\cos^2\Delta\varphi + \sin^2\Delta\varphi)$$
$$+ (\cos^2\Delta\varphi \cos^2\Omega + \sin^2\Delta\varphi \sin^2\Omega)$$
$$+ (\cos^2\Delta\varphi \sin^2\Omega + \sin^2\Delta\varphi \cos^2\Omega)]. \quad (2.74)$$

Recognizing trigonometric identities Eq. 2.74 can be rewritten as Eq. 2.75

$$D_1^2 + D_2^2 = 16\, A_o^2\, A_r^2\, \{1 + 2\cos\Omega + [\cos^2(\Delta\varphi - \Omega) + \sin^2(\Delta\varphi + \Omega)]\}. \quad (2.75)$$

Using the relation $(\sin^2 x + \cos^2 x) = 1$ Eq. 2.75 reduces to the form shown in Eq. 2.76

$$D_1^2 + D_2^2 = 16\, A_o^2\, A_r^2\, (1 + 2\cos\Omega + 1). \quad (2.76)$$

Rewriting Eq. 2.76 the solution for $D_1^2 + D_2^2$ becomes Eq. 2.77

$$D_1^2 + D_2^2 = 32\, A_o^2\, A_r^2\, (1 + \cos\Omega). \quad (2.77)$$

Using the half angle identity of Eq. 2.78

$$(1 + \cos\Omega) = 2\cos^2(\Omega/2), \quad (2.78)$$

Eq. 2.77 can be reduced to Eq. 2.79

$$[D_1^2 + D_2^2]^{1/2} = 8\, A_o A_r \cos(\Omega/2). \quad (2.79)$$

Equation 2.79 represents the static viewing image. In order to obtain the displacement data for the EOH system the fringe locus function Ω must be determined. In order to do so the same procedure used to obtain Eq. 2.77 must be followed for the subtraction of Eqs. 2.64 and 2.67 as well as Eqs. 2.65 and 2.67 as shown in Eqs. 2.80 and 2.81.

$$(I_1 - I_3) - (I_2' - I_4') = 4\, A_o\, A_r\, [(1 - \cos\Omega)\cos\Delta\varphi + \sin\Delta\varphi \sin\Omega] \quad (2.80)$$

and

$$(I_2 - I_4) - (I_1' - I_3') = 4\, A_o\, A_r\, [(1 - \cos\Omega)\sin\Delta\varphi - \cos\Delta\varphi \sin\Omega] \quad (2.81)$$

Equations 2.80 and 2.81 are then squared and added together as shown in Eq. 2.82

$$[(I_1 - I_3) - (I_2' - I_4')]^2 + [(I_2 - I_4) - (I_1' - I_3')]^2 =$$
$$16A_o^2A_r^2[(1-\cos\Omega)\cos\Delta\varphi + \sin\Delta\varphi \sin\Omega]^2$$

$$+ 16A_o^2A_r^2[(1- \cos \Omega) \sin\Delta\varphi - \cos\Delta\varphi\sin \Omega]^2 . \quad (2.82)$$

Let $[(I_1 - I_3) - (I_2' - I_4')]^2 + [(I_2 - I_4) - (I_1' - I_3')]^2$ be denoted as $D_3^2 + D_4^2$ and Eq. 2.82 can then be expanded to Eq 2.83

$$D_3^2 + D_4^2 = 16A_o^2A_r^2\{[\cos^2\Delta\varphi + \sin^2\Delta\varphi] - 2\cos^2\Delta\varphi\cos\Omega + [\cos^2\Delta\varphi\cos\Omega + \sin^2\Delta\varphi\sin\Omega] - 2\sin^2\Delta\varphi\cos\Omega + \sin^2\Delta\varphi\cos^2\Omega + \cos^2\Delta\varphi\sin^2\Omega\}. \quad (2.83)$$

Recognizing the identity $(\cos^2\Delta\varphi + \sin^2\Delta\varphi) = 1$ and $(\cos^2\Delta\varphi\cos\Omega + \sin^2\Delta\varphi\sin\Omega) = \cos^2(\Delta\varphi - \Omega)$ Eq. 2.83 reduces to Eq. 2.84

$$D_3^2 + D_4^2 = 16A_o^2A_r^2\{1 - 2\cos^2\Delta\varphi\cos\Omega + \cos^2(\Delta\varphi - \Omega) - 2\sin^2\Delta\varphi\cos\Omega + \sin^2\Delta\varphi\cos^2\Omega + \cos^2\Delta\varphi\sin^2\Omega\}. \quad (2.84)$$

Grouping similar terms Eq. 2.84 can be rewritten as Eq. 2.85

$$D_3^2 + D_4^2 = 16A_o^2A_r^2\{1 + (-2\cos^2\Delta\varphi\cos\Omega - 2\sin^2\Delta\varphi\cos\Omega) + \cos^2(\Delta\varphi - \Omega) + (\cos^2\Delta\varphi\sin^2\Omega + \sin^2\Delta\varphi\cos^2\Omega)\}. \quad (2.85)$$

Using the identity $(\cos^2\Delta\varphi\sin^2\Omega + \sin^2\Delta\varphi\cos^2\Omega) = \sin^2(\Delta\varphi - \Omega)$ Eq. 2.85 reduces to Eq. 2.86

$$D_3^2 + D_4^2 = 16A_o^2A_r^2\{1- 2\cos\Omega(\cos^2\Delta\varphi + \sin^2\Delta\varphi) + \cos^2(\Delta\varphi - \Omega) + \sin^2(\Delta\varphi - \Omega)\}. \quad (2.86)$$

Next, using $(\sin^2 x + \cos^2 x) = 1$ Eq. 2.86 becomes

$$D_3^2 + D_4^2 = 16A_o^2A_r^2\{1 - 2\cos\Omega + 1\}, \quad (2.87)$$

which reduces to Eq. 2.88

$$D_3^2 + D_4^2 = 32A_o^2A_r^2(1 - \cos\Omega). \tag{2.88}$$

Equation 2.77 is subtracted from 2.88 to yield Eq. 2.89

$$D = (D_1^2 + D_2^2) + (D_3^2 + D_4^2) = 64\ A_o^2A_r^2\cos\Omega \tag{2.89}$$

Thus far there are two unknowns Ω and D and only one equation, so an additional equation is needed in order to solve for Ω. The second equation will be formed by following the same procedure as was used to determine D but instead of working with the combinations of Eqs. 2.64 with 2.66 and Eqs. 2.65 with 2.67 the combination will be switched to Eqs. 2.64 with 2.67 and Eqs. 2.66 with 2.65. This procedure is as follows

$$(I_1 - I_3) + (I_2' - I_4') = 4\ A_o^2\ A_r^2\ [(1 + \sin\Omega)\cos\Delta\varphi + \sin\Delta\varphi\cos\Omega], \tag{2.90}$$

$$(I_2 - I_4) + (I_1' - I_3') = 4\ A_o^2\ A_r^2\ [(1 + \sin\Omega)\sin\Delta\varphi - \cos\Delta\varphi\cos\Omega] \tag{2.91}$$

and

$$(I_1 - I_3) - (I_2' - I_4') = 4\ A_o^2\ A_r^2\ [(1 - \sin\Omega)\cos\Delta\varphi - \sin\Delta\varphi\cos\Omega], \tag{2.92}$$

$$(I_2 - I_4) - (I_1' - I_3') = 4\ A_o^2\ A_r^2\ [(1 - \sin\Omega)\sin\Delta\varphi + \cos\Delta\varphi\cos\Omega]. \tag{2.93}$$

Where $[(I_1 - I_3) + (I_2' - I_4')]^2$ will be denoted as N_1^2 and $[(I_2 - I_4) + (I_1' - I_3')]^2$ will be denoted as N_2^2. The sum of these two terms yields

$$N_1^2 + N_2^2 = 32\ A_o^2\ A_r^2\ (1 + \sin\Omega). \tag{2.94}$$

Let $[(I_1 - I_3) - (I_2' - I_4')]^2$ be denoted as N_3^2 and $[(I_2 - I_4) - (I_1' - I_3')]^2$ be denoted as N_4^2 and the sum of these two terms yields

$$N_3^2 + N_4^2 = 32\ A_o^2\ A_r^2\ (1 - \sin\Omega) \tag{2.95}$$

These two terms are then subtracted and denoted by the letter N for simplicity

$$N = (N_1^2 + N_2^2) + (N_3^2 + N_4^2) = 64\ A_o^2\ A_r^2 \sin\Omega. \tag{2.96}$$

Dividing Eqs. 2.96 by 2.97 yields Eq. 2.97

$$\frac{N}{D} = \frac{64A_o^2A_r^2\sin\Omega}{64A_o^2A_r^2\cos\Omega}. \tag{2.97}$$

Recognizing the trigonometric identity tan Ω = sin Ω / cos Ω, Eq. 2.97 can be solved for Ω, the fringe locus function in terms of N and D as shown in Eq. 2.98

$$\Omega = \tan^{-1}(N/D). \tag{2.98}$$

Finally, the displacement data can be determined using Eq. 2.30 as shown in Section 2.3.

2.5 DYNAMIC MEASUREMENTS

This section provides a detailed mathematical derivation of the physical and analytical processes required to obtain quantitative vibrational amplitude measurements using EOH. Dynamic measurements are made using the time-averaged hologram method discussed in section 2.2, where Eq. 2.13 gives the fringe intensity distribution. The intensity can be rewritten as Eq. 2.37 and multiplied by the characteristic equation of Eq. 2.21 to yield Eq. 2.99.

$$I_{nt}(x,y) = I_{ot} + I_{rt} + 2\, A_{ot}\, A_r \cos[\Delta\varphi_t + \Delta\theta_n]M(\Omega_t). \tag{2.99}$$

The images of intensity are gathered in a series of sequential frames as shown by Eq. 2.99, where the n indicates the n^{th} sequential frame [3], which varies as a function of time given as the subscript t. M is the characteristic function and is the modulating term of Eq. 2.99, which is evaluated as the zero-order Bessel function of the first kind.

2.5.1 DYNAMIC EOH THEORY

Just as in the static case, Eq. 2.99 contains four unknowns I_{to}, I_{rt}, $\Delta\phi_t$ and Ω_t. In order to determine the fringe locus function from the interferogram of a vibrating object, four sequential frames are recorded with the phase of the reference beam incremented in steps of 90° between each frame. This process is represented by the following set of simultaneous equations:

$$I_{t1} = I_{to} + I_r + 2A_{ot}A_r \cos(\Delta\phi + 0^{\circ})M(\Omega_t) \tag{2.100}$$

$$I_{t2} = I_{to} + I_r + 2A_{ot}A_r \cos(\Delta\phi + 90^{\circ})M(\Omega_t) \tag{2.101}$$

$$I_{t3} = I_{to} + I_r + 2A_{ot}A_r \cos(\Delta\phi + 180^{\circ})M(\Omega_t) \tag{2.102}$$

$$I_{t4} = I_{to} + I_r + 2A_{ot}A_r \cos(\Delta\phi + 270^{\circ})M(\Omega_t)\,. \tag{2.103}$$

In the above equations the argument (x, y) has been dropped for simplification and the subscript t indicates the time varying parameters. Following the same procedure used for static measurements the equations are reduced to

$$I_{1t} = I_{ot} + I_r + 2A_{ot}A_r \cos(\Delta\phi_t)M(\Omega_t)\,, \tag{2.104}$$

$$I_{2t} = I_{ot} + I_r + 2A_{ot}A_r \sin(\Delta\phi_t)M(\Omega_t)\,, \tag{2.105}$$

$$I_{3t} = I_{ot} + I_r - 2A_{ot}A_r \cos(\Delta\phi_t)M(\Omega_t)\,, \tag{2.106}$$

$$I_{4t} = I_{ot} + I_r - 2A_{ot}A_r \sin(\Delta\phi_t)M(\Omega_t)\,, \tag{2.107}$$

then by subtraction

$$I_{1t} - I_{3t} = 4A_{ot}A_r \cos(\Delta\phi_t)M(\Omega_t) \tag{2.108}$$

and

$$I_{2t} - I_{4t} = 4A_{ot}A_r \sin(\Delta\phi_t)M(\Omega_t)\,. \tag{2.109}$$

Using a similar method as was used for the static measurements and using the relation

$$M(\Omega_t) = J_0(|\Omega|) \tag{2.110}$$

the data image for the time-average frames will become

$$(I_{1t} - I_{3t})^2 + (I_{2t} - I_{4t})^2 = 16\, A_o^2\, A_r^2\, J_o^2(|\Omega_t|). \tag{2.111}$$

Here the subscript t has been dropped from the amplitude variable for simplicity. The objective is to determine the fringe locus function Ω_t, which is the argument of the Bessel

function. The preferable method involves modulating the phase of either the object or the reference beams sinusoidally at the same phase and frequency as the test structure. This uses the fact that it is possible to shift J_o fringes similar to the method in which phase modulation shifts consinusoidal fringes in conventional double exposure holographic interferometry [3, 5]. Adding a modulation step, a vibrating mirror with a known optical phase, into the process makes it possible to solve for the argument of J_o. Mathematically, this modulation step is accomplished by adding a known variable into the argument of the Bessel function denoted as B. The variable B is commonly known as the phasor bias and takes the form of Eq 2.112

$$M(\Omega_t, B) = J_0(|\Omega - B|). \tag{2.112}$$

Generally the intensity distribution can be expressed as Eq. 2.113

$$I_{nt} = I_{at} + I_{mt} J_o^2[\Omega_t - B] \tag{2.113}$$

Where I_{at} represents the intensity or the energy of the local, average background of the scattered light and I_{mt} is the local, maximum intensity of the scattered lighted. Equation 2.111 a special case of Eq. 2.113 as demonstrated by the following equations

$$I_{nt} = (I_{1t} - I_{3t})^2 + (I_{2t} - I_{4t})^2 \tag{2.114}$$

where the local, average background intensity is equal to zero in Eq. 2.115

$$I_{at} = 0, \tag{2.115}$$

and

$$I_{mt} = 16\, A_o^2\, A_r^2\, J_o^2(|\Omega_t|). \tag{2.116}$$

The Bessel function is non-separable and in order to solve for Ω_t one should estimate the $J_o^2(|\Omega_t|)$ intensity distribution as a cosine function, cos Ω_t [4].. This substitution can be made because the correlation between the crossings of the x – axis, the cosine function

and the Bessel function nearly coincide [3]. Recall that a black fringe can be represented by every touching of the x-axis by the $J_o^2(|\Omega_t|)$ function. The general equation can now be rewritten as Eq. 2.117

$$I_{nt} = I_{at} + I_{mt}\cos^2[\Omega_t - B]. \tag{2.117}$$

Using the cosine half-angle theorem, $\cos^2 x = \frac{1}{2}(1 + \cos 2x)$ Eq. 2.117 becomes Eq. 2.118

$$I_n = I_a + I_m\frac{1}{2}\ (1 + \cos[2\Omega - 2B]) \tag{2.118}$$

Multiplying the cosine half angle through Eq. 2.117 the new solution becomes Eq. 2.118

$$I_n = I_a + \frac{1}{2}I_m + \frac{1}{2}I_m\cos[2\Omega - 2B]), \tag{2.119}$$

where

$$I_a = I_a + \frac{1}{2}I_m, \tag{2.120}$$

and

$$I_m = \frac{1}{2}I_m. \tag{2.121}$$

So, Eq. 2.118 reduces to Eq. 2.122

$$I_h = I_a + I_m\cos[2\Omega - 2B]. \tag{2.122}$$

Where the bias modulation B is maintained at the same frequency as the object vibration. With three known values of B, (0, B and –B) Eq. 2.122 can be solved for the fringe locus function as follows:

$$I_{n1} = I_a + I_m\cos 2\Omega, \tag{2.123}$$

$$I_{n2} = I_a + I_m\cos[2\Omega - 2B], \tag{2.124}$$

$$I_{n3} = I_a + I_m\cos[2\Omega + 2B], \tag{2.125}$$

Where I_{n1}, I_{n2} and I_{n3} are the intensities of EOH images, each with a different phasor bias value. Using the cosine addition and subtraction formulas,

$$\cos(x-y)=\cos(x)\cos(y)+\sin(x)\sin(y) \tag{2.126}$$

and

$$\cos(x+y)=\cos(x)\cos(y)-\sin(x)\sin(y) \tag{2.127}$$

the three values of B can effectively be used to solve for Ω_t. First, solving for the average background intensity I_a from Eq. 2.123 gives

$$I_a = I_{n1} - I_m \cos 2\Omega. \tag{2.128}$$

Plugging Eq. 2.128 into Eq. 2.124 yields

$$I_{n2} = I_{n1} - I_m \cos 2\Omega + I_m [\cos 2\Omega \cos 2B + \sin 2\Omega \sin 2B] \tag{2.129}$$

Combining like terms gives Eq. 2.130 and then Eq. 2.131

$$I_{n2} = I_{n1} + I_m [\cos 2\Omega \cos 2B + \sin 2\Omega \sin 2B - \cos 2\Omega] \tag{2.130}$$

then

$$I_{n2} = I_{n1} + I_m [(\cos 2B - 1)\cos 2\Omega + \sin 2\Omega \sin 2B] \tag{2.131}$$

Solving for the local maximum intensity I_m gives the following equations

$$I_{n2} - I_{n1} = I_m [(\cos 2B - 1)\cos 2\Omega + \sin 2\Omega \sin 2B] \tag{2.132}$$

$$I_{n2} - I_{n1} = - I_m [(1 - \cos 2B)\cos 2\Omega - \sin 2\Omega \sin 2B] \tag{2.133}$$

$$I_m = \frac{I_{n1} - I_{n2}}{(1-\cos 2B)\cos 2\Omega - \sin 2\Omega \sin 2B} \tag{2.134}$$

Substituting Eq. 2.134 in Eq. 2.125 yields Eq. 2.134

$$I_{n3} - I_{n1} = \frac{(I_{n1} - I_{n2})\cos 2\Omega}{(1-\cos 2B)\cos 2\Omega - \sin 2\Omega \sin 2B} + \frac{(I_{n1} - I_{n2})\cos\Omega \cos 2B - \sin 2\Omega \sin 2B}{(1-\cos 2B)\cos 2\Omega - \sin 2\Omega \sin 2B} \tag{2.135}$$

Expansion of Eq. 2.135 gives Eq. 2.136

$$I_{n3}(1-\cos 2B)\cos 2\Omega - I_{n3}\sin 2\Omega \sin 2B \quad I_{n1}(1-\cos 2B)\cos 2\Omega$$
$$+ I_{n1}\sin 2\Omega \sin 2B = - I_{n1}\cos 2\Omega + I_{n2}\cos 2\Omega$$
$$+ I_{n1}\cos \Omega \cos 2B \quad I_{n1}\sin 2\Omega \sin 2B - I_{n2}\cos 2\Omega \cos 2B$$
$$+ I_{n2}\sin 2\Omega \sin 2B \tag{2.136}$$

Solving Eq. 2.136 for Ω yields Eq. 2.137

$$\Omega(x,y)_{approx} = \frac{1}{2}\tan^{-1}\left[\frac{(1-\cos 2B)(I_{n3}-I_{n2})}{(\sin 2B)(-2I_{n1}+I_{n2}+I_{n3})}\right] \tag{2.137}$$

If the three intensities I_{n1}, I_{n2}, I_{n3} corresponding to three time-average EOH images with different phasor bias are substituted into Eq. 2.137 the result gives the approximate solution of the fringe locus function. Recall that the cosine function is merely an approximation used to solve for the argument of the Bessel function and though the two functions are similar they are not exact. Thus, Eq. 2.137 is only an approximate solution for Ω_t where Ω_t can be expressed as

$$\Omega_t = \Omega_{t\,approx} + \varepsilon \tag{2.138}$$

where ε is the difference between the true Bessel function solution and the approximated cosine solution. Figure 2.8 is the plot of $J_0^2(\Omega_t)$ solution versus the cosine solution, where the x-axis is the optical phase (fringe locus function) and the y-axis is the normalized fringe intensity [4]. Here it can be seen that the cosine function and the Bessel function do not match up exactly, which illustrates Eq. 2.137 is only the approximate solution. It should be noted that as the magnitude of the optical phase increases, the Bessel function and the cosine function more closely match up. It is for this reason that the squared Bessel function can be approximated by the cosine function squared.

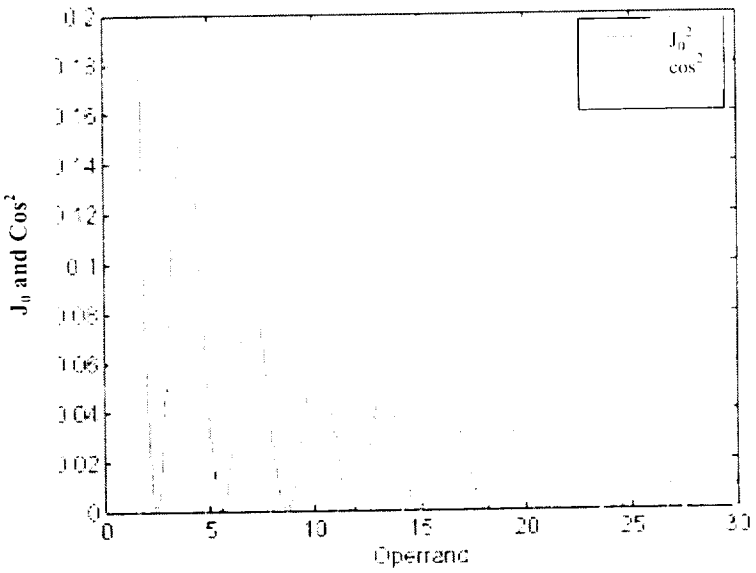

Figure 2.8: Bessel function vs. Cosine Function.

To correct for the error, ε, a Bessel function look up table is created. The look up table is a table of the approximate cosine solution versus the exact Bessel function solution and is stored as a two dimensional array in computer memory [4]. The purpose of the table is to save computational time while the computer is processing the displacement data. Rather than spend the time computing the equations for each displacement condition, the computer will simply compute the approximate solution and then reference a preexisting table to find the exact solution.

After computing Ω_{approx}, the holographic image may look something like Fig. 2.9. This image is known as a wrapped phase map, where the greyscale represent relative optical phase. The greyscale levels in this image have been scaled such that a greyscale level of 0 (black) represents an optical phase of (0*π), whereas a greyscale level of 255 (white) represents an optical phase of (2*π). Thus the abrupt, discontinuous transitions

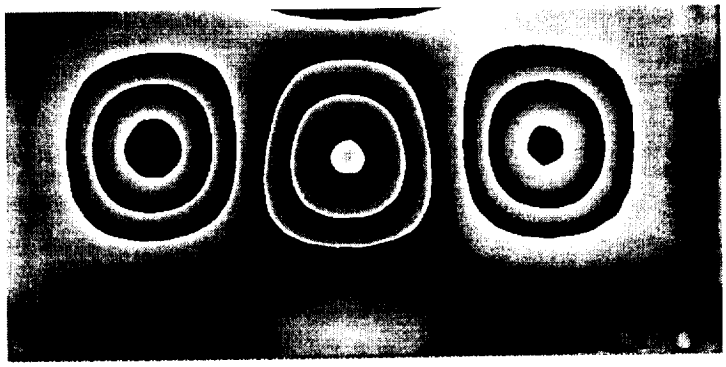

Figure 2.9: EOH wrapped phase map [4].

from black to white denote the occurrence of an EOH fringe, or additional multiple of 2π optical phase. Naturally the object surface does not have sharp discontinuities as implied by the wrapped phase map. The 0 to 2π (black to white) phase jumps are merely an artifact of the inverse tangent function used to compute the phase. To compute the final vibration amplitude map, the wrapped phase map must be "unwrapped" to remove the 2π discontinuities. Phase unwrapping is often the most difficult part of EOH data processing, and there are numerous phase unwrapping algorithms in the literature ranging in scope of applicability and complexity. Conceptually, unwrapping is done by scanning a row of pixels across the image and adding up all of the 2π changes [4]. The 2π changes will be positive or negative depending on whether the change on the wrapped phase map has gone from black to white or white to black. For example, if a single row of pixels is extracted from the center of Fig. 2.9 the line plot of Fig. 2.10 would be produced [4]. Here, each black peak represents a phase change of 2π. These changes are added or subtracted together to produce the unwrapped phase map (the red line). Finally, by dividing the unwrapped phase by the wave number, $k = 2\pi/\lambda$, and the sensitivity vector K of equation 2.37, the displacement is found.

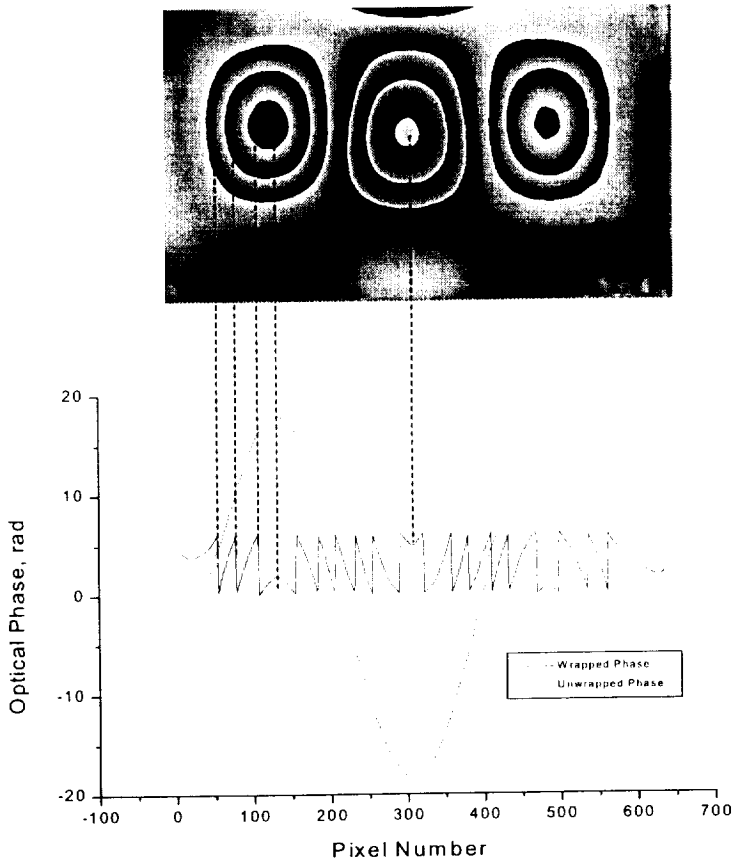

Figure 2.10: Unwrapped phase map with corresponding wrapped phase map [4]

CHAPTER 3.0

FRINGE CONTROL

Electro-Optic Holography (EOH) is laser-based, diagnostic technique used to measure micron-sized displacements of static and/or dynamically loaded structures. Dynamically loaded structures are of greatest interest for this research project, where the displacement of the structure is great enough to cause the interferogram to become densely compacted with interference fringes. When the fringe density exceeds the ability of the software to clearly identify individual fringes the upper measurement limit of the technique is compromised. By modulating the current source of the laser diode, the number of fringes can be reduced as a function of the modulation order. This also changes the intensity distribution as to that of higher order Bessel functions. Thus, by increasing the order, the sensitivity of the EOH system is decreased allowing for larger displacement measurements to be made. The reduction of fringes is theoretically unlimited but physically limited by the frequency bandwidth of the signal generator. This EOH fringe control method is known as Frequency Translated Electro-Optic Holography (FTEOH).

This chapter focuses on the techniques and development for FTEOH. Section 3.2 introduces FTEOH, where section 3.3 derives the theory behind the technique. Section

3.4 presents the methodology for estimating fringe density, which is followed by section 3.5, which explains the FTEOH fundamentals.

3.1 NOMENCLATURE

A_o	Amplitude of the object beam, the laser beam directed onto the test object.
A_n	Amplitude of sideband components.
A_r	Amplitude of the reference beam, the laser beam directed into the CCD camera.
A_υ	Amplitude of frequency shift.
c	Speed of light in a vacuum.
CCD	Charged Couple Device camera.
d	Temporary Variable, whose quantity is equal to $\left[e_o^2\upsilon^2 + \Delta L^2 \Delta \upsilon_n^2 - 2e_o \upsilon \Delta L \Delta \upsilon_n \cos(\Omega - \phi_\upsilon)\right]^{1/2}$.
e	General Amplitude of displacement.
E_o	The time dependent displacement of a point on a vibrating object.
e_o	Amplitude of the test object during cyclic vibration.
EOH	Electro-Optic Holography.
E_r	The time dependent displacement of the PZT.
e_r	Amplitude of the PZT during vibration.
F	Object frequency in Hertz.
f	Frequency in radians.
F_o	The object light field, the beam of light that illuminates the test object.
F_r	The reference light field, the beam of light that is directed into the CCD camera.
F_υ	The light field reflected off of the vibrating structure.

FTEOH	Frequency Translated Electro-Optic Holography.
g_o	A geometrical factor with $g_o = 2$ for displacements perpendicular to the object surface and with normal incidence.
g_r	A geometrical factor with $g_o = 2$ for displacements perpendicular to the object surface and with normal incidence.
I	The light intensity of the laser beam.
J_n	n^{th} order Bessel function of the first kind.
K	Sensitivity Vector, the vectorial difference between the propagation vectors.
k	The wave number whose magnitude is given by $2\pi/\lambda$.
L_o	Optical path length for the object leg.
L_r	Optical path length for the reference leg.
ΔL	Optical path difference between the object and reference legs $\lvert L_o - L_r \rvert$.
MF	Number of fringes masked by modulation.
M_T	Characteristic function.
n	Integer value used to increase the frequency of modulation.
n_c	Index of refraction of the cladding material for the fiber optic cable.
n_o	Index of refraction of the core material for the fiber optic cable.
P	Proportionality constant.
p	Integer value used to increase the frequency of modulation.
RF	Remaining number of fringes after modulation.
T	Exposure time of the CCD camera.
t	Time in seconds.
TF	Total number of fringes without modulation.
X	Temporary variable whose value is equal to $e_o \upsilon \sin(\omega t + \Omega)$.

Y	Temporary variable whose value is equal to $\Delta\upsilon L_o \sin(\omega t + \phi_\upsilon)$.
Z	Temporary variable whose value is equal to $\Delta\upsilon L_r \sin(\omega t + \phi_\upsilon)$.
$\Delta\upsilon$	Frequency shift of laser diode.
δ	Dirac delta function.
ϕ_o	Optical phase of the object beam.
ϕ_r	Optical phase of the reference beam.
ϕ_υ	Unknown Phase, induced by modulation.
η	Fringe multiplication factor.
λ	The wavelength of the laser light used for interference.
θ_m	The max angle beyond which rays that enter the fiber are no longer confined within the fiber.
θ'_m	The critical angle beyond which rays will be bounded within the fiber.
Ω_{approx}	The approximate omega solution, made by approximating the Bessel function as a cosine function.
$\Omega(t)$	The fringe locus function.
Ω_d	Distance from origin to the maximum of the first peak of the J_n^2 curve.
Ω_{step}	The step function for intensity jumps, which is equal to 2π radians.
Ω_t	The exact fringe locust solution.
Ω_{unwrap}	The approximated omega with the addition of the step function.
$\Omega_{unwrapFT}$	The unwrapped omega for the FTEOH technique.
ω	Angular frequency in radians of the test object.
ω_c	Laser diode emission frequency, rad/s.
υ	Laser diode emission frequency, Hz.

3.2 INTRODUCTION TO FTEOH

The image of Fig. 3.1 illustrates a typical dynamic EOH fringe pattern, whereas the image of Fig. 3.2 illustrates how laser diode current modulation has reduced the number of fringes. The objective of this thesis is to develop a fringe control method that will allow the user to represent the displacement field of Fig. 3.1 with a fringe pattern like that shown in Fig. 3.2.

Techniques to perform this type of fringe control have been developed for holography. For example, Aleksoff [5] presented a conventional film based holographic method that involved modulation of the reference beam using a mirror mounted on a PZT stack as means of controlling fringe characteristics. The mirror was forced at harmonics of the object vibration causing the frequency of the reference beam to be modulated. He stated that by modulating the reference wave any number of fringes corresponding to smaller displacements could be eliminated, thereby alleviating the holographic image of high fringe density. Although this type of fringe control has been applied to conventional holographic interferometry, fringe reduction has not yet been established for the EOH technique.

The ideas of laser modulation presented by Aleksoff have been expanded upon in this thesis study and applied to the EOH technique. This new technique for obtaining large amplitude displacements has been given the name Frequency Translated Electro-Optic Holography (FTEOH). For the sake of definition it is best that the term fringe reduction be understood as it is applied to FTEOH. By masking the group of fringes that represent areas on the test structure undergoing the small amplitude displacement (i.e.

those fringes nearest the zero order fringe) the image can be phase unwrapped and the displacement can be realized. However, the displacement that each fringe represents can no longer be approximated as $\frac{\lambda}{2}$ but now must be approximated as $\eta\frac{\lambda}{2}$ where η is a fringe multiplication factor and is related to the order or the harmonic of frequency modulation of the laser diode current source.

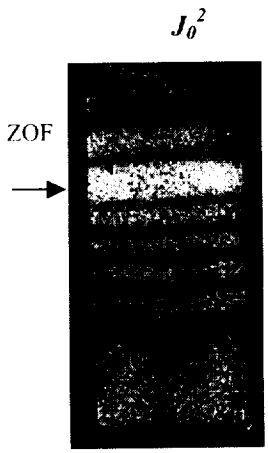

Figure 3.1: Typical dynamic EOH image of a cantilever beam.

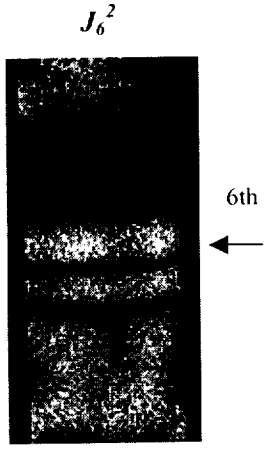

Figure 3.2: The desired result of modulation. The density of the fringes from Fig. 3.1 have been reduced.

Prior to the development of FTEOH many researchers [19, 28-30] used a technique in which the location of the zero order fringe was manipulated as means for determining large amplitude displacements. This method, known as phase mapping, is a relatively new technique which involves laser diode wavelength modulation as a means to determine the vibration amplitude of large displacements. Phase mapping heterodynes an external sinusoidal signal with the laser diode current source to produce a new current signal that in turn modulates the original laser beam and hence the phase of both the reference and object beams. Adjusting the amplitude and phase of an external signal controls the order of desired modulation. As a result, the location of the first bright fringe

is shifted from the nodal position to those points that vibrate at the same amplitude and phase as the reference beam [16, 19, 25-27]. By adjusting the phase and the amplitude of the external modulating signal the zero order fringe is shifted across the EOH image making it possible to map the vibrational amplitudes that may otherwise be too great to be observed in the unmodulated case [25].

One of the big problems with the phase masking technique is that the zero order fringe must be driven to various positions on the object and more or less qualitatively reconstruct the vibrational amplitudes. Thus phase mapping, at least where image processing is concerned, is a non-automated process. This can be a significant problem in practical testing scenarios. Whereas the FTEOH technique has automated processing capabilities.

From this phase mapping technique a fringe, FTEOH was developed. FTEOH differs from phase mapping by utilizing the frequency variation of the external signal rather than the phase manipulation of the signal. The frequency of the signal is varied to produce an image with fewer fringes. These images have an intensity distribution related to higher order Bessel functions, which produces images where the fringes related to areas on the structure undergoing small displacement are masked as a result of modulation.

The verification of the FTEOH theory allows the useful range of the EOH system to be extended well beyond former limitations, thereby making it possible to generate displacement data for amplitudes previously too great to be measured by the EOH system but too small to be measured through other conventional methods. Therefore, the theory

and practice of the FTEOH technique closes the gap between established structural displacement analysis and EOH.

3.3 FTEOH THEORY

The underlying theory of the FTEOH technique is presented in this section. The focus of the presentation is on the effects generated by modulating the current to the laser diode. In this thesis, the term "modulation" refers to modulating the current, which results in a corresponding modulation in the laser emission frequency. Physically, the laser diode current is modulated using a function generator connected to the laser diode current source.

3.3.1 FTEOH REFERENCE AND OBJECT BEAMS

In FTEOH the laser output is split into two beams, the reference beam and the object beam. The object beam illuminates the test structure. Light scattered from the vibrating test structure for the unmodulated case can be expressed as shown in Eq. 3.1

$$F_v(x,y) = A_o \exp[i\phi_o(x,y,t)]. \tag{3.1}$$

In Eq. 3.1, the light of the reflected beam is spatially varying depending greatly on where on the test structure the light is reflected. A_o is the amplitude of the reflected light and ϕ_o is the phase [16]. The phase of the object beam is given as Eq. 3.2

$$\phi_o(x,y,t) = \frac{2\pi g_o E_o(x,y,t)}{\lambda}, \tag{3.2}$$

$2\pi/\lambda = k$ is called the wave number, g_o is a geometrical factor with $g_o = 2$ for displacements perpendicular to the object surface with normal incidence[16]. E_o is the

time dependent displacement of the point of interest on the vibrating test object and is expressed as Eq. 3.3

$$E_o(x,y,t) = e_o \sin(\omega t + \Omega(t)) \tag{3.3}$$

where e_o is the amplitude of vibration of the object, ω is the angular frequency of the object, and $\Omega(t)$ the phase. The object beam can now be expressed as Eq. 3.4

$$F_o(x,y) = A_o \exp\left[i\frac{4\pi}{\lambda} e_o \sin(\omega t + \Omega(t)) \right]. \tag{3.4}$$

The same evaluation can be given for the reference beam as shown by the following equations. Eq. 3.5 represents the unmodulated reference beam

$$F_r(x,y) = A_r \exp(i\phi_r(x,y,t)) \tag{3.5}$$

where A_r and ϕ_r are the amplitude and phase of the reference light respectively.

The reference phase is then expressed as Eq. 3.6

$$\phi_r(x,y,t) = \frac{2\pi g_r E_r(x,y,t)}{\lambda} \tag{3.6}$$

where E_r is the time dependent amplitude of laser diode current modulation and is given by Eq. 3. 7

$$E_r(x,y,t) = e_r \sin(\omega t + \phi_r(x,y,t). \tag{3.7}$$

The variables e_r and ϕ_r are the maximum amplitude and phase of the laser diode current modulation for the reference beam [25]. The reference beam can now be expressed as Eq. 3.8

$$F_r = A_r \exp\left[i\frac{4\pi}{\lambda} e_r \sin(\omega t + \phi_r) \right], \tag{3.8}$$

where the argument (x, y, t) has been dropped for simplification. Eqs. 3.4 and 3.8 can be given as the Fourier expansion (frequency spectrum) [5, 30] as shown by Eqs. 3.9 and 3.10

$$F_o(f) = \sum_{n=-\infty}^{\infty}\left[J_n(\frac{4\pi}{\lambda}e_o)\right]\exp(in\Omega)\delta(f-nF), \tag{3.9}$$

$$F_r(f) = \sum_{n=-\infty}^{\infty}\left[J_n(\frac{4\pi}{\lambda}e_r)\right]\exp(in\phi_r)\delta(f-nF) \tag{3.10}$$

where (f) indicates that the light beam equations are given in terms of the frequency domain [5], $\omega = 2\pi F$, F is the object frequency in hertz and $J_n(\frac{4\pi}{\lambda}e_o)$ is the n^{th} order Bessel function of the first kind with modulation depth $(\frac{4\pi}{\lambda}e_o)$. It should be noted that the Bessel function appears in the Fourier expansion of the object and reference beam equations.

3.3.2 THEORY OF MODULATION EFFECTS

The major point of interest in laser diode current modulation, as far as FTEOH is concerned, is that both the reference and object beams are modulated, which forces Eqs. 3.4 and 3.7 to be expressed as Eqs. 3.11 and 3.12 [25, 26].

$$F_o = A_o\exp\left[i\frac{4\pi}{c}\{e_o\upsilon\sin(\omega t+\Omega(t))+\Delta\upsilon L_o\sin(n\omega t+\phi_o)\}\right] \tag{3.11}$$

and

$$F_r = A_r\exp\left[i\frac{4\pi}{c}\Delta\upsilon L_r\sin(n\omega t+\phi_o)\right] \tag{3.12}$$

In Eqs. 3.11 and 3.12 the wavelength of light is defined as $\frac{\upsilon}{c} = \frac{1}{\lambda}$ from Eqs. 3.9 and 3.10. L_o and L_r are the optical path lengths for the object and reference beams, respectively. The constant $\Delta\upsilon$ is the amplitude of the frequency shift induced by modulation, and ϕ_υ is the unknown phase caused by reflection off of the vibrating test structure [25].

The intensity of the resulting modulated fringe pattern is determined by adding the reflected scatted light of Eq. 3.11 and the reference light of Eq. 3.12, and then multiplying by the complex conjugate as shown in Eq. 3.13, where * denotes complex conjugate.

$$I = (F_o + F_r)(F_o + F_r)^* \tag{3.13}$$

Expanding Eq. 3.13 the intensity becomes Eq. 3.14

$$I = \left\{ A_o \exp\left(i\left[\frac{4\pi}{c}\left(e_o \upsilon \sin(\omega t + \Omega) + \Delta\upsilon L_o \sin(n\omega t + \phi_\upsilon)\right)\right]\right) + A_r \exp\left(i\left[\frac{4\pi}{c}\Delta\upsilon L_r \sin(n\omega t + \phi_\upsilon)\right]\right)\right\}$$

$$\bullet \left\{ A_o \exp\left(-i\left[\frac{4\pi}{c}\left(e_o \upsilon \sin(\omega t + \Omega) + \Delta\upsilon L_o \sin(n\omega t + \phi_\upsilon)\right)\right]\right),\right.$$

$$\left. + A_r \exp\left(-i\left[\frac{4\pi}{c}\left(\Delta\upsilon L_r \sin(n\omega t + \phi_\upsilon)\right)\right]\right)\right) \tag{3.14}$$

which can be rewritten as Eq. 3.15

$$I = \left\{ A_o \left[\exp i\frac{4\pi}{c} X \right]\left[\exp i\frac{4\pi}{c} Y \right] + A_r \left[\exp i\frac{4\pi}{c} Z \right]\right\}$$

$$\bullet \left\{ A_o \left[\exp -i\frac{4\pi}{c} Y \right]\left[\exp i\frac{4\pi}{c} Z \right] + A_r \left[\exp -i\frac{4\pi}{c} Z \right]\right\} \tag{3.16}$$

where

$$X = e_o \upsilon \sin(\omega t + \Omega), \tag{3.17}$$

$$Y = \Delta v L_o \sin(n\omega t + \phi_v) \tag{3.18}$$

and

$$Z = \Delta v L_r \sin(n\omega t + \phi_v). \tag{3.19}$$

The expansion of Eq. 3.15 yields Eq. 3.20

$$I = A_o^2 + A_r^2 + A_o A_r \left[\exp i\frac{4\pi}{c}X\right]\left[\exp i\frac{4\pi}{c}Y\right]\left[\exp -i\frac{4\pi}{c}Z\right]$$

$$+ A_o A_r \left[\exp i\frac{4\pi}{c}X\right]\left[\exp -i\frac{4\pi}{c}Y\right]\left[\exp i\frac{4\pi}{c}Z\right]. \tag{3.20}$$

Substituting Eqs. 3.17 - 3.19 into the third and fourth terms of Eq. 3.20 is given as Eq. 3.21

$$I = A_o^2 + A_r^2 + A_o A_r \exp i\left[\frac{4\pi}{c}(e_o v \sin(\omega t + \Omega) + \Delta v(L_o - L_r)\sin(n\omega t + \phi_v))\right]$$

$$+ A_o A_r \exp i\left[\frac{4\pi}{c}(e_o v \sin(\omega t + \Omega) + \Delta v(L_r - L_o)\sin(n\omega t + \phi_v))\right]. \tag{3.21}$$

Since the CCD camera is a photon integrating device, the camera will only record the average light intensity during the camera exposure time. As a result, Eq. 3.21 must be integrated over time in order to obtain the correct intensity relation.

$$\frac{1}{T}\int_0^T I dt = A_o^2 + A_r^2 + \frac{1}{T}F_r \int_0^T F_v^* dt + \frac{1}{T}F_r^* \int_0^T F_v dt \tag{3.22}$$

The final term of Eq. 3.22 is of primary importance. It governs the intensity characteristics of the FTEOH interference pattern and is expressed as Eq. 3.23.

$$\frac{1}{T}F_r^* \int_0^T F_v dt$$

$$= \frac{1}{T}\int_0^T A_o A_r \exp i\left\{\frac{4\pi}{c}[e_o v \sin(\omega t + \Omega) + \Delta v(L_r - L_o)\sin(n\omega t + \varphi_v)]\right\} \tag{3.23}$$

Let the path length difference between the object leg and the reference leg be given as $\Delta L = |L_o - L_r|$. The intensity for the image can be expressed as Eq. 3.24

$$I = |M_T|^2 = \left| \frac{1}{T} \int_0^T \exp i \left\{ \frac{4\pi}{c} [e_o \upsilon \sin(\omega t + \Omega) + \Delta \upsilon \Delta L \sin(n\omega t + \varphi_o)] \right\} \right|^2 \tag{3.24}$$

where $M_T = J_n(\Omega_l)$ is the characteristic function that denotes the interference of the two fields as a result of sinusoidal motion [3]. Using the trigonmeteric identities of Eqs. 3.25 and 3.26

$$\sin(x + y) = \sin x \cos y + \cos x \sin y \tag{3.25}$$

$$\cos(x - y) = \cos x \cos y + \sin x \sin y \tag{3.26}$$

let

$$d^2 = e_o^2 \upsilon^2 + \Delta \upsilon^2 \Delta L^2 - e_o \upsilon \Delta \upsilon \Delta L \cos(\Omega - \varphi_o), \tag{3.27}$$

where d^2 is the square of exponential term of Eq. 3.24 (excluding $\frac{4\pi}{c}$), as shown in equation 3.28

$$d^2 = [e_o \upsilon \sin(\omega t + \Omega) + \Delta \upsilon \Delta L \sin(n\omega t + \varphi_o)]^2 . \tag{3.28}$$

The characteristic equation can now be rewritten as Eq. 3.29

$$M_T = \frac{1}{T} \int_0^T \exp i(-n\omega t) \exp i \left(\frac{4\pi}{c} d \right) dt . \tag{3.29}$$

Using the Bessel function identity of Eq. 3.30

$$\exp i(d \sin \omega t) = \sum_{m=-\infty}^{\infty} J_m(d) \exp i(m\omega t) \tag{3.30}$$

the characteristic equation can be written in terms of the Bessel function as shown in Eq. 3.31

$$M_T = \sum_{m=-\infty}^{\infty} \exp i(-n\omega t) J_m\left(\frac{4\pi}{c} d\right) \exp i(im\omega t). \tag{3.31}$$

The expansion of Eq. 3.31 yields Eq. 3.32

$$M_I = \sum_{m=-\infty}^{\infty} J_m \left\{ \frac{4\pi}{c} \left[e_o^2 \upsilon^2 + \Delta\upsilon^2 \Delta L^2 - 2e_o \upsilon \Delta\upsilon \Delta L \cos(\Omega - \varphi_\upsilon) \right]^{\frac{1}{2}} \right\} \cdot$$

$$\frac{1}{T} \int_0^T \exp[i(m-n)\omega t] dt. \tag{3.32}$$

The final expression of Eq. 3.32 will be equal to zero for all cases except when $m = n$, that is to say that the final term of Eq. 3.32 behaves as the Dirac delta function as shown in Eq. 3.33

$$\frac{1}{T} \int_0^T \exp[i(m-n)\omega t] dt = \delta(m-n). \tag{3.33}$$

Thus, Eq. 3.33 only exists when the modulating frequency and the structural frequency of the test object match. The intensity distribution of Eq. 3.24 can now be expressed as Eq. 3.34

$$I = |M_T|^2 = J_m^2\left(\frac{4\pi}{c} d\right) \tag{3.34}$$

Increasing the frequency of the modulating signal by harmonics of the test structure frequency changes the intensity distribution of the time average interference pattern. The intensity pattern is no longer governed by the square of the zero order Bessel function. Instead the pattern is governed by the n^{th} order Bessel function whose initial maximum occurs for increasing arguments of the Bessel function as shown in the Fig. 3.3.

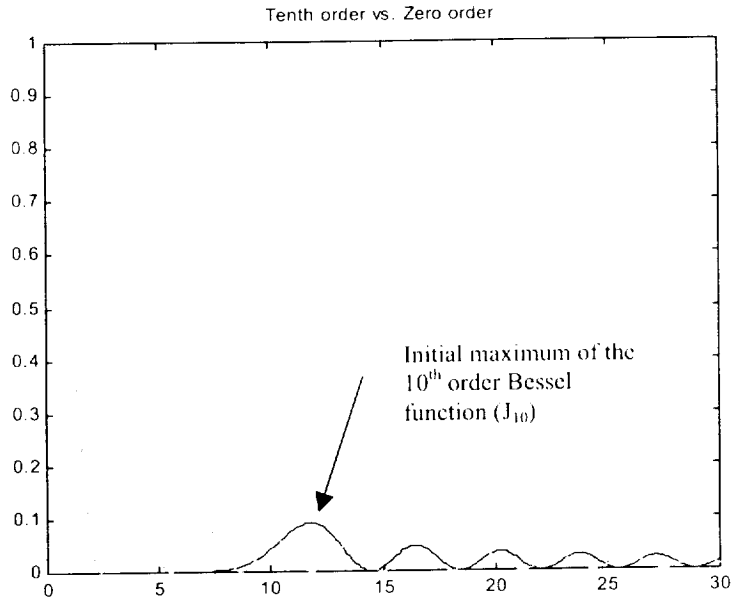

Figure 3.3: The initial maximum of the 10^{th} order Bessel function occurs at a larger argument with respect to the initial maximum of the zero order Bessel

3.3.3 Bessel Functions and the Intensity Distribution

An EOH phase map is essentially a contour or mode shape map of the deflections incurred by the object during excitation. Thus each fringe represents a positive or negative out-of-plane displacement. The large, bright fringe about the periphery of the mode shape of Fig. 3.4 is known as the zero order fringe and is analogous to the term node or nodal point, which is a location of zero displacement on a vibrating object. When the laser diode current source is modulated at a sufficiently high order, the zero order fringe is eliminated from the image. This is also true of all sufficiently small amplitude fringes.

Laser diode current modulation acts as a displacement filter that filters out or masks those fringes that represent the areas on the test structure experiencing low

amplitude displacements. In Fig. 3.5, page 72, all three illustrations represent the same cantilever beam experiencing the same sinusoidal vibration. Figure 3.5 (a) is the interference pattern produced by conventional EOH techniques, i.e. no fringe masking. Figure 3.5 (b) is an exaggerated side view of the cantilever beam in oscillation, and Fig. 3.5 (c) is an image of the interference pattern produced by modulating the current to the laser diode. The dotted horizontal line that crosses through Fig. 3.5 locates the zero order fringe, the nodal position for the mode of oscillation. Notice that the number of fringes has been reduced from the fringe pattern on the right and the zero order fringe has gone black as a result of modulation. Regardless, the displacement field for both interference patterns is the same.

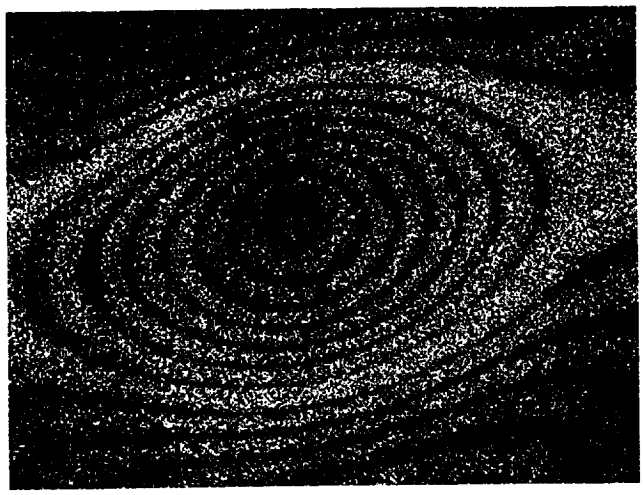

Figure 3.4: No modulation with an excitation amplitude of 2 volts and a total of 7 fringes.

Each successive increase in modulation order forces the initial maximum of the Bessel function to occur at larger and larger operands. Thus, as the order of the frequency modulation is increased it takes a greater object displacement to cause the initial bright fringe to occur. For those displacements that are too small no substantial phase change is seen and the image reports these areas as a dark null that increases with successive modulation order. The fringes that remain within the image are representative of areas experiencing of large amplitude displacement. The first bright, higher order fringe is not a nodal point as it is in the unmodulated case, but an area on the object with a

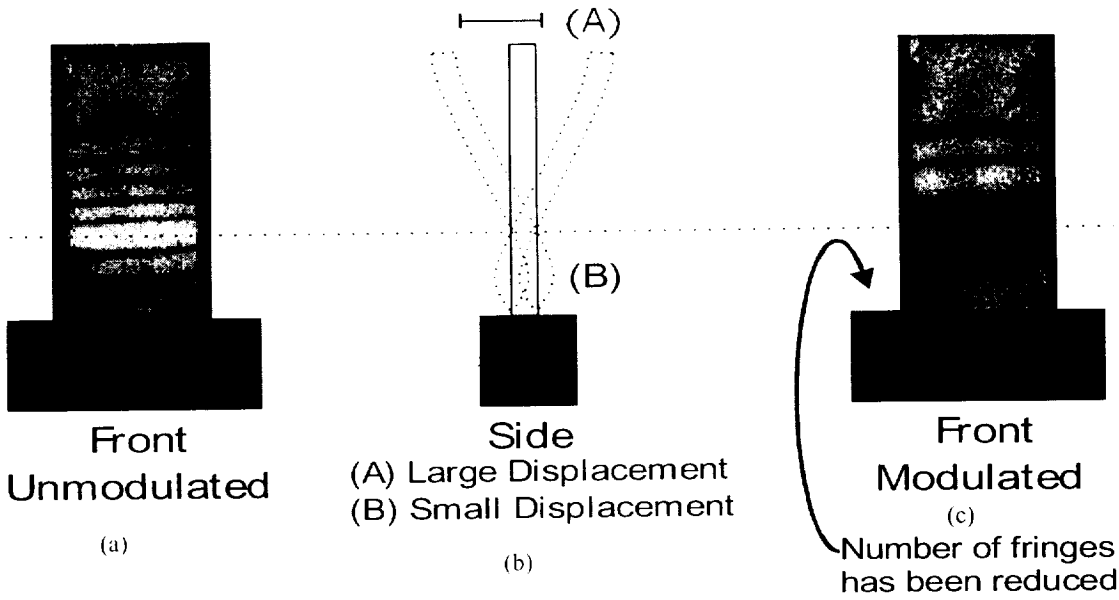

Figure 3.5: Results of using the FTEOH method on a cantilever beam with sinusoidal excitation. The left image is of the unmodulated case while the right is the modulated case. Note the making of the low order fringes for the modulated case.

displacement large enough to cause a significant phase change [25, 26]. This comparison can be seen in Fig. 3.6 and Fig. 3.7 the $J_o^2(\Omega)$ vs. $J_5^2(\Omega)$ and $J_5^2(\Omega)$ plots respectively.

In short, as the modulating frequency order is increased, the intensity distribution changes as a function of the n^{th} order Bessel function where each successive order masks

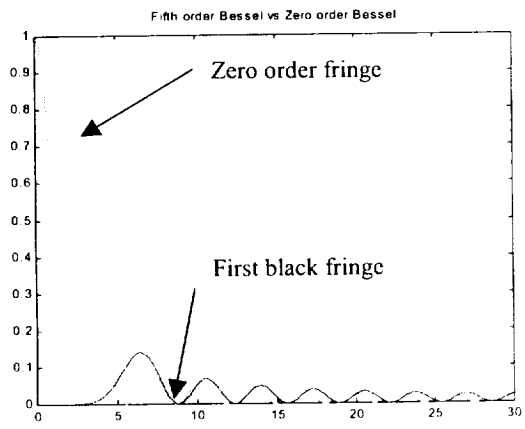

Figure 3.6: J_0 vs. J_5

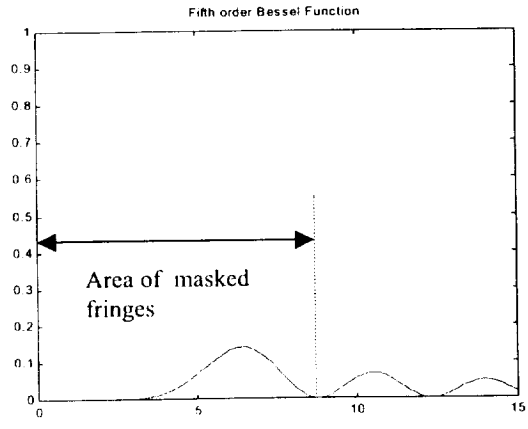

Figure 3.7: Fifth order Bessel function.

the lower order fringes. Larger structural displacements can now be measured where before frequency modulation the fringe density would have been too high to resolve individual fringes. Now with the masking of lower order fringes each remaining fringe is clearer than before modulation, allowing phase unwrapping to be completed. By modulating the laser diode current source the number of fringes that will be unwrapped is fewer than the unmodulated case. Therefore, in order to obtain the correct structural displacement the distance that each fringe would represent would increase with increasing modulation order.

3.3.4 MORE BESSEL FUNCTION EXAMPLES

The following pages are examples of FTEOH and the fringe masking technique. Figure 3.8 illustrates a typical EOH image with it corresponding FTEOH image. Note the number of fringes masked in the FTEOH image and how it correlates directly with the plot of the zero order and fourth order Bessel functions. Figures 3.9-3.11 all show similar fringe reduction.

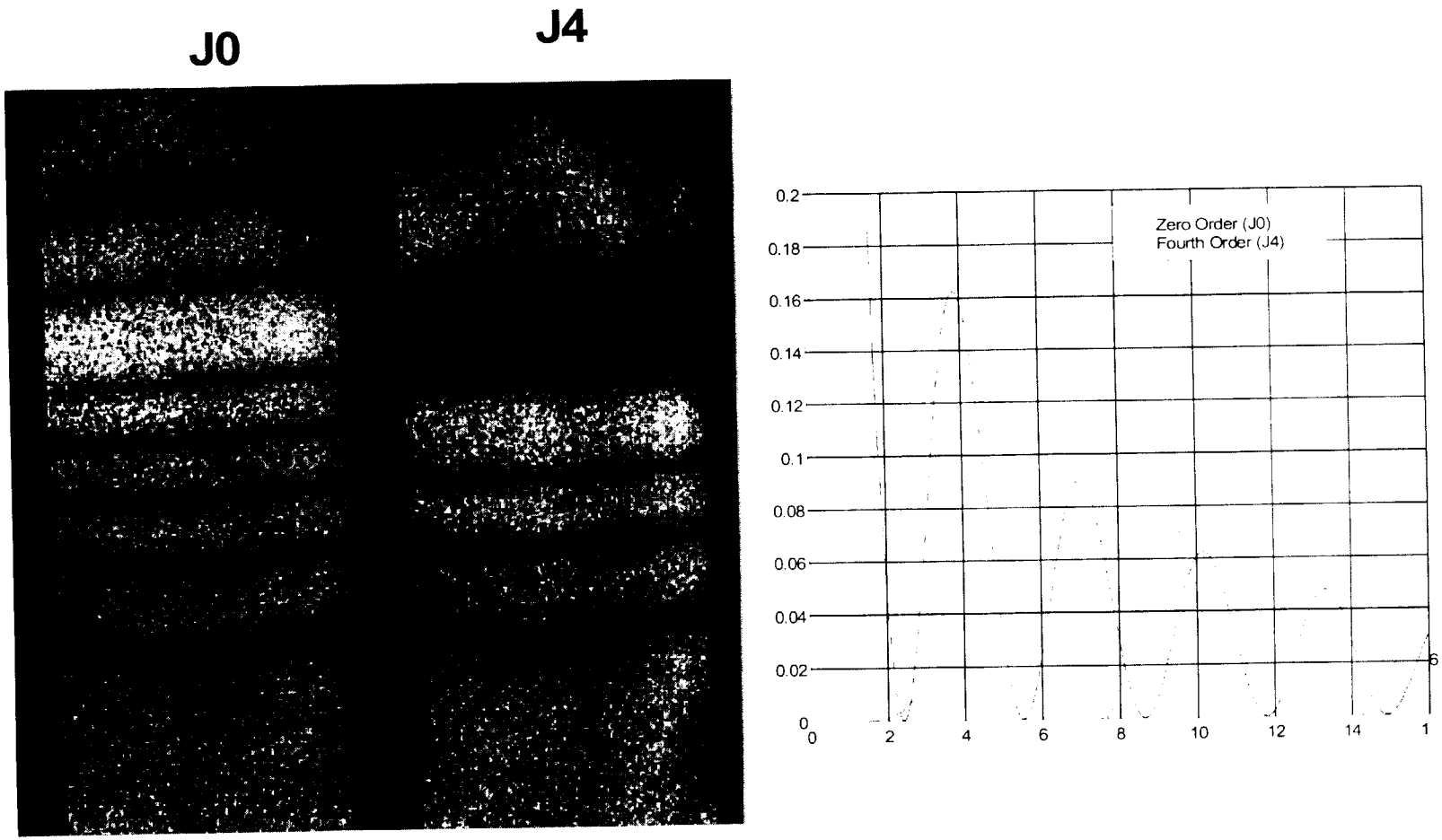

Figure 3.8: EOH image and its corresponding FTEOH image. Here a 4th order modulation was used to mask two fringes from the FTEOH image.

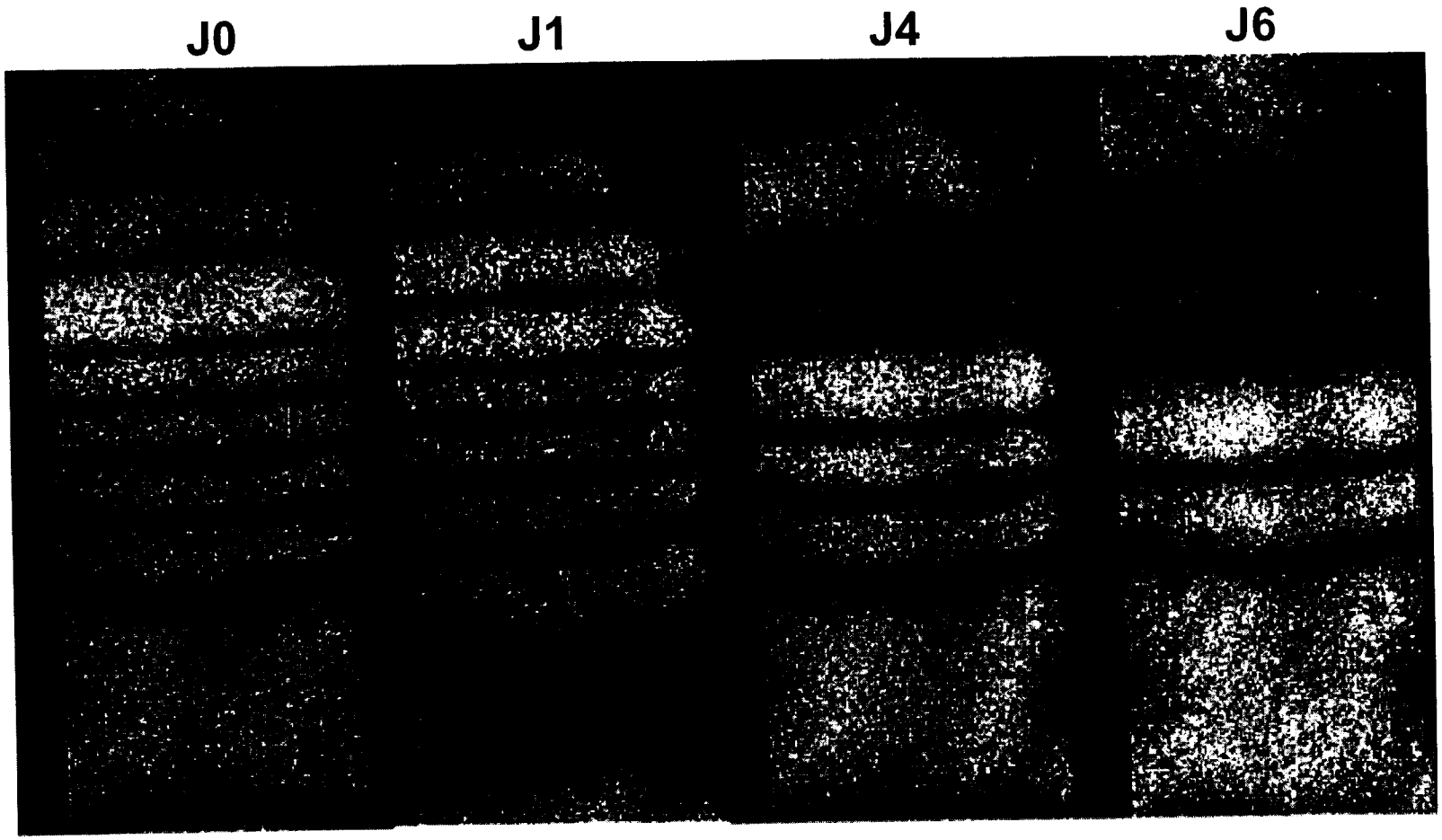

Figure 3.9: Cantilever beam shown as first the EOH image and then with corresponding FTEOH images. It can be seen that by increasing the modulation order the interference fringes are in fact masked by a dark null.

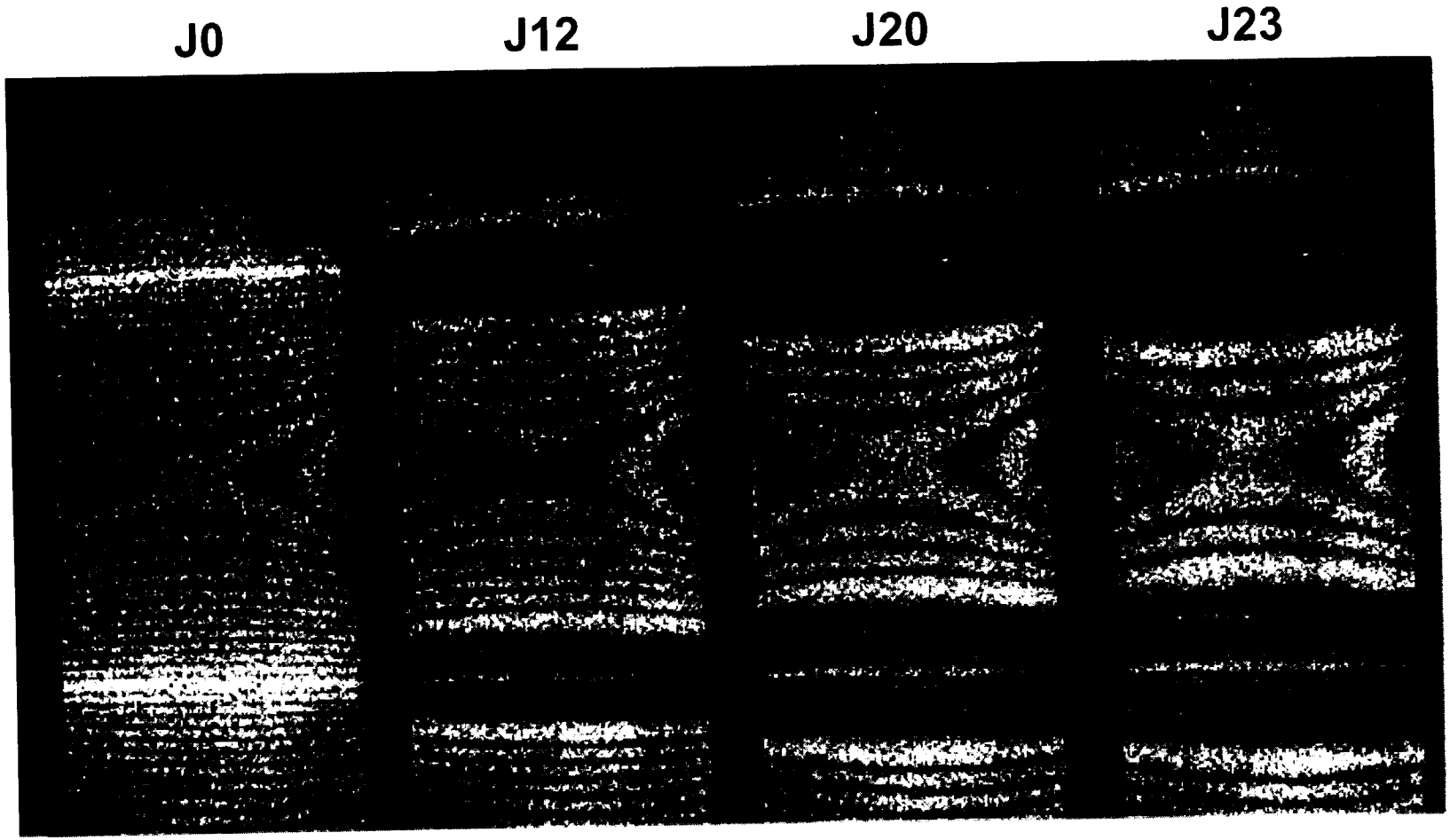

Figure 3.10: More FTEOH images. The images here show a greater number of fringes, yet as the order of modulation is increased the fringes become more resolvable.

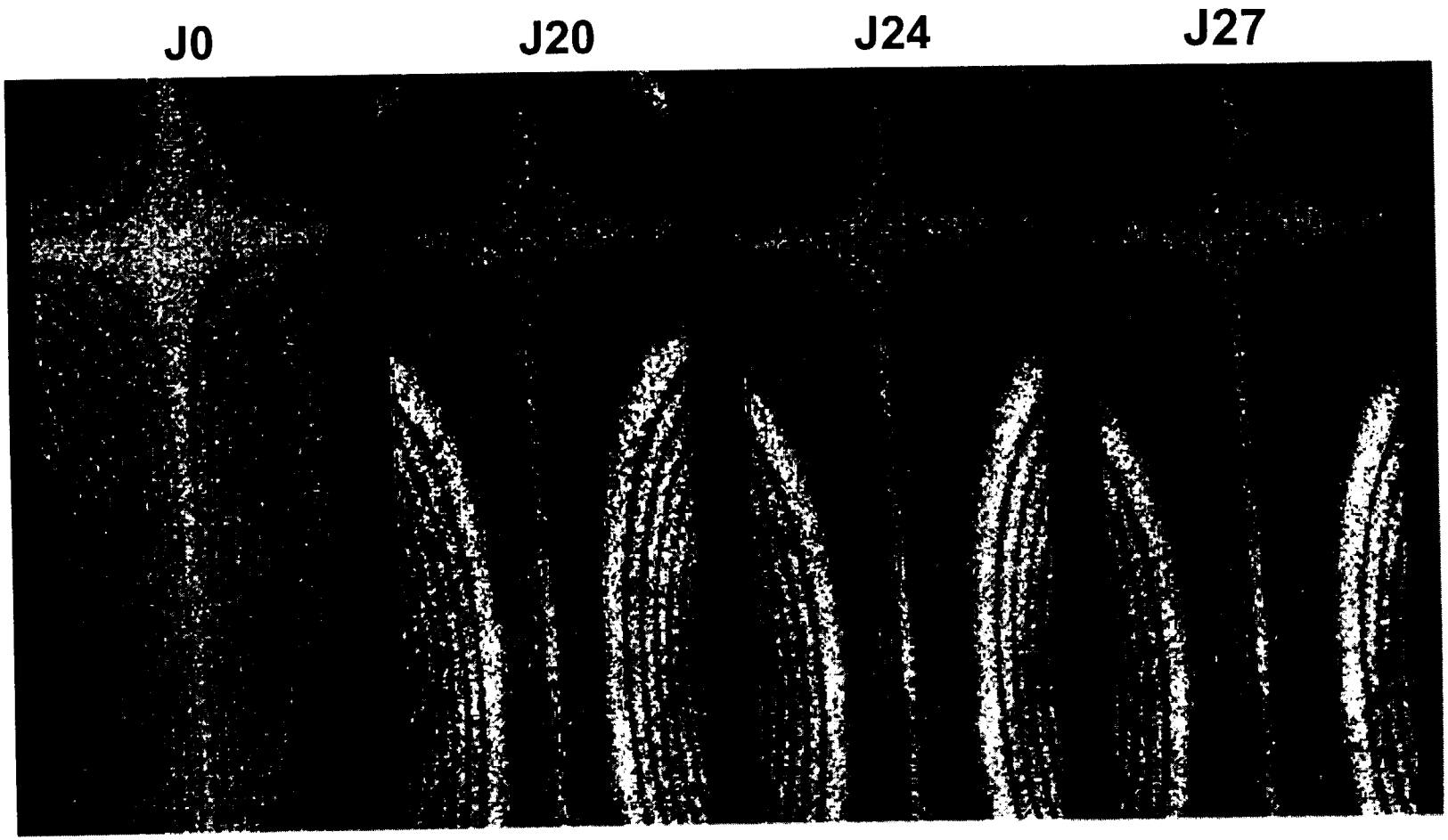

Figure 3.11: A cantilever beam excited at a frequency which has induced a torsion mode. Once again, as the modulation order is increased the interference fringes become more resolvable. Note that the zero order fringe is still visible, this effect may be corrected by controlling the shuttering of the CCD camera.

3.3.5 LOOK-UP TABLES

Equation 3.35 demonstrates how the approximate omega solution can be determined by approximating the Bessel function with a cosine function, derivation shown in Section 2.5.

$$\Omega(x,y)_{approx} = \frac{1}{2}\tan^{-1}\left[\frac{(1-\cos 2B)(I_{n3}-I_{n2})}{(\sin 2B)(2I_{n1}-I_{n2}-I_{n3})}\right] \tag{3.35}$$

If the three intensities I_{n1}, I_{n2}, I_{n3} corresponding to three time-average EOH images with different phasor bias are substituted into Eq. 3.35 the result is the approximate solution of the fringe locus function.

The $\tan^{-1}$ function can take values between π and $-\pi$ and Eq. 3.35 will exist between $\pi/2$ and $-\pi/2$. Thus, the results of Eq. 3.35 will exhibit a discontinuity every time the phase increases or decreases by 2π rad. These discontinuities will be resolved in order to obtain a continuous phase map of the displacement. This process is obtained by adding or subtracting 2π rad (Ω_{step}) every time a discontinuity is encountered. Therefore, when the computer searches the wrapped phase map it searches for those discontinuities in the wrapped phase map that jump from black to white. If a discontinuity is found the step function, Ω_{step}, is added or subtracted to the approximate solution of Eq. 3.35 to obtain the unwrapped solution of Eq. 3.36.

$$\Omega_{unwrap} = \Omega_{approx} \pm \Omega_{step} \tag{3.36}$$

The cosine function is only an approximation of the Bessel function. Thus, Eq. 3.35 is the approximation for the exact solution Ω_t, where Ω_t is expressed as:

$$\Omega_t = \Omega_{unwrap} + \varepsilon \tag{3.37}$$

where ε is the difference between the true Bessel function and the approximated cosine solution. To correct for the error, ε, a Bessel function look up table is created. The look up table is a table of the approximate cosine solution versus the exact Bessel function solution and is stored as a two dimensional array in the computer memory [4]. The exact Bessel function solution is obtained by substituting the phasor bias B (0, $-B$, B) into Eq. 2.116 to obtain Eqs. 3.38 - 3.40.

$$I_z = 16A_o^2A_r^2J_0^2(\Omega_t - 0) \tag{3.38}$$

$$I_p = 16A_o^2A_r^2J_0^2(\Omega_t + B) \tag{3.39}$$

$$I_n = 16A_o^2A_r^2J_0^2(\Omega_t - B) \tag{3.40}$$

where I_z, I_p, and I_n are the images captured with a zero, positive and negative phasor bias at each of the four phase steps of 0°, 90°, 180°, and 270°. Replacing the approximated values of Eq. 3.35 with those of Eqs. 3.37 – 3.40 the unwrapped solution becomes that of Eq. 3.41

$$\Omega_{unwrap} = \frac{1}{2}\tan^{-1}\left[\frac{1-\cos(2B)}{\sin(2B)}\frac{J_0^2(\Omega_t - B) - J_0^2(\Omega_t + B)}{2\cdot J_0^2(\Omega_t) - J_0^2(\Omega_t - B) - J_0^2(\Omega_t + B)}\right]. \tag{3.41}$$

The purpose of the table is to save computational time while the computer is processing the displacement data. Rather than spend the time computing the equations for each displacement condition, the computer will simply compute the approximate solution and then reference a preexisting table to find the exact solution. The resulting plot of a typical correction lookup table (B = $\pi/3$) is shown in Fig. 3.12, on page 81.

3.3.5.1 LOOK-UP TABLE FOR FTEOH

The Bessel function look up table for FTEOH must account for the order of harmonic used to obtain the frequency modulated image. For example, if the fifth order harmonic was used to obtain a masked fringe image, the unwrapped omega, Ω_{unwrap}, of Eq. 3.41 would need to be a function of $J_5^2(\Omega)$. In general the unwrapped omega for the FTEOH technique is given as Eq. 3.42

$$\Omega_{unwrapFT} = \frac{1}{2}\tan^{-1}\left[\frac{1-\cos(2B)}{\sin(2B)}\cdot\frac{J_n^2(\Omega_t - B) - J_n^2(\Omega_t) + B}{2\cdot J_n^2(\Omega_t) - J_n^2(\Omega_t - B) - J_n^2(\Omega_t + B)}\right] \qquad (3.42)$$

The result of plotting the unwrapped omega for the modulated case, Eq. 3.42, versus the exact solution Ω_t, is shown in Fig. 3.13.

The plot of $\Omega_{unwrapFT}$ versus Ω_t will not provide the correct solution because $\Omega_{unwrapFT}$ is approximated using the cosine function, which does not contain any modulated components. Thus, the plot of the newly calculated look up table is shifted down with respect to the original Ω_{unwrap} look up table. A comparison of the two plots is shown in Fig. 3.14 where both the vertical and horizontal axes are in units of π. This downward shift is a result of FTEOH modulation and correlates directly to the area of masked fringes in a raw speckle image. As was discussed throughout chapter 3, the FTEOH image will contain a large dark null where lower order fringes have been masked as a result of modulation. Therefore, when the image is unwrapped the computer will see the masked area as having no intensity change, this corresponds directly to the zero amplitude area between the origin and approximately 6.4 Ω_t in Fig. 3.13, on page 81.

In order to correct the downshift of Fig. 3.13, the curve will need to be shifted up a distance, Ω_d, which is the distance from zero to the maximum of the first initial peak of the $J_n^2(\Omega)$ curve to the origin, as shown in Fig. 3.15. This shift will allow the curve of Fig. 3.13 to nearly imitate the lookup table of Fig. 3.12. By applying the Ω_d shift to the unwrapped omega, Eq. 3.43 will be obtained.

$$\Omega_{unwrapFT} = \Omega_{unwrapFT} + \Omega_d \tag{3.43}$$

Graphically the addition of the shift will nearly overlay the Ω_{unwrap} curve with that of the $\Omega_{unwrapFT}$, as shown in Fig. 3.16. This relation is again shown in Fig. 3.17 for J_0^2 J_5^2, J_{10}^2 and J_{15}^2, where J_0^2 is the typical EOH Ω_{unwrap} look up table curve. Here it can be seen that the addition of Ω_d to $\Omega_{unwrapFT}$ will approximate the $J_0^2(\Omega)$ look up table curve. A list of Ω_d 's are given in Table 3.1.

The solution for the FTEOH unwrapped displacement will not be the exact solution with respect to the EOH unwrapped displacement but will be a close approximation to the actual solution, hence the difference between the Ω_{unwrap} lookup table and the $\Omega_{unwrapFT}$ lookup table.

The last and final step is to obtain the structural displacement for the test structure. Using the equations derived in Chapter 2 the displacement can be determined using Eq. 3.44.

$$L = k\frac{\Omega_t}{K} \tag{3.44}$$

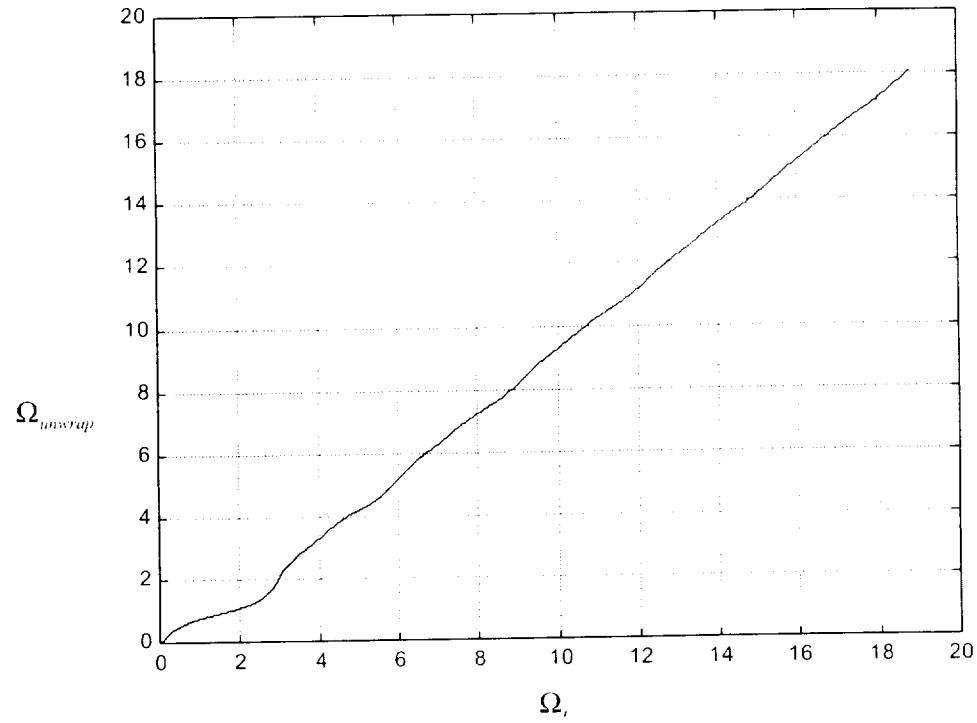

Figure 3.12: The look up table is plotted by graphing the exact fringe locus function vs. the approximate fringe locus function for the zero order Bessel function case. The axes are shown in units of π radians.

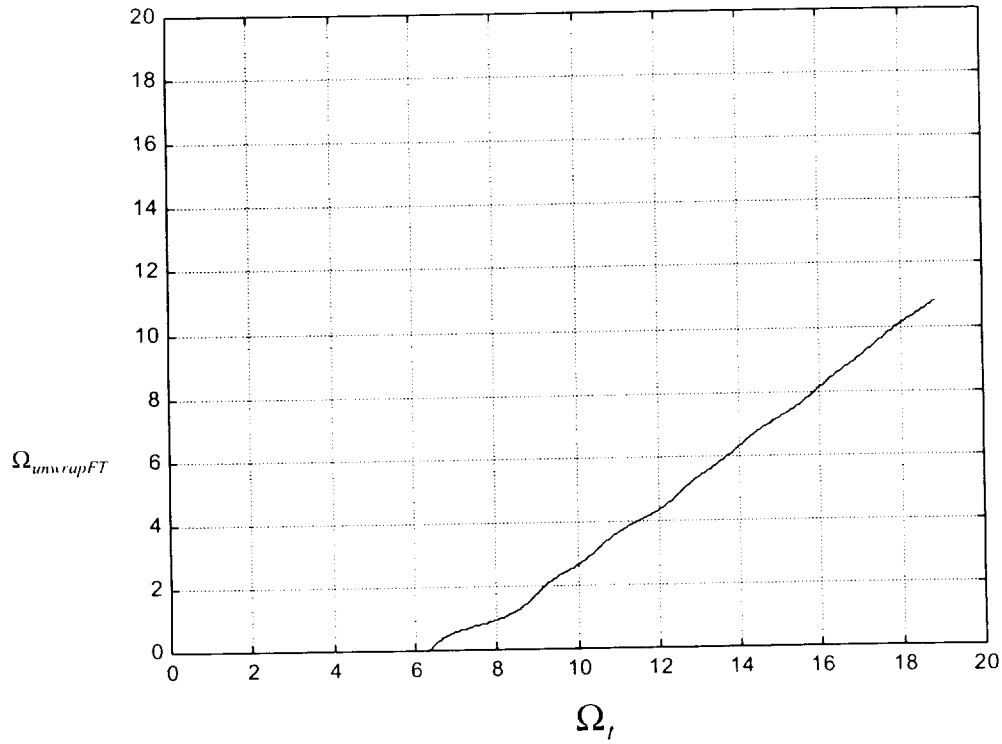

Figure 3.13: Exact fringe locus function vs. the approximate fringe locus function for the fifth order Bessel function case. The axes are shown in units of π radians.

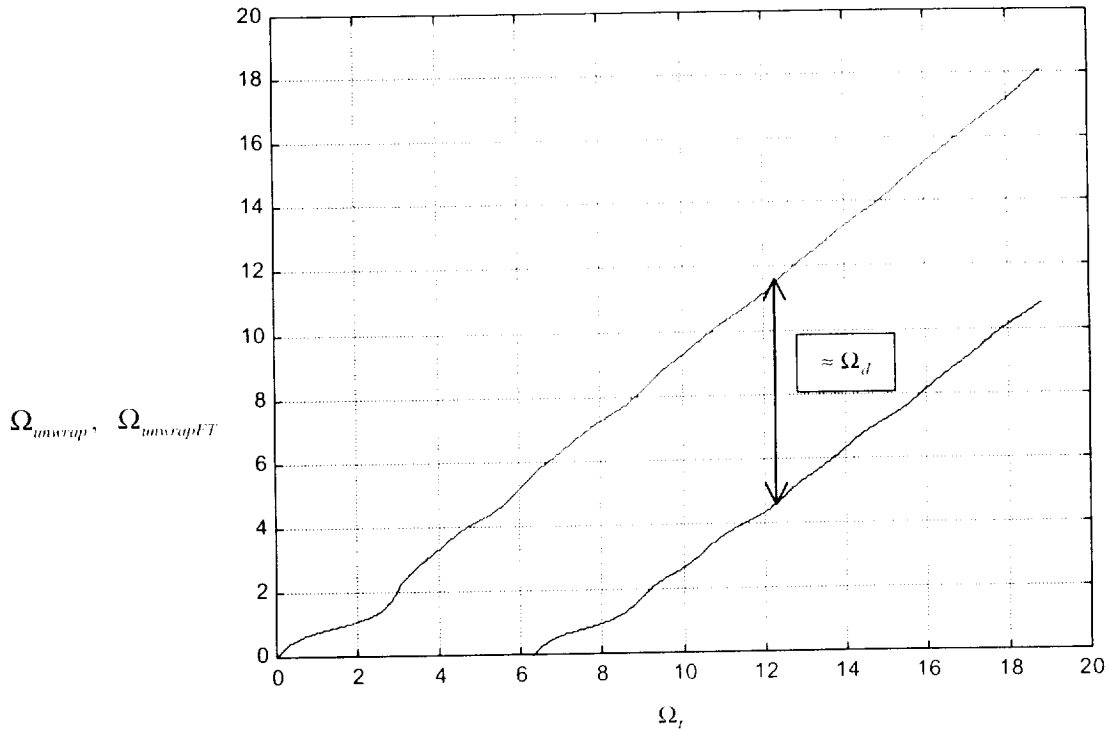

Figure 3.14: The exact fringe locus function vs. the approximate fringe locus function for the zero order and fifth order Bessel function cases, respectively. The axes are shown in units of π radians.

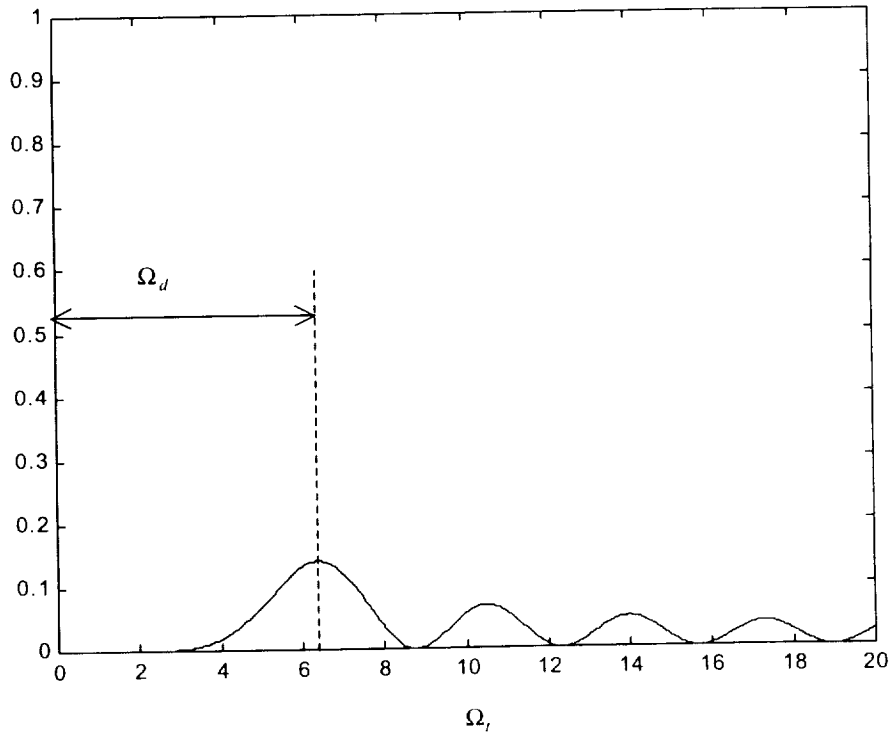

Figure 3.15: Plot of $J_5^2(\Omega_t)$ and Ω_d. The horizontal axis is shown in units of π radians, the vertical is noramlized intensity

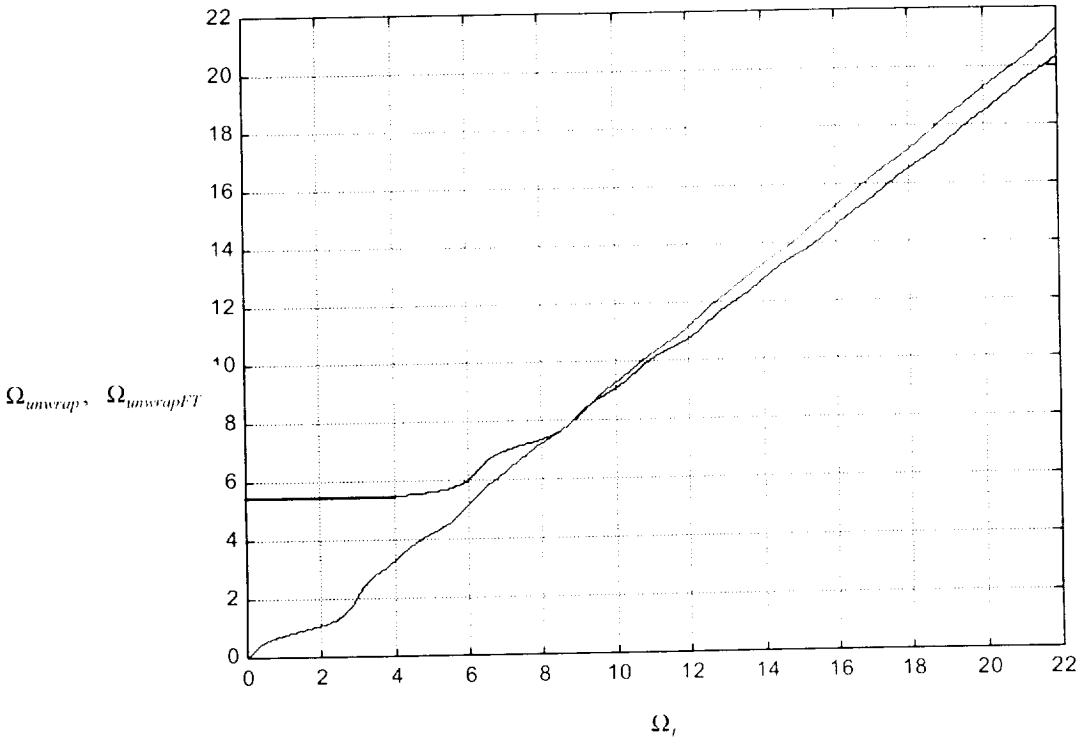

Figure 3.16: The exact fringe locus function vs. the approximate solution for the zero order and fifth order (+ Ω_d) cases. The axes are shown in units of π radians.

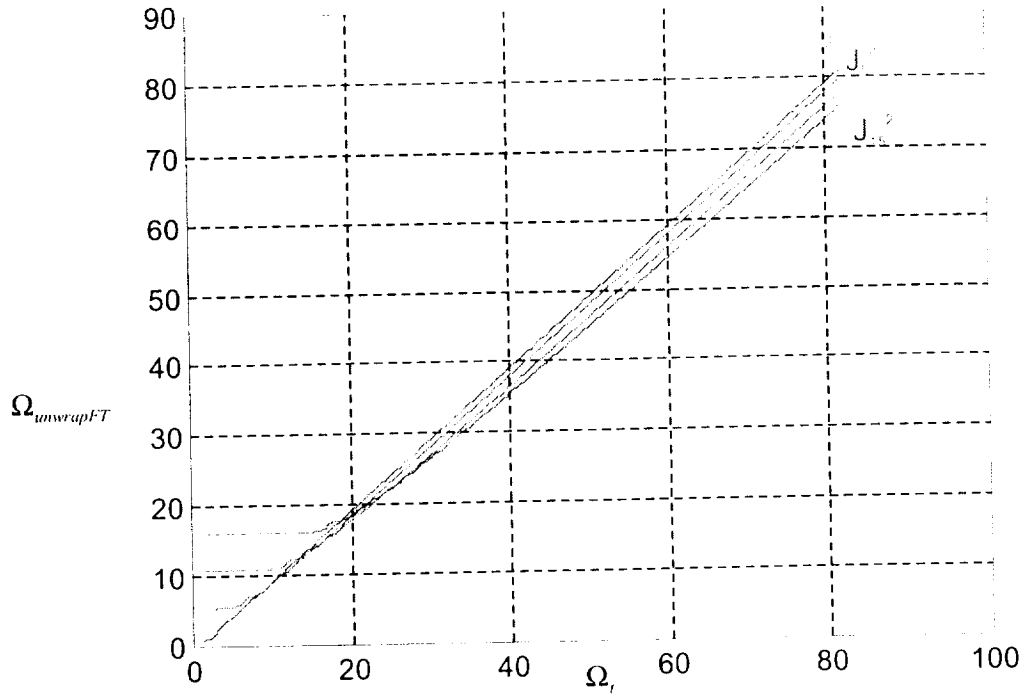

Figure 3.17: The overlay of $J_{15}^2(\Omega)$, $J_{10}^2(\Omega)$, $J_5^2(\Omega)$ and $J_0^2(\Omega)$ look up tables. For this figure $\Omega_{unwrapFT}$ indicates all look up tables where FT varies in value from 0 to 15 in steps of 5. Note that the $J_0^2(\Omega)$ look up table is an approximation for the higher order look up tables. The axes are shown in units of π rads.

Table 3.1: The n^{th} order Bessel function and the location of the maximum of the first initial peak.

n	Locus of maximum	n	Locus of maximum
5	6.42	23	25.32
6	7.50	24	26.36
7	8.58	25	27.38
8	9.65	26	28.41
9	10.72	27	29.45
10	11.77	28	30.48
11	12.825	29	31.51
12	13.88	30	32.54
13	19.43	31	33.57
14	15.98	32	34.59
15	16.96	33	35.62
16	18.06	34	36.64
17	19.09	35	37.67
18	20.15	36	38.70
19	21.18	37	39.71
20	22.215	38	40.74
21	23.25	39	41.77
22	24.28	40	42.79

3.4 ESTIMATING THE FRINGE DENSITY

This section details the method for estimating fringe using the FTEOH technique. This is not a phase unwrapping technique but rather a simple method for quickly estimating the vibration amplitude. The displacement field for the FTEOH interference pattern can be estimated using a simple linear relation that lies within the family of Bessel functions and their relation to fringe masking. The number of fringes masked is a function of the Bessel function order, and as will be shown, not every modulation order will reduce the number of fringes from the FTEOH image. Modulating the laser diode current source at any arbitrary harmonic will introduce a small error to the estimated displacement. Choosing a harmonic in which the first dark fringe of the higher order Bessel function approximately aligns with a dark fringe in the unmodulated or the zero order Bessel function case can help to reduce this error. The alignment can be seen by plotting J_0^2 versus the n^{th} order Bessel function and choosing the function, which gives the best fringe alignment. The number of fringes that will be masked by the modulation order can be determined by counting the number of times to the left of the alignment the $J_o^2(\Omega)$ touches the x-axis. Remember that touching the x-axis by a Bessel function represents a single dark fringe in the interference pattern. For example, in Fig. 3.18 the first dark fringe of the thirteenth order modulation (J_{13}^2) aligns with the 6th dark fringe of the unmodulated case (J_0^2). Here it can be seen that 5 complete fringes will be removed and the 6th fringe of the J_0^2 case aligns with the 1st dark fringe of the J_{13}^2 case. Choosing the 13th harmonic as the modulation order guarantees that no more, or no less than 5

fringes will be removed from the image. This particular alignment procedure can be found at every third harmonic starting at the 5th harmonic (i.e., 5, 8, 10, 13, 16, 19, . . .).

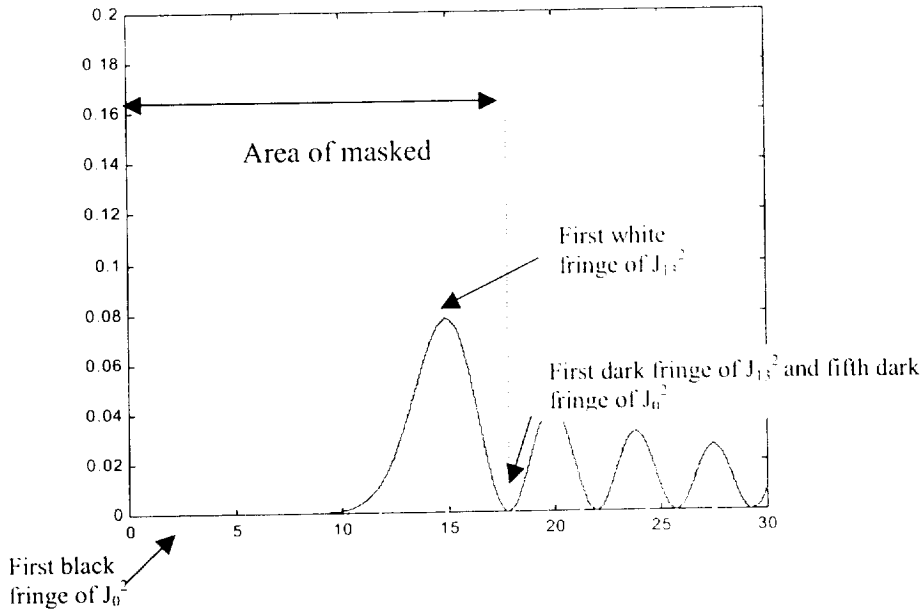

Figure 3.18: J_{13}^2 vs. J_0^2. The 1st dark fringe of J_{13}^2 is the 5th dark fringe of J_0^2.

3.4.1 THE "EVERY THIRD ORDER" RULE

To show that the "every third order" rule is merely an approximation, the zeros of the n^{th} order Bessel function are listed in Table 3.2 along with the corresponding zeros of the zero order Bessel function. The alignment of the zeros is not exact but is relatively close. By using every third harmonic a simple linear relationship develops between the number of masked fringes and the modulation order as shown in Eq. 3.45

$$MF = \frac{1}{3}n + \frac{2}{3} \tag{3.45}$$

where n is the n^{th} harmonic of the object's frequency and MF is the number of masked fringes masked as a result of modulation. Figures 3.19-3.21 are plots of the zero order

Bessel function versus higher order Bessel functions shown as an example of how Eq. 3.45. In Fig. 3.15 J_{16}^2 is compared to J_0^2, here it can be seen that the alignment of the first dark fringe of J_{16}^2 occurs at the 7th dark fringe of J_0^2 and as predicted by Eq. 3.45 six white to black fringes have been masked.

Table 3.2: J_n Zeros and the corresponding J_0 zeros.

J_n	First zero of J_n (Value of Fringe Locus)	The corresponding zero of J_0	Difference
5	8.77	8.653	0.117
8	12.225	11.791	0.434
10	14.478	14.930	-0.452
13	17.801	18.071	-0.270
16	21.085	21.213	-0.128
19	24.352	24.352	0.000
22	27.570	27.493	0.077
25	30.780	30.635	0.145
28	33.875	33.776	0.099
31	37.156	36.918	0.238
34	40.330	40.058	0.272
37	43.487	43.199	0.288
40	46.645	46.341	0.304

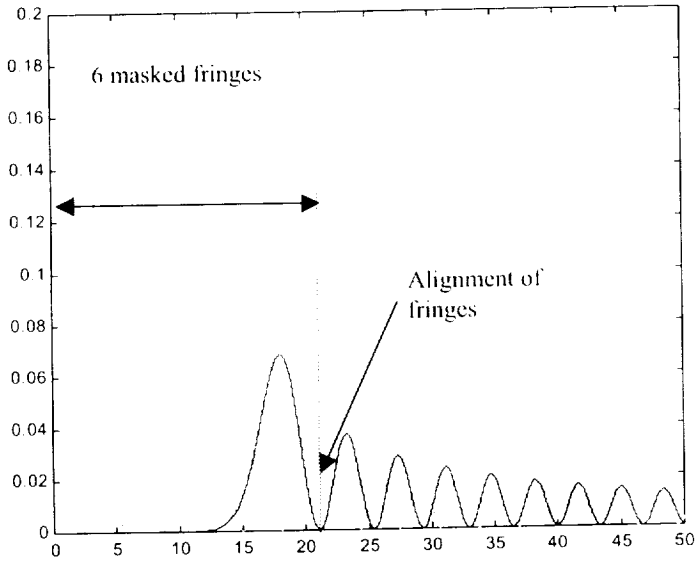

Figure 3.19: J_{16}^2 vs. J_0^2. The 1st dark fringe of J_{16}^2 aligns with the 7th dark fringe of J_0^2.

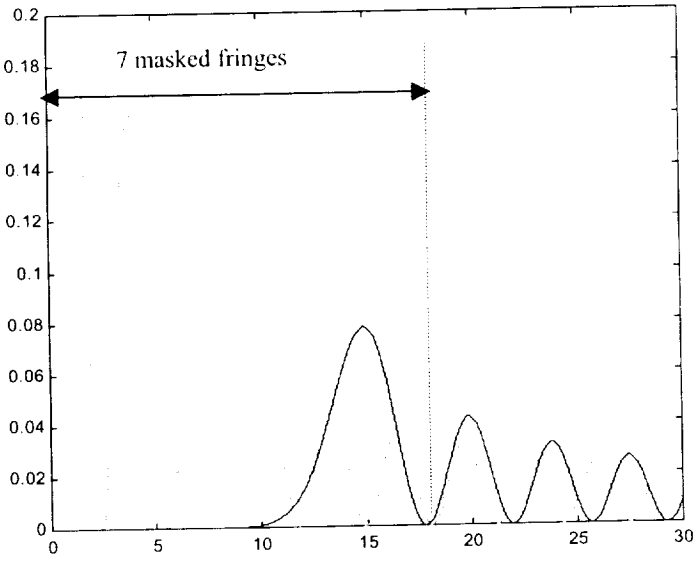

Figure 3.20: J_{19}^2 vs. J_0^2. The 1st dark fringe of J_{19}^2 aligns with the 1st dark fringe of J_0^2.

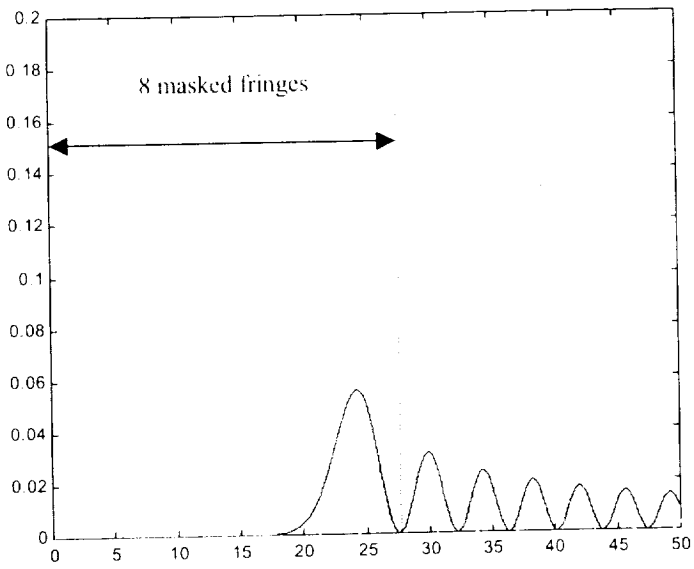

Figure 3.21: J_{22}^2 vs. J_0^2. The 1st dark fringe of J_{22}^2 aligns with the 8th dark fringe of J_0^2.

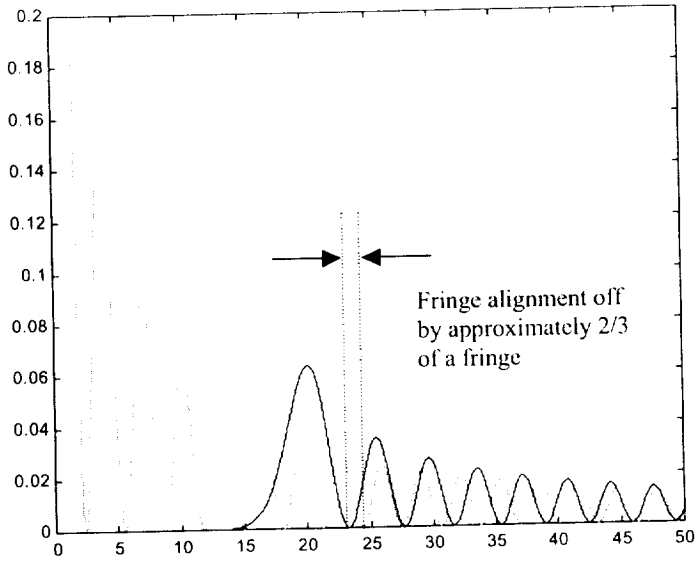

Figure 3.22: J_{18}^2 vs. J_0^2. the 1st dark fringe of J_{18}^2 sits 2/3 of the way between the 6th and the 7th fringe of J_0^2 which introduces error into the unwrapped measurement.

If a non-optimum harmonic is used, like was done in Fig. 3.22, the last masked fringe is not completely covered. Instead, the 1st dark fringe of J_{18}^2 is found to sit two-thirds of the way between two dark fringes of the J_0^2 case. Even though the interference pattern of the FTEOH method will produce a fringe that is slightly masked, the fringe may be incorrectly counted as a whole fringe. If this is the case the estimated vibration amplitude will be erroneously too large. Therefore to eliminate this error it is best to choose one of the optimum harmonics and not have to correct for fractions of fringes when estimating the displacement.

3.4.2 THE "EVERY THIRD ORDER" RULE AND ESTIMATING THE DISPLACEMENT

Although showing how the "every third order" rule works on plots of the Bessel function, it is beneficial, to show how this relation actually corresponds to the pictorial representations of Fig. 3.18 - 3.22. In Fig. 3.19-3.27 the test object was excited at 925 Hz. The images here show successive increase in modulation order starting with no modulation Fig. 3.23 and increasing to the tenth order in Fig. 3.31. The first order of modulation is not represented due to an increase in the sensitivity level [5, 31, 32], which results in an increase in the number of fringes. The second order modulation actually brings the number of fringes

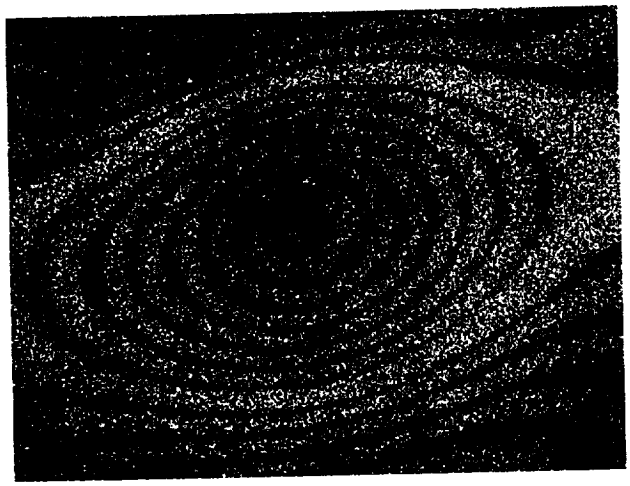

Figure 3.23: No modulation, 7 total fringes.

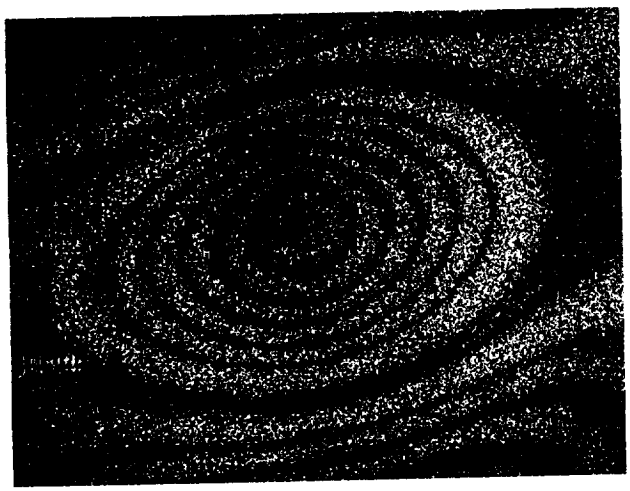

Figure 3.24: 3rd modulation order, 5 remaining fringes.

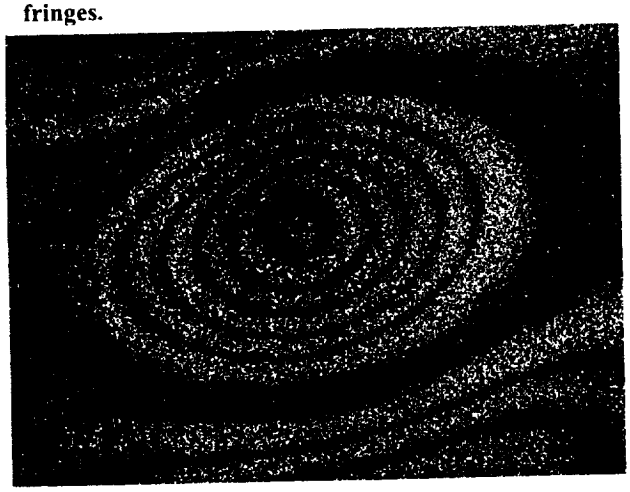

Figure 3.25: 4th modulation order, 5 remaining fringes.

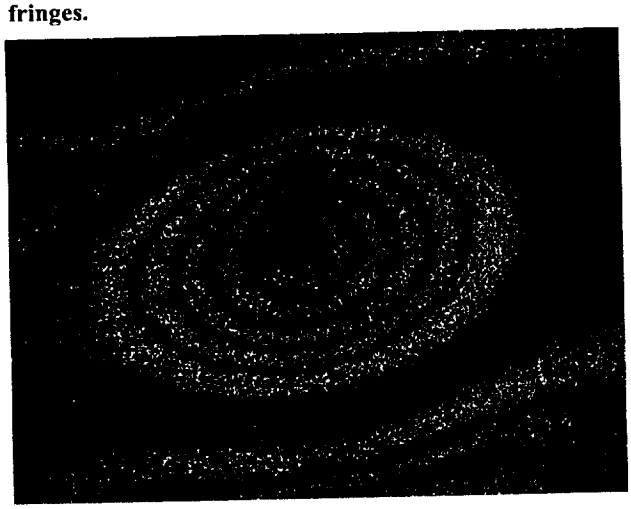

Figure 3.26: 5th modulation order, 5 remaining fringes

back to the original count by masking one fringe, so the first order in which fringes have been noticeably masked does not occur until the third order.

Third order modulation has eliminated two fringes as shown in Fig. 3.24 when compared to the unmodulated image of Fig.3.23. These fringes were masked from the image by means of the third order of modulation, however, two fringes have also been removed from figures 3.25 and 3.26, which use the forth and fifth modulation orders. Nevertheless, the image of Fig. 3.23 should be used for estimating displacement according to the "every third order" rule, which predicts the alignment of fringes. According to the plot of J_5 vs. J_0, the first dark fringe of J_5 aligns with the third dark fringe of J_0, making the fifth modulation order the optimal choice

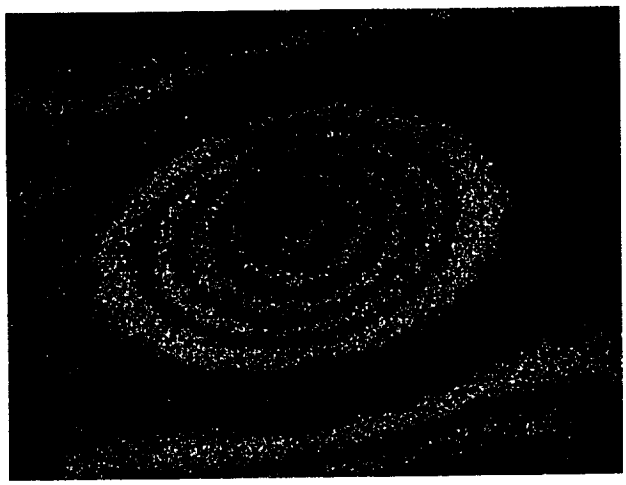

Figure 3.27: 6th modulation order, 4 remaining fringes.

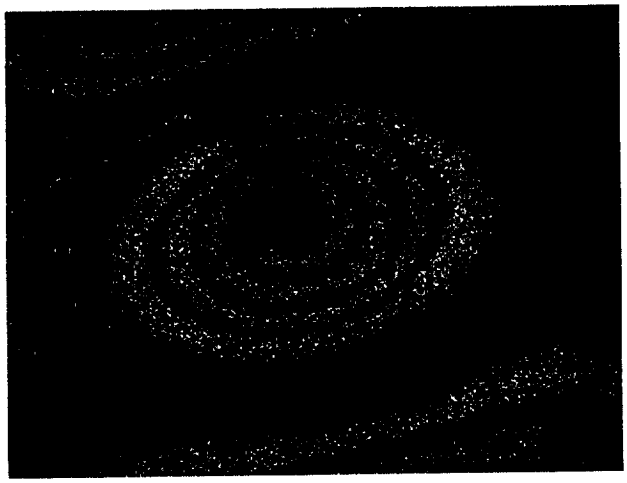

Figure 3.28: 7th modulation order, 4 remaining fringes.

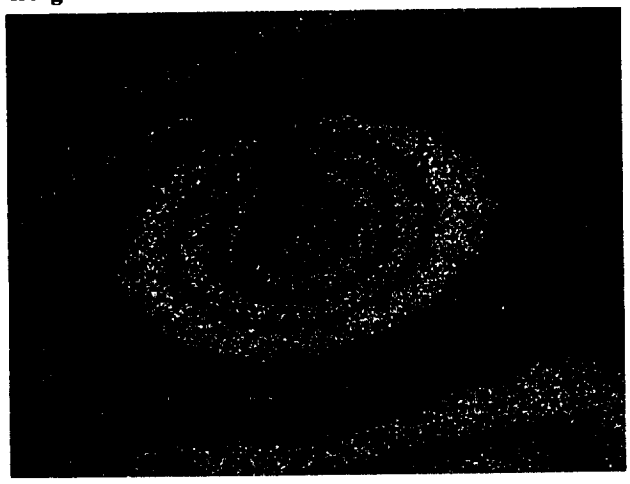

Figure 3.29: 8th modulation order, 3 remaining fringes.

over the third and forth modulation orders. This entire synopsis is repeated for Figs. 3.27-3.31 where the optimal modulation order is shown in Fig. 3.28 and 3.31, which are the eighth and tenth modulation orders respectively. This order will more closely yield the correct displacement.

By using the "every third order" rule the structural displacement of the object can be easily calculated. To determine the estimated displacement, once the proper modulation order has been chosen, the operator will need to count the number of fringes in the FTEOH image denoted to as *RF* (Remaining Fringes). The *RF* number is then be added to the *MF* number of Eq. 3.42 to determine the total fringe count ($TF=MF+RF$) of the unmodulated case. Next, a fringe multiplication factor η, is determined by dividing *RF* into *TF*

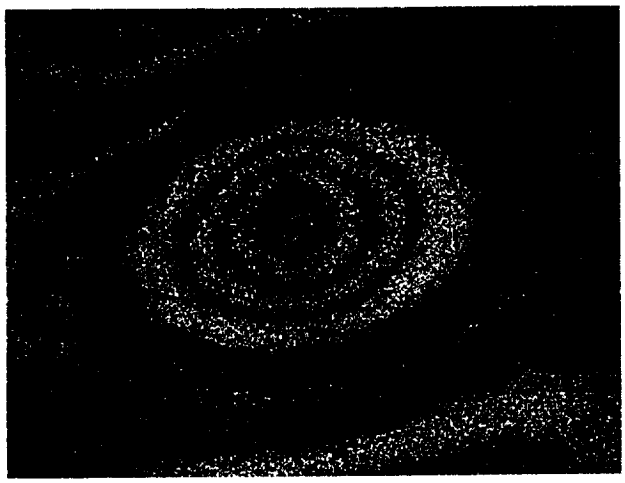

Figure 3.30: 9th modulation order, 3 remaining fringes.

Figure 3.31: 10th modulation order, 3 remaining fringes.

number $\eta = \frac{TF}{RF}$, which is then multiplied by $\frac{\lambda}{2k}$. For the modulated case a single black to white fringe has a displacement greater than one fringe in the unmodulated case. Thus, the multiplication factor η is used to determine the linear displacement the structure for the masked fringe image. For example, if a 13th order modulated image contained 4 fringes (*RF*) the fringe multiplication factor is

$$MF = \frac{1}{3}(13) + \frac{2}{3} = 5 \tag{3.46}$$

$$\eta = \frac{MF + RF}{RF} = \frac{TF}{RF} = \frac{9}{4} = 2.25 \tag{3.47}$$

each fringe now has a displacement value equal to $2.25\left(\frac{\lambda}{2k}\right)$. However, this methodology only works when optimum modulation orders are used, partial fringes are not accounted for in Eqs. 3.46 and 3.47.

3.4.3 THEORY SUMMARY

Modulating the laser diode drive current results in a laser emission frequency modulation proportional to the input signal. Sawtooth variations of the external signal cause the phase relationship of the scattered object light to change and interact differently with respect to the unmodulated case. As a result, the optical intensity of the EOH images change such that each successive frequency variation ($n\omega$) causes the fringe intensity distribution to vary the EOH image as the n^{th} order Bessel function. Graphically speaking, the zero order fringe and all other sequentially lower order fringes from $n = 0, 1, \ldots n\text{-}1$ are essentially masked by the initial null of the n^{th} order Bessel function shown as an example in Fig. 3.32 using J_0^2 and J_{10}^2. According to this plot, the 5th dark fringe that will appear in the unmodulated, J_0^2, image will be the same as the first dark fringe in the modulated, J_{10}^2 image. The first bright fringe seen in the modulated image is not a

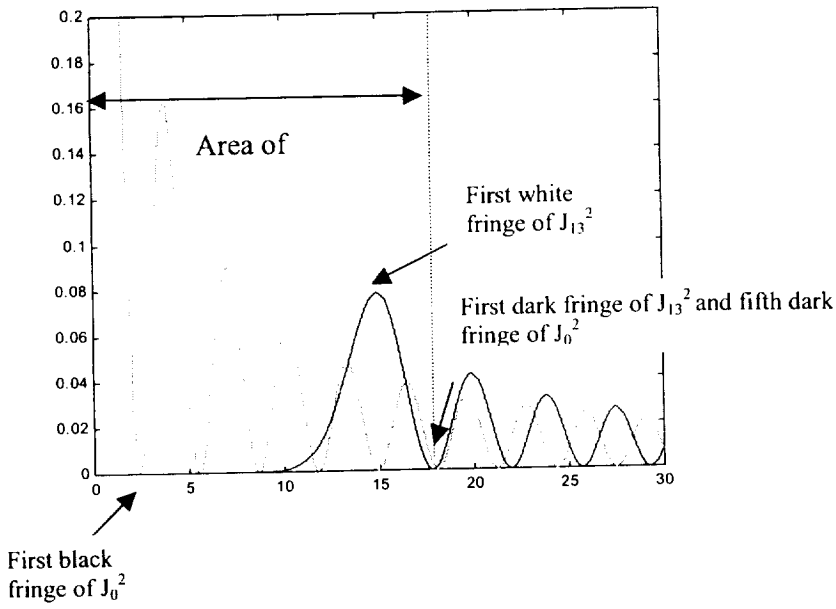

Figure 3.32: J_{13}^2 vs. J_0^2. The 1st dark fringe of J_{13}^2 is the 5th dark fringe of J_0^2.

nodal point but an area on the object with large enough displacement to cause a significant phase change between the object and reference beams to create the n^{th} order bright fringe. This phenomenon is again illustrated in Fig. 3.33 and 3.34 with a J_0^2, unmodulated image and a J_{10}^2, modulated image. Here it can be seen that five fringes have been masked in Fig. 3.34, thereby verifying the higher order Bessel function intensity distribution theory.

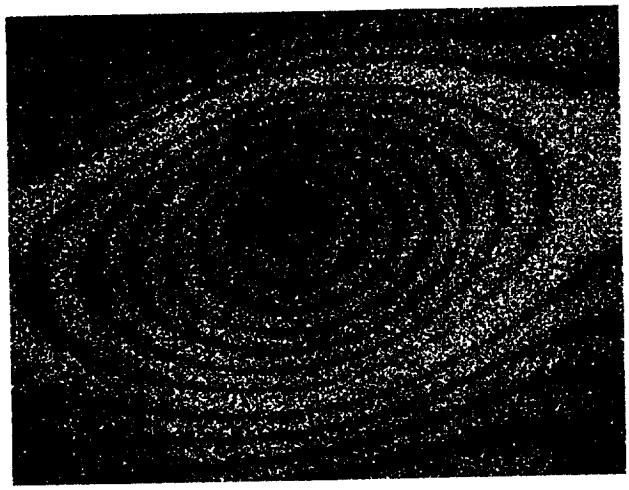

Figure 3.33: No modulation, 7 total fringes.

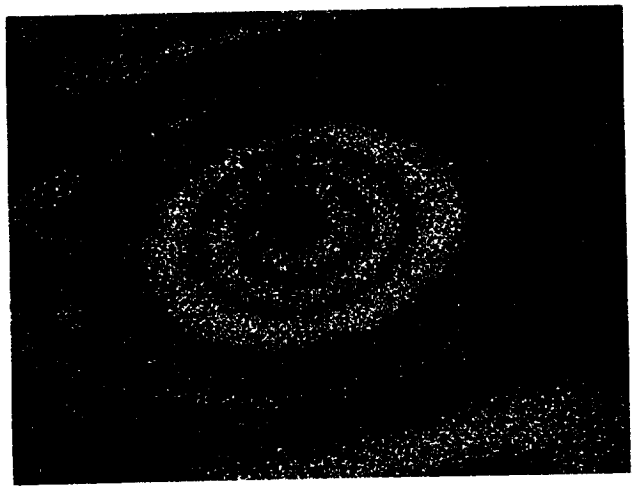

Figure 3.34: 10^{th} modulation order, 3 remaining fringes.

3.5 FUNDAMENTALS OF FTEOH

The goal of this section is to provide insight into how the FTEOH technique works based on signal analysis. This section does this by discussing the object, reference, and interference light beams in terms of their frequency content.

Figure 3.35 is an enlargement of a portion of the FTEOH system. The figure shows a camera lens capturing a portion of the light scattered by the test structure and recombining it with the reference beam through a beam splitter. A CCD camera then captures the combined beam. Figure 3.35 illustrates the frequency content and physical signal processing that occurs in the FTEOH technique. A second order modulation was chosen merely to explain the theory of the FTEOH technique.

It is shown that the light scattered from the object has been spatially modulated by integer harmonics of the vibrating test structure centered about the laser carrier frequency. The analysis uses the fact that a coherent light beam reflected by a vibrating object is temporally and spatially modulated in a way that depends on the type of vibration [11]. This is shown by the a_0, a_1, a_2 and a_3 spectral lines denoted in the object beam plot of Fig. 3.35. The relative amplitudes of these harmonic components are only estimated in the figure and will actually vary. The important point is that independent of the amplitude a component exists at harmonic frequencies.

The reference beam is shown to have a clean second harmonic modulation from the carrier frequency, a single sideband suppressed carrier. This is obtained by using the sawtooth modulation, which is discussed section 3.5.2. Serrodyning (sawtooth modulation) inherently suppresses all harmonics of the current modulation as shown by the reference beam.

The CCD camera integrates the intensity of the recombined object and reference beams to produce the interference beam signal shown in Fig. 3.35. The process of capturing the recombined light using a CCD camera is the same as performing a cross correlation of the two signals. A cross correlation is an operation between two different, yet continuous time energy signals. Upon combination of the two signals a third, unique signal is produced. The correlation between two continuous-time energy signal, such as the reflected object beam and the reference beam, given as $F_v(x,y)$ and $F_r(x,y)$ respectively, will have a cross correlation given by Eq. 3.48 [33]

$$r_{F_v,F_r}(\tau) = \int_{-\infty}^{\infty} F_v(t)F_r(t-\tau)dt\,. \tag{3.48}$$

The term $(t-\tau)$ is the time convolution of the reference beam, however the same result can be obtained if the convolution of the reflected object beam were taken instead [33].

Figure 3.35 illustrates that the diode laser current was modulated at twice the test object frequency; this is seen by the large single spike at the J_2 position in the reference beam spectral profile. In the cross correlation process the J_2 component of the reference beam combines with the a_2 component of the object beam. Because of the cross correlation effect, the CCD camera sees the correlated portions of the signals as a constant. Since the second harmonic was the correlated part of the two beams the resulting interference pattern will have a fringe pattern governed by the square of the second order Bessel function. An additional feature of the CCD camera that can be applied is shuttering. This is an area that requires more research but the idea is that shuttering can be used to apply a sinc filter (sinc = $\frac{\sin \pi T}{\pi T}$, where T is the exposure period) about the zero frequency component, which in turn suppresses the sidebands of

the zero frequency signal content even further. It should be noted that in Figs. 3.8-3.11 and all of the FTEOH images, that the original zero order fringe is still present. It is expected that by reducing the shuttering speed, which in turn would decrease the width of the sinc function, the presence of the zero order fringe in FTEOH images could be reduced. The mathematics for the shuttering effect of Fig. 3.35 is discussed below, where the time averaged intensity of the captured image over the period of exposure is given by Eq. 3.49 [5].

$$I = \frac{1}{T}\int_0^T F_r^*(t)F(t)_v dt \tag{3.49}$$

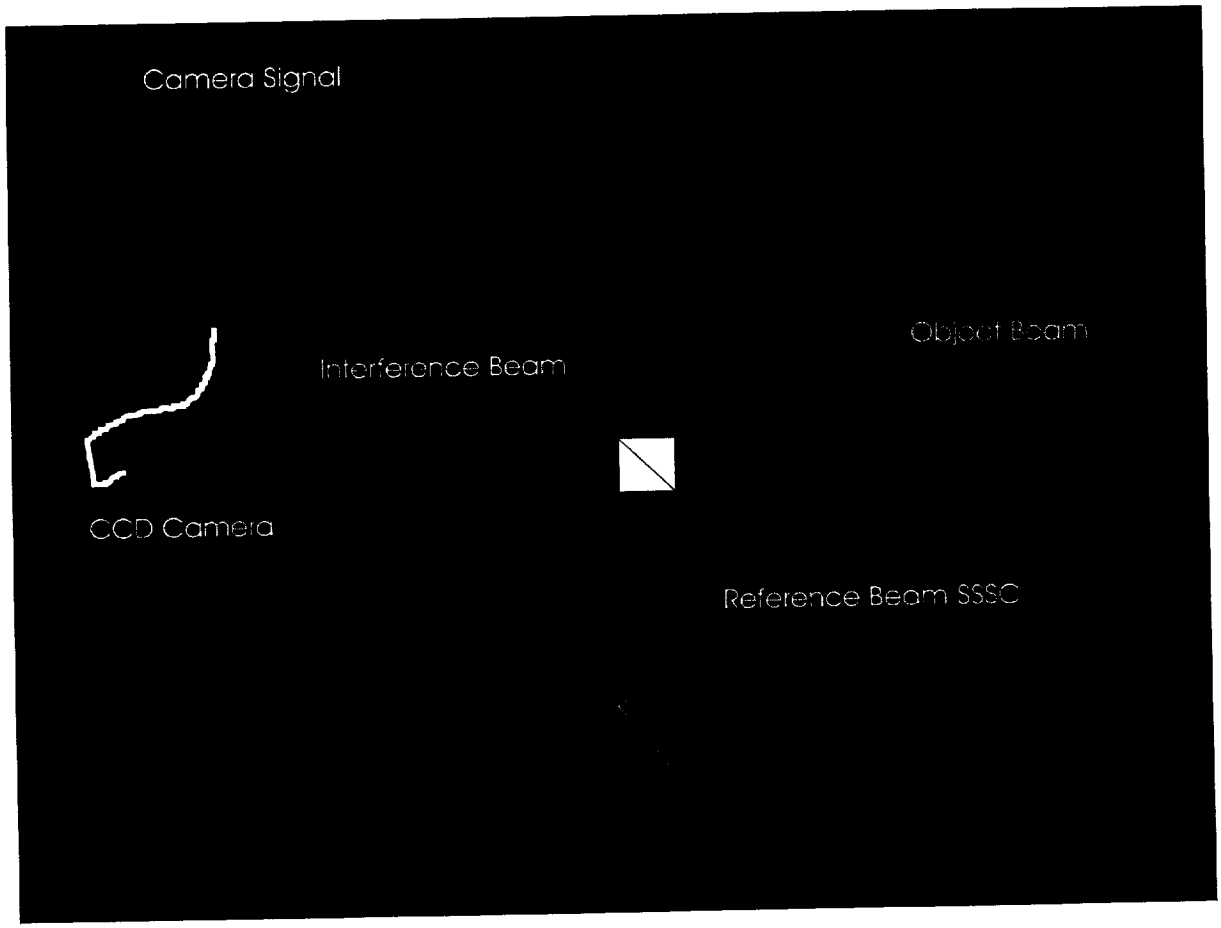

Figure 3.35: Frequency content and physical signal processing that occurs in the FTEOH technique

In Eq. 3.49 I is the time averaged combined intensity of the object and reference beams, $F^*_r(t)$ is the complex conjugate of the reference light beam, $F_o(t)$, is the reflected object beam. By taking the Fourier transform of Eq. 3.49, where the Fourier transform of the intensity is denoted by i, Eq. 3.50, which is a product of the sinc function, is obtained.

$$i = \chi(f) \cdot T \operatorname{sinc} Tf \tag{3.50}$$

where

$$\chi(f) = F_r^*(f) * F_o(f) \tag{3.51}$$

$\chi(f)$ is the cross correlation of the complex conjugate of the reference beam with that of the object beam [5].

$$\operatorname{sinc} Tf = \frac{\sin \pi f}{\pi f}. \tag{3.52}$$

This relation says that as T increases the width of the sinc function decreases and filters out the frequency components that are not centered at zero. This effect is shown in Fig. 3.35 where the range of the desired frequency components converge to $f = 0$ [5] . If the limits of the intensity are evaluated as the period T approaches infinity, as shown in Eq. 3.53

$$i = \lim_{T \to \infty} i_{ro}(fT) = \chi(0)\delta(f) \tag{3.53}$$

where $\delta(f)$ is the Dirac delta function, then the function only exists at the desired freequency. With a long exposure time the value of the cross-correlation spectrum at the origin is the only value that becomes applicable [5]. This is why the FTEOH images are related to the higher order Bessel functions.

3.5.1 SCATTERING OF THE OBJECT LIGHT

This section and section 3.5.2 discuss the scattering of the object beam and how to take advantage of the spectral components that result from reflection through use of the sawtooth function. Modulation through use of the sawtooth or ramp function is known as serrodyning, which will produce a signal with a single sideband suppressed carrier (SSSC), which is instrumental in producing an FTEOH image with clean resolvable fringes.

The reflection of the coherent object beam with that of the test structure is temporally and spatially modulated in a manner that depends on the type of vibration [5, 31, 32]. In this particular study, the vibration of the object is of a sinusoidal manner. When the light is reflected off of the object's surface, the modulated terms can be expressed as $(\exp(in\Omega)\delta(f-nF))$. That is, the reflected light is phase $(\exp(in\Omega))$ as well as frequency modulated $\delta(f-nF)$ and can be expressed in terms of higher order Bessel functions, as previously shown [5, 31].

The spectral composition of the light scattered by the vibrating object will contain the carrier frequency of the laser (ω_c) with side bands at integer multiples of the object frequency $(\omega_c \pm n\omega)$, where ω is the object frequency and n is the n^{th} harmonic of the object frequency. The modulated spectrum is shown in Fig. 3.36 [5, 32].

The scattered object beam contains several different frequency components, although in comparison to the carrier frequency (GHz), the components (Hz – MHz) might be considered inconsequential but in fact these components are of major interest for phase mapping methodology [5, 25, 26, 31, 32]. Using traditional modulation methods (i.e. a PZT actuated mirror), a conventional holographic image would be

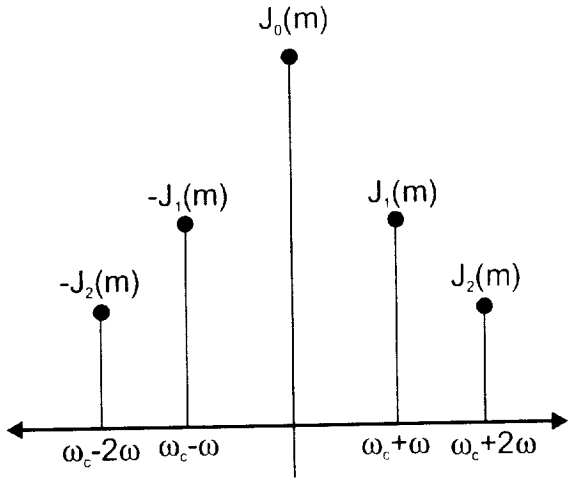

Figure 3.36: Fourier Transform of the phase modulated spectrum of reflected light off of a sinusoidally moving object [34].

obtained by modulating the reference beam at integer multiples of the object frequency (i.e., $\omega_c \pm n\omega$) [5]. As a result, the synchronous or correlated component of the scattered object light and the modulated reference light is no longer the carrier signal ω_c, but is at $\omega_c \pm n\omega$, which is located at the n^{th} order side band [5, 31, 32] as shown in Fig. 3.36 [34]. The interaction of the scattered object wave with the modulated reference wave produces an image whose intensity is related to higher order Bessel functions. The order of the Bessel function is directly related to the n^{th} harmonic of the structure's excitation frequency, the frequency for which the reference beam is modulated. This method has been used by several authors [5, 31, 32] to increase as well as decrease the sensitivity of conventional holography.

3.5.2 SERRODYNING

The spectral composition of the light reflected off a vibrating object for the frequency modulated case is similar to that shown in Fig. 3.36 but the carrier frequency contains a time dependent component and is characterized by $\omega_c = \omega_c \pm \Delta\upsilon \sin p\omega t$ as shown in Fig 3.37 [34]. Each successive side band of Fig. 3.37, like those shown in Fig. 3.36, contain a component of harmonic object frequency where the central component is

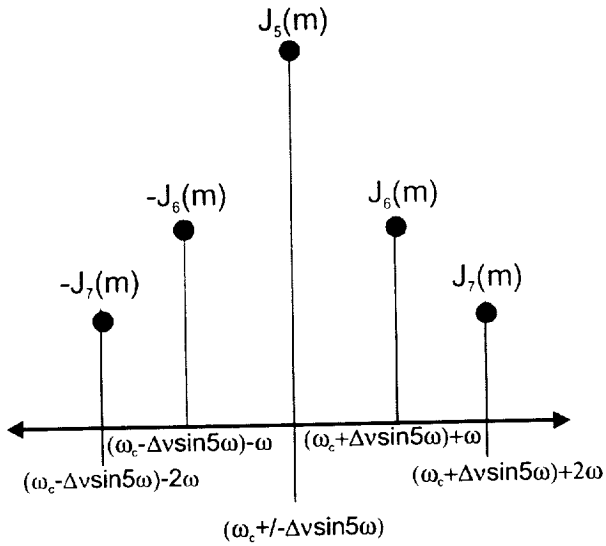

Figure 3.37: The modulated spectral composition of the scattered object wave

the desired, modulated signal. The remaining components are the result of reflection off of a sinusoidally moving object. Unlike traditional modulation, these side bands do not contribute to the final EOH image. Instead, the synchronous component of the scattered object beam and the reference beam will always be the central frequency component, like the one shown in Fig. 3.33, regardless of the order of modulation. By modulating the laser diode current source both the object and reference beams have an equivalent spectral composition ($\omega_c = \omega_c \pm \Delta\upsilon \sin p\omega t$). The only difference between the two beams

is that the object beam contains products of reflection and the reference beam does not. Therefore, when the light of the two beams recombine back at the CCD camera, the cross correlation will occur using the central frequency component of both the scattered object beam and the reference beam because these are the synchronous components of both signals. To insure that the intensity distribution of the interference pattern is governed by a desired higher order Bessel function a sawtooth waveform is used to suppress any sideband components. These sideband components are a result of laser diode current modulation via a sine function.

3.5.2.1 SERRODYNING AT THE SOURCE

Supposing that the external modulating signal is a sine function, instead of a sawtooth waveform, with a frequency equal to that of the test object's excitation frequency [25], the optical frequency of the laser diode will oscillate in a sinusoidal manner about the lasing frequency with a frequency shift of $\Delta\upsilon$, as shown in Fig. 3.38.

For the particular case of FTEOH, an external periodic signal, generated by a function generator, is applied to the laser diode current source. However, the external modulating signal, given that it is a sinusoidal, causes the signal to oscillate about the lasing frequency at a frequency equal to that of the external modulating signal. The

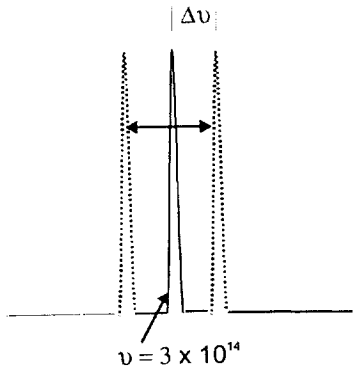

Figure 3.38: Frequency shift of the laser diode. The solid line frequency spike represents the original lasing frequency. The dotted line is the frequency shift $\Delta\upsilon$, which oscillates about the lasing frequency and is expressed as $\Delta\upsilon \sin(\omega t)$, the modulating frequency. Where the modulating frequency = the test structure excitation. However, the mean frequency over the period of oscillation for the frequency is still the lasing frequency υ.

optical frequency change can be expressed as shown in Eq. 3.54, where $\Delta\upsilon$ is the amplitude of the frequency shift and ϕ_υ is the phase of the source frequency modulation [25, 26].

$$A_\upsilon = \Delta\upsilon \sin(\omega t + \phi_\upsilon) \tag{3.54}$$

A small problem exists at the central frequency of both the scattered object beam and the reference beam. When a sine wave is used to modulate the frequency shift of the laser diode, the shift will contain a time dependent component. There is no guarantee that the components of the two beams will match up exactly. The scattered object beam component may contain the positive carrier signal $\omega_c = \omega_c + \Delta\upsilon \sin p\omega t$, while the reference beam may contain the negative carrier signal $\omega_c = \omega_c - \Delta\upsilon \sin p\omega t$.

If the Fourier transform of function shown in Fig. 3.38 is taken, the signal would contain several different spectral components within the frequency range $\omega_c = \omega_c + \Delta\upsilon \sin p\omega t$ to $\omega_c = \omega_c - \Delta\upsilon \sin p\omega t$, which is not acceptable and highly noticeable within the viewing FTEOH images when the frequency of the modulating signal is increased. To correct for this, the sinusoidal waveform of the modulating signal is replaced by a sawtooth waveform. The sawtooth waveform will bias the signal to the positive side suppressing all undesirable sideband components. Modulating the laser diode current source by means of a sawtooth wave is known as serrodyning. The amplitudes of the residual sidebands after serrodyning can be expressed by Eq. 3.55 [39].

$$A_n = \frac{\omega}{2\pi}\int \exp(-i(\Omega\omega - n\omega))dt$$

$$= \frac{1}{2\pi(\Omega - n)}\{\exp[-i(\Omega - n)] - 1\} \tag{3.55}$$

In Eq. 3.55 ω is the modulation frequency and A_n is the amplitude of the sidebands. The result, given that the frequency is modulated in integer steps, is a single sideband suppressed carrier (SSSC) with all residual sideband amplitudes suppressed to zero [39].

In terms of its Fourier series expansion, the sawtooth function can be given as Eq. 3.56, which can then be simplified as the summation of Eq. 3.57.

$$y = \frac{2A}{\pi}\left(\sin\omega t + \frac{1}{2}\sin 2\omega t + \frac{1}{3}\sin 3\omega t + \ldots\right) \tag{3.56}$$

$$y = \frac{2A}{\pi}\sum_{n=1}^{\infty}\left[\frac{1}{n}\sin\omega t\right] \tag{3.57}$$

In the above equations A is the amplitude of the modulating signal. By substituting the Fourier series of Eq. 3.57 into Eqs. 3.11 and 3.12, the object and reference beams can now be expressed as shown in Eqs. 3.58 and 3.59.

$$F_v = A_o \exp\left\{i\frac{4\pi}{c}\left[e_o v\sin(\omega t + \Omega) + \Delta v L_r \sum_{n=1}^{\infty}\frac{1}{n}\sin(\omega t + \varphi_v)\right]\right\} \tag{3.58}$$

$$F_r = A_r \exp\left\{i\frac{4\pi}{c}\Delta v L_r \sum_{n=1}\frac{1}{n}\sin((\omega t + \varphi_r)\right\} \tag{3.59}$$

The Fourier transform of Eqs. 3.58 and 3.59 are given in Eqs. 3.60 and Eqs. 3.61

$$F_v = \sum_{n=-\infty}^{\infty}\left\{J_n\left[\frac{4\pi}{c}(e_o v + \Delta v L_o)\right]\exp(in(\Omega + \varphi_v))\delta(f - n\omega)\right\} \tag{3.61}$$

$$F_r = \sum_{n=-\infty}^{\infty}\left[J_n\left(\frac{4\pi}{c}\Delta v L_r\right)\right]\exp(in\varphi_r)\delta(f - n\omega) \tag{3.61}$$

Thus, because of the presences of the Dirac delta function the above equations only exist at $n\omega$, giving rise to the single sideband at $n\omega$ with complete suppression of all spurious components.

3.5.3 WAVEFORMS, VERIFYING THE SAWTOOTH THEORY

Based on the cross correlation analysis described above, a sine waveform cannot be used to perform laser diode current modulation because its spectral composition will contain more than one component. After the first harmonic, using the sine wave, the images lose their contrast and definition and it is virtually impossible to clearly identify individual fringes. This same phenomenon is also true of the triangular waveform. However, if a sine, square or triangular waveform were used to perform laser diode current modulation, a synchronous component is not guaranteed and as a result the fringes are unclear and difficult to distinguish, which is the case in Figs. 3.39 – 3.42. In Fig. 3.39 a sine waveform was used to modulate the laser diode current source at the 4^{th} harmonic of the test structure's frequency. It can be seen that the fringes are difficult to define and do not resemble the fringe pattern of Fig. 3.39, an image created by a ramp waveform. In Fig. 3.41 a square wave was used as the modulating waveform, although the image is clear and all the fringes are resolvable, there is no fringe reduction. Therefore it can be concluded that the square waveform does not allow fringe reduction for the FTEOH method. Next, a triangular waveform was used to create the modulated image of Fig. 3.42. Unlike the case of the square wave, the number of fringes has been reduced with respect to Fig. 3.39; however, individual fringe resolution is poor, which makes displacement analysis extremely difficult. Based on the information obtained for these four waveforms it can be concluded that the best results for the case of FTEOH fringe reduction will occur when using a sawtooth waveform for modulation of the laser diode current source.

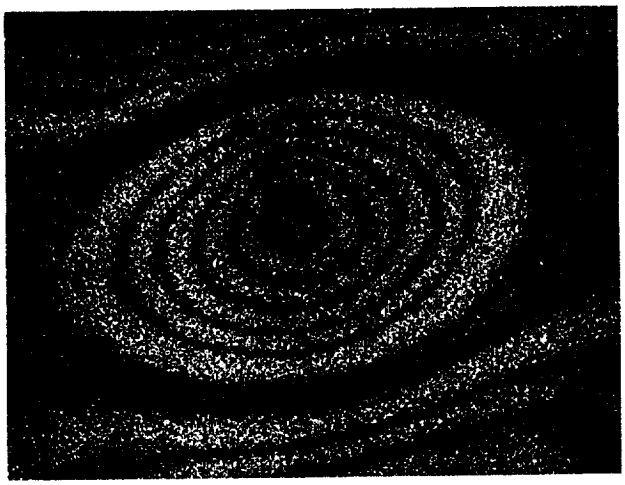

Figure 3.39: Forth order modulation obtained with ramp waveform fringe resolution is clean and distinguishable.

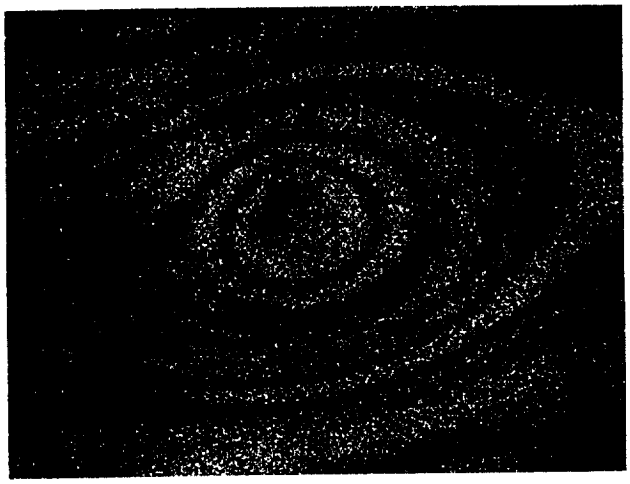

Figure 3.40: Forth order modulation obtained by using a sine waveform fringe resolution has been greatly reduced.

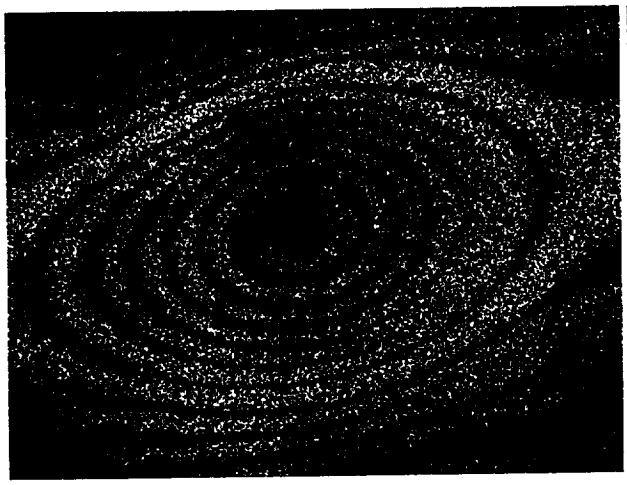

Figure 3.41: Forth order modulation obtained with square waveform. The image shows no signs of fringe reduction.

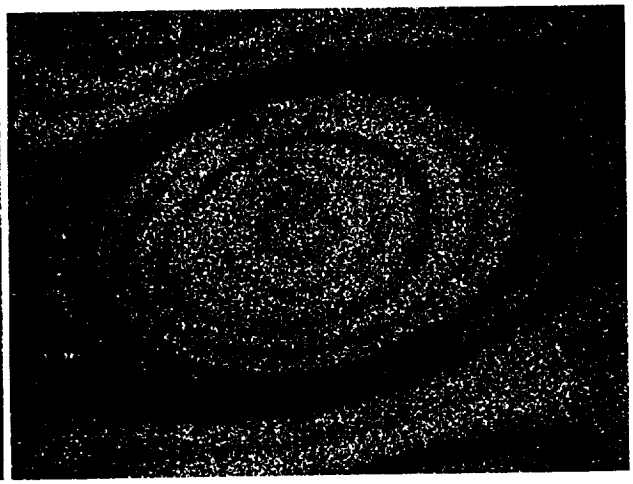

Figure 3.42: Forth order modulation obtained with a triangular waveform. The fringe resolution is degraded.

CHAPTER 4.0

EXPERIMENTAL SET UP AND PROCEDURE

This chapter details the experimental setup used to obtain the data for FTEOH analysis. It includes a discussion of each optical component and how laser light propagates through the optical fiber based system. Although the system described here is fiber based, the FTEOH technique will work in exactly the same manner on a mirror based system. A fiber-based system was chosen for ease of optical component movement.

4.1 THE EXPERIMENTAL SET UP

The experiments used to perform fringe reduction for the FTEOH system were done on the optical set up illustrated in Fig. 4.1. The ray trace of Fig. 4.2 was drawn to help visualize the laser beam path for Fig. 4.1. The optical system consisted of, in order of the journey of the laser beam:

- 100 mW laser diode, discussed in Appendix B.
- A telescope assembly consisting of:
    - A collimator, anamorphic prism pair and two converging lenses, all used to collimate, compress and shape the light beam.

- A Faraday isolator to prevent back reflection into the laser diode, a beam splitter used to create two beams (the object and the reference beam) from the original laser beam.
- Fiber optic couplers, used to direct the laser light into the fiber optic cable.
- Phase stepper and PZT mounted mirror, used to change the optical path length of object and reference leg respectively.
- CCD camera, used to capture the interference patterns.

These optical pieces, which are discussed in detail in this section, were an integral part of producing FTEOH interference patterns for this thesis study.

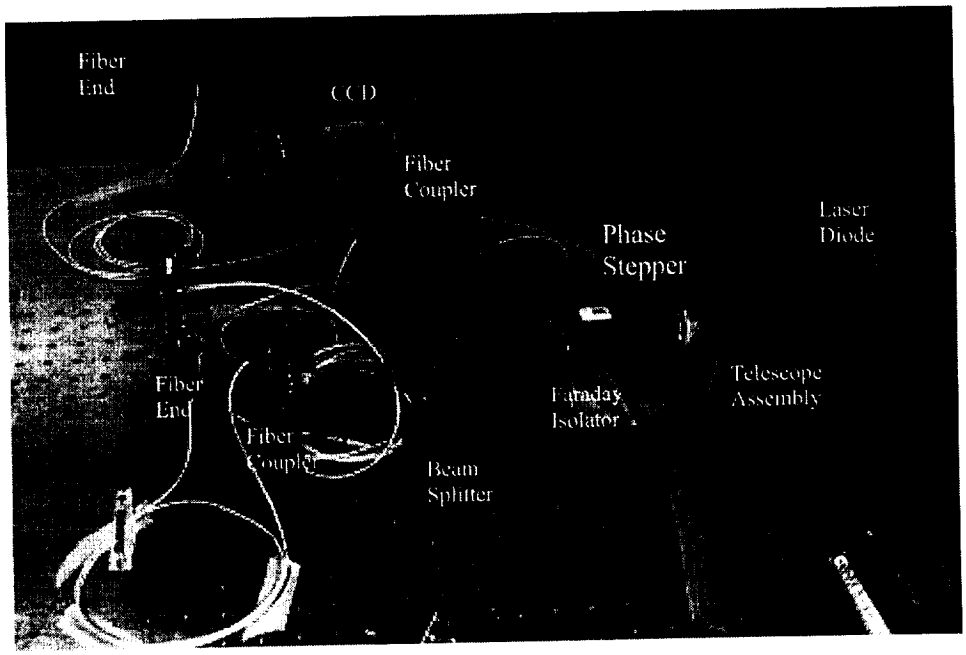

Figure 4.1: FTEOH Optical set up

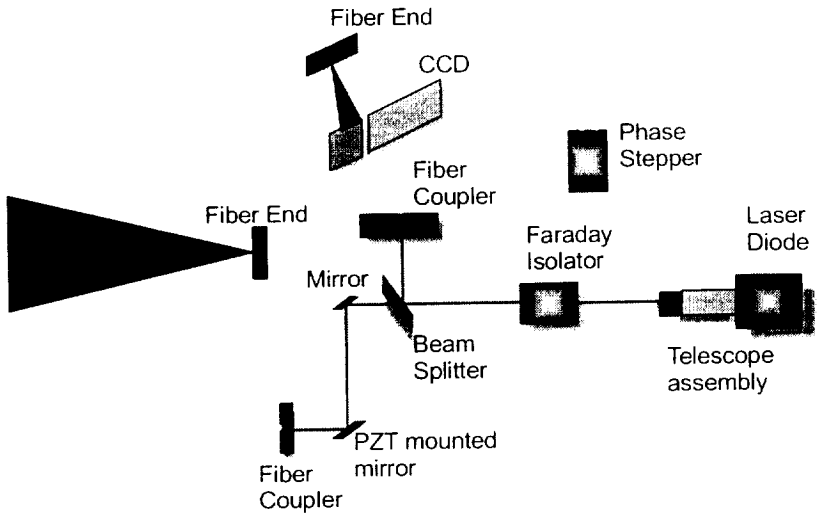

Figure 4.2: FTEOH optical path.

4.1.1 TELESCOPE ASSEMBLY

As shown in Fig. 4.2, the light emitted from the laser diode is immediately directed through the telescope assembly shown in Fig. 4.3. This assembly is a combination of lenses and prisms that collimate and contract the diameter of the elliptically divergent beam of the laser diode. The telescope assembly was placed into the optical set up to more efficiently pass the laser light through the aperture of the Faraday Isolator shown as the right most element in Fig. 4.3.

The first element in the telescope assembly is the collimator, illustrated in Fig. 4.4 as a dotted cylinder. The light emitted from the laser diode is not a collimated beam with a circular beam profile, as is the case with all other gas and solid-state lasers. Instead, light emitted from the laser diode is highly divergent, with an elliptical beam profile that expands very rapidly from the laser aperture. Light emitted from the laser diode is not a

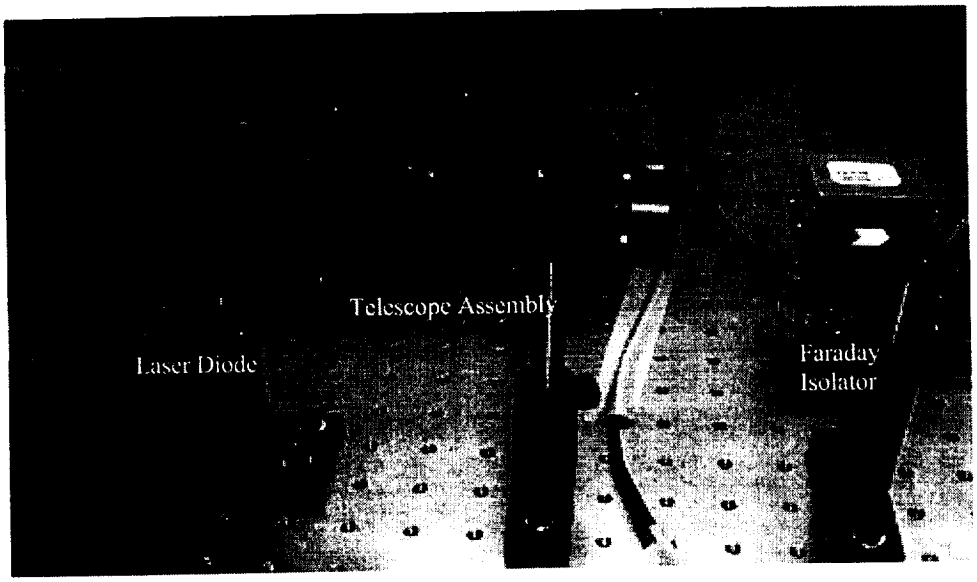

Figure 4.3: Telescope assembly and Faraday Isolator.

collimated beam but a highly divergent, elliptical beam that expands very rapidly from the aperture of the laser diode. To correct the divergence of the beam, a collimator is used. The purpose of the collimator is to optically correct for the divergence using lenses, thus achieving a more collimated less diverging beam of light. The objective is to focus this point far enough away that the beam, in the area of interest, appears to be a long narrow column of light. Once the light is '"collimated" it is directed through other optics with greater efficiency. The second element in the telescope assembly is the anamorphic prism pair shown as a cross-section in Fig. 4.5. This optic reshapes the elliptical beam into a nearly circular beam by magnifying along only one meridian [42]. The light from the laser diode is characteristically elliptical, which causes a problem when attempting to pass light through a small circular aperture. Thus, an anamorphic prism is used to magnify the elliptical beam along one meridian creating a nearly circular beam. The transmitted beam is displaced laterally as a result of magnification as shown in Fig. 4.5.

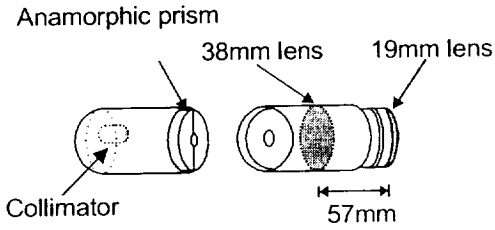

Figure 4.4: Cut-away of the Telescope assembly.

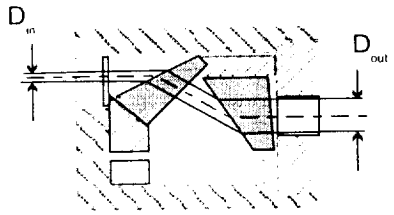

Figure 4.5: Cross-section of the Anamorphic prism pair [1].

The third and final element in the telescope assembly is a pair of double convex converging lenses. These lenses act together to contract the diameter of the circular beam. The beam expander was used to contract the laser beam diameter to obtain maximum light throughput through the Farady isolator aperture.

The first lens in the telescope assembly of Fig. 4.4 is a 38 mm converging lens. Light passing through this lens will converge at a focal point 38 mm from the lateral axis and then will begin to diverge. If the second lens is placed at a distance of 19 mm from the focal point of the 38 mm lens the beam the now divergent beam of Fig. 4.6 will regain its collimated characteristics but will have a diameter one half the size of the original beam.

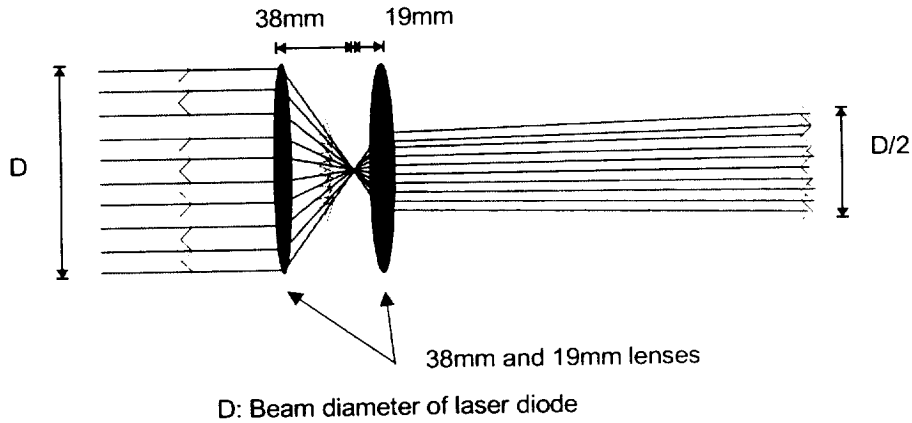

Figure 4.6: Ray trace of the contracted beam.

4.1.2 THE FARADAY ISOLATOR

After the light has passed through the telescope assembly it is directed through the Faraday isolator, a magneto-optic, used to prevent reflection from re-entering the cavity of the laser diode. A Faraday isolator is a unidirectional device based on the Faraday effect [43]. That is, the light will only pass through the device in the forward direction. The Faraday isolator is a magneto-optic device used to prevent external reflections from re-entering the laser diode cavity. Any light re-entering the cavity will disrupt the laser emission frequency stability.

The isolator is comprised of polarizers, an optical crystal, and strong magnets. Combining the magnets and optical crystal produces a Faraday rotator, which can be used to rotate the polarization of the light passing through it [43]. This phenomenon, discovered by Michael Faraday, was found to occur when an isotropic dielectric, such as a crystal, is placed in a relatively strong magnetic field. The presence of the magnetic field causes the dielectric crystal to become optically active, which in turn causes a beam of light, polarized the direction of the field, passing through the crystal, to become rotated in the direction of the magnetic field [36].

Light passing through in the forward direction, as shown in Fig. 4.7, of the isolator will initially pass through the input polarizer and become polarized along the

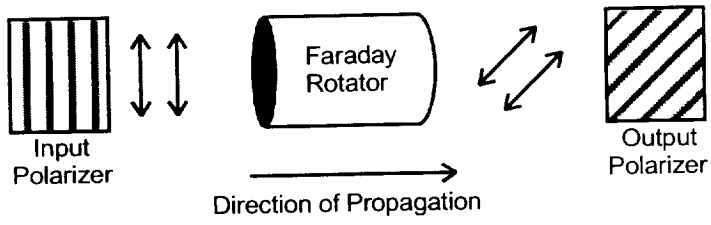

Figure 4.7: The three major components of the Faraday Isolator. In this figure the light is traveling through the isolator in the forward direction [42].

vertical plane. Upon passing through the Faraday rotator, the plane of polarization will be rotated 45°. The output polarizer, which has been aligned 45° relative to the input polarizer, will then let the light pass through unimpeded [43].

The isolator was designed to prevent back reflections from re-entering the cavity of the laser diode. Any reflection into this sensitive chamber will cause the diode to lose emission stability. In order to prevent this from occurring the isolator is placed in the direct path of the emitting beam. Any reflected light traveling in the opposite direction must pass through the output polarizer first and become polarized at an angle of 45°, the light then passes through the Faraday rotator and experiences and additional 45° rotation. The light is now polarized along the horizontal plane and will not be able to pass through the input polarizer, which only allows light polarized in the vertical plane to pass through unimpeded [43]. The case for light traveling in the reverse direction is shown in Fig. 4.8.

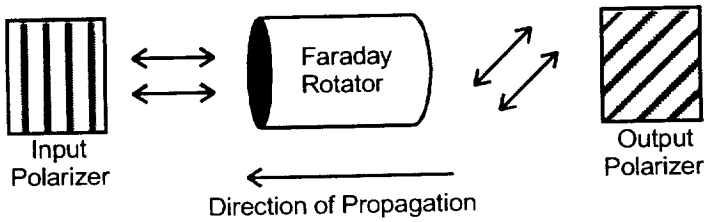

Figure 4.8: The polarization of back reflected light traveling in the reverse direction through the isolator. Light traveling in this direction will not be able to pass through the input polarizer and hence will be permitted from re-entering the cavity of the laser diode [39].

4.1.3 BEAM SPLITTER

After passing through the isolator the beam interacts with a pane of glass that behaves as a beam splitter. The light both reflects and transmits through the glass creating two beams, which are at 90° angles to each other. The transmitted beam has been denoted as the reference and the reflected beam the object leg in Fig. 4.2. The reference beam

contains most of the laser energy while the reference beam is typically only a small fraction, 5%, of the laser energy [4].

4.1.4 FIBER OPTIC COUPLERS AND CABLE

From the beam splitter the object and reference legs are directed along separate paths. Both legs, however, are eventually directed to fiber optic couplers. The fiber optic coupler has an optical lens placed at the head of a fiber optic cable. The fiber optic coupler receives the collimated laser light and focuses it down to a spot at the fiber optic core. The light successful focuses onto the core can then propagate through the fiber. Coupling the light into the fiber is a little more difficult than simply aligning the light through a small aperture. Figure 4.9 and 4.10 show both the front and the back of the fiber coupler used to direct the light of the reference leg into the fiber optic cable.

Figure 4.9: Front of reference leg fiber coupler.

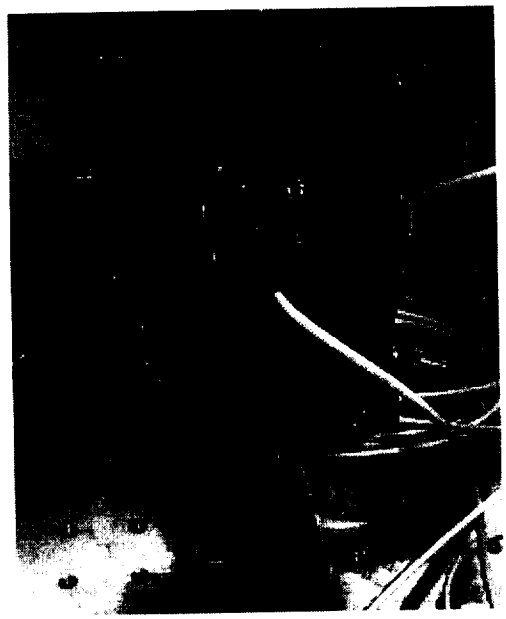

Figure 4.10: Back of reference leg fiber coupler.

The optical fiber is made from silicon dioxide (SiO_2) and dopant materials used to control the refractive index. Most fibers are constructed with an inner core with an index of refraction n_o slightly higher than the surrounding material n_c called the cladding [44]. The diameter of the fiber is approximately one optical wavelength wide and if not perfectly aligned through the center of the fiber the light will be dispersed in to the cladding material [44]. For example, the light propagating through the fiber cross section of Fig. 4.11 is shown at two different angles. In the first case the light is at too great of an angle and enters the cladding material preventing propagation along the core. In the second case the light is shown at the maximum angle at which the light rays will be confined within the core. Thus, it is extremely important to guarantee alignment into the fiber is correct. Alignment using both the vertical and horizontal directions is important, however, the fibers tend to be more sensitive to the pan and tilt adjustment. One will know when alignment has been properly achieved when the maximum amount of light has propagated to the end of the fiber. Alignment into the fiber for this experiment was made easier with the addition of the fiber collimator and the photo diode. The fiber collimator, just like the collimator used to collimate the beam of the laser diode, focus the light into the fiber. The collimator has an index of refraction that changes from the periphery radially to the center of the lens, which causes light to bend differently

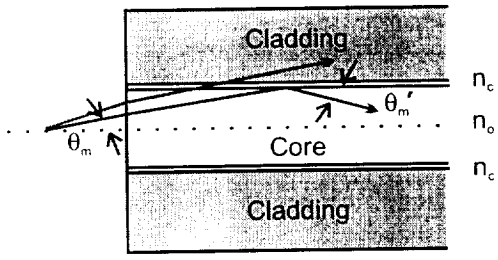

θ_m : The max angle beyond which rays that enter the fiber are no longer confined within the Fiber

θ_m' :The critical angle beyond which rays will be bounded with in the fiber

Figure 4.11: Propagation of light through a fiber optic cable, n_c is the index of refraction for the cladding and n_o is the index of refraction for the core [44].

along the radius of the lens. Light not in direct alignment with the fiber collimator will bend into the cladding material thus preventing light to travel the length of the fiber.

The second element that aids in alignment is the photodiode. A photo diode greatly increases the ease with which the light beam can be coupled into the fiber by providing a signal that reacts when light has traveled the length of the fiber. The photo diode is placed into an open loop circuit, which is attached to the end of the optical fiber and an oscilloscope. The oscilloscope monitors the voltage change that occurs as the photo diode comes in contact with light. Once the light has been roughly adjusted into the index graded lens in the x and y position, the pan and tilt are adjusted until the reading on the oscilloscope indicates the maximum amount of light has been coupled through the fiber. The fiber ends for both the object and reference legs are then disconnected from the photodiode and placed back into the optical set-up.

The light transgressing through the object leg travels through three meters of fiber before reaching the fiber end, as shown in Fig. 4.1 and 4.2. Once the light reaches the end of the fiber where it is no longer confined to the boundaries of the fiber core it begins to diverge very rapidly. The diverging light travels an additional meter through air upon reaching and illuminating the test structure of Fig. 4.12. This fiber end is placed at such a distance that the divergent light emitted from the fiber illuminates the entire face of the object. This type of illumination

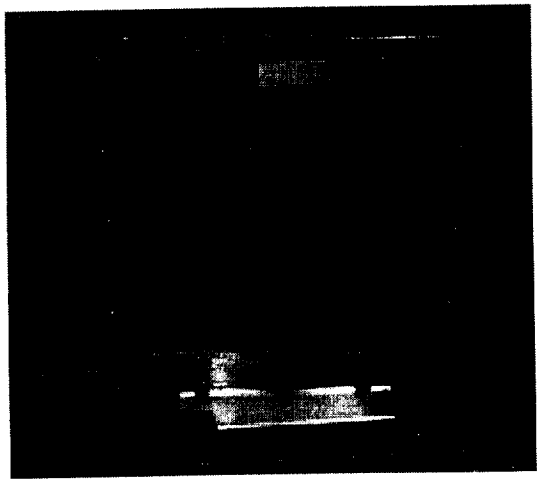

Figure 4.12: Test Object.

gives the operator the ability to choose a localized area or the entire surface of the object to study.

The structure, shown in Fig. 4.12, is an aluminum plate confined by a heavy frame and fixed at the base. The frame was used to increase the stiffness of the structure. On the backside of the structure a piezoelectric (PZT) actuator was placed near the centroid and was the source of dynamic excitation during testing.

4.1.5 PHASE STEPPER

The light traveling through the reference leg of the FTEOH system travels through approximately one meter of fiber before encountering the phase stepper shown in Fig. 4.13 and 4.14. The phase stepper is composed of a one inch diameter by one inch high piezoelectric cylinder, fiber optic cable and electrical leads with which voltage is supplied to the cylinder and cause the cylinder to expand. Approximately one meter of fiber was wrapped around the piezoelectric cylinder. Thus when the cylinder expands so

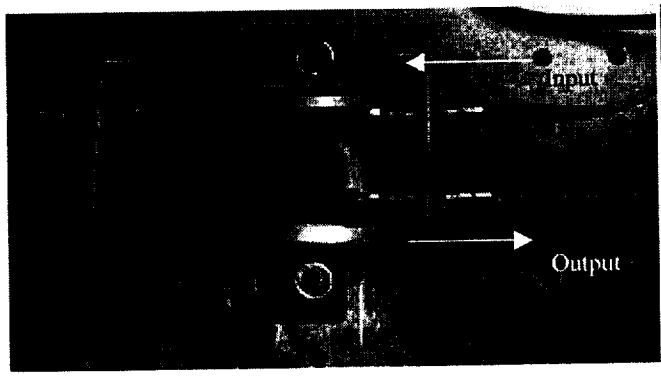

Figure 4.13: Top view of the phase stepper

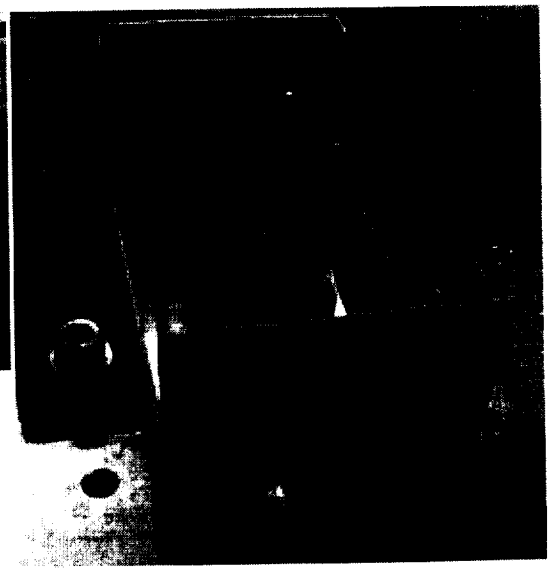

Figure 4.14: Side view of the Phase stepper

too does the fiber. The cylinder is excited by a stepped voltage, which causes the cylinder to expand and increase the optical path length of the reference leg. This expansion will travels and two additional meters before reaching the fiber end where the light is projected onto a beam splitter cube and directed onto the CCD array as shown in Fig 4.15.

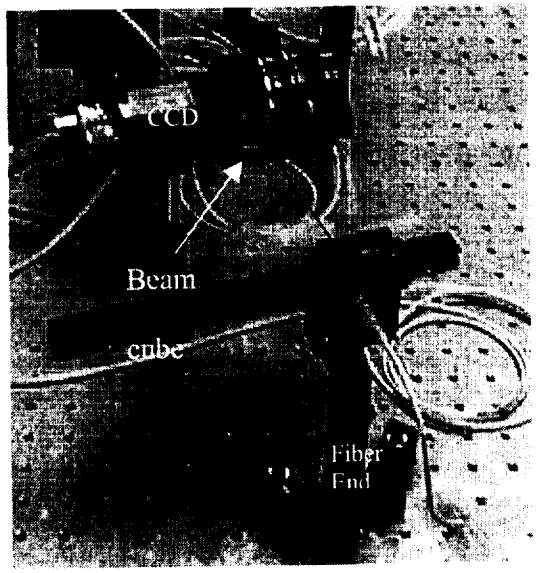

Figure 4.15: Reference light directed into the CCD

4.1.6 CCD CAMERA

When the reference light is directed onto the beam cube splitter and recombined with the scattered object light speckle will be attained. If speckle is not seen the interference fringes will also not been seen. Thus, it is vitally important that proper adjustment of the reference leg be attained. The speckle size of the speckles is also plays a major role in the unwrapping process. Specular interference (speckle) will result when the object and reference beams are combined at the beam splitter are the conditions of

mutual coherence and alignments are properly met. The observation of speckle is a prerequisite of achieving EOH and/or FTEOH interferograms.

Speckle size is also an important factor in the generation of interferograms. Ideally the speckle size should be approximately equal to or slightly larger than the physical size of a pixel on the CCD array. If the speckle size is too small, a single pixel may collect photons from multiple speckles whose interference may be out of phase. This results in an averaging effect that reduces interferogram contrast.

Speckle size can be estimated by Eq. 4.1

$$DS = 2.44\lambda \frac{f}{\#}, \tag{4.1}$$

where DS is the diameter of the speckle, λ is the laser wavelength and $\frac{f}{\#}$ is the f-number. The lens f-number is the ratio of the lens focal length divided by the lens aperture diameter [42]. It is best to have speckles about the size of a single pixel, which can be controlled by adjusting the aperture of the camera lens.

4.2 PROCEDURE

Once proper alignment of the optical elements has been attained, acquisition of the data can begin. The lights in the laboratory were lowered to minimize background light collect by the CCD camera. The signal generator was turned on and the PZT, was excited at a fundamental frequency of the test structure. The amplitude of excitation was such that it induced a high fringe density. Next, the external signal connected to the laser diode current source, was excited at integer multiples of the structure's frequency until the number of fringes reduced from the FTEOH image was satisfactory to the operator.

With the phase stepper operating in four-step increments the data was captured and then unwrapped to yield the final results discussed in Chapter 5 Results and Conclusion.

CHAPTER 5.0

RESULTS AND DISCUSSION

In the previous chapters the theory of FTEOH was presented. This chapter will detail the experiment and results that verify the FTEOH theory followed by a discussion on the future work for FTEOH.

5.1 LIST OF EQUIPMENT

Including the equipment discussed in chapter 4 the following components were used in obtaining the results for the FTEOH technique.

- Infrared Laser diode:
  - Micro Laser Systems Lepton IV Series System
  - Model # L4852S-115-TE-4
  - S/N 247
  - Power: 115 mW
  - Wavelength: 851 nm
  - Beam Diameter
    - Horiz: 4.2 mm
    - Vert.: 3.8 mm

- Laser Diode Current Driver
  - ILX Lightwave Laser Diode Controller
  - Model # LCD-3724
  - S/N 37241228

- Function Generator
    - Hewlett Packer Multifunction Synthesizer
    - Model # 8904A DC-600 kHz
    - S/N 3518A08207
    - Opt 8ZE, 002

- Cantilever Beam
    - Length 7 in.
    - Width 2 in.
    - Depth 0.125 in.

The cantilever beam used for analysis is shown in Fig. 5.1. The shaded area of Fig. 5.2 represents the actual area of study.

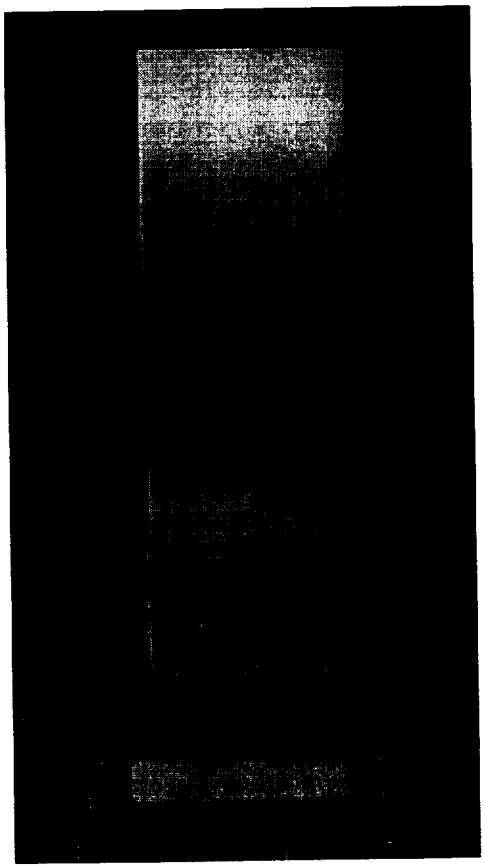

Figure 5.1: Cantilever beam used to obtain EOH and FTEOH data analysis.

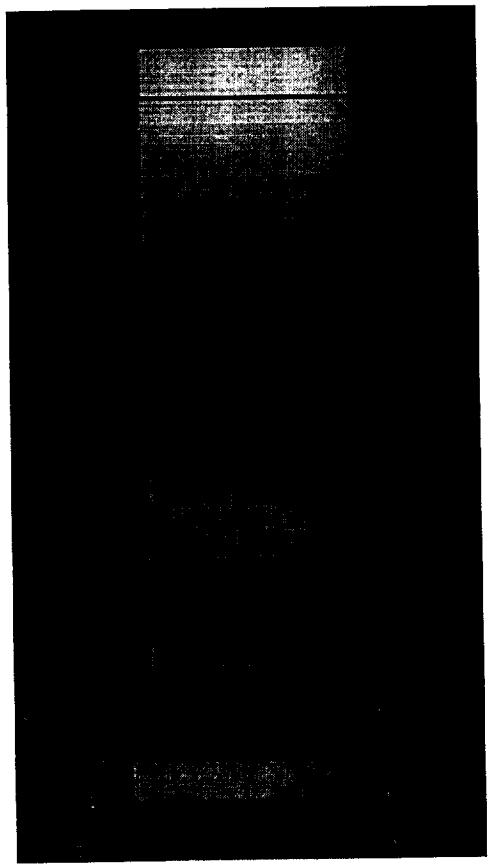

Figure 5.2: Shaded area represents the area used to during data acquision of this study.

5.2 THE EXPERIMENT AND DATA CAPTURE

Experimental verification of the FTEOH theory was accomplished using a vertically mounted cantilever beam. The beam was sinusoidally excited using a PZT mounted at the beam center near the free end. The cantilever beam was excited at 428 Hz with amplitude of 3.30 V. In this test setup only a portion of the cantilever beam of Fig. 5.1 was analyzed as illustrated in Fig. 5.2.

Data was captured in two sets. The first set was acquired using conventional EOH techniques, i.e. no laser diode current modulation. The second set was acquired using FTEOH techniques with sawtooth modulation applied at 2140 Hz, the fifth harmonic of the test structure excitation. The test structure excitation amplitude was constant for both cases.

In previous test cases the phasor bias settings were determined separately for the modulated case. The process of determining these settings is not as easily followed as in conventional EOH, mainly because the peak of the first fringe of a higher order Bessel function is more difficult to identify when the object excitation is turned off. This is a result of a lower peak intensity for the ever increasing Bessel function. It was also determined in those cases where the phasor bias settings were calculated precisely, that they were nearly the same as the setting for the conventional EOH system. Thus, it was decided to approximate the amplitude for the phasor bias to that of the conventional EOH phasor bias amplitude the results would produce the same displacement.

Here it can be seen that two fringes have been masked from the FTEOH image leaving behind a dark null. Although less apparent, the two masked fringes can be seen

in Fig. 5.4, these effects were discussed in Section 3.3. The procedure used for capturing data for both the EOH and FTEOH technique is detailed in Table 5.3. Figures 5.3 and 5.4 show the interferograms viewed for conventional EOH and FTEOH , respectively.

Table 5.1: Data capture procedure for both the EOH and FTEOH techniques.

step	Procedure for data capture
1	The first step is to determine the amplitude (voltage) at which the phase stepper will be operating to produce the 0°, 90°, 180° and 270° phase shift required in Eqs. 3.35-3.37.
2	Produce a static interference pattern.
3	Slowly increase the amplitude of the phase stepper, from zero, until the static fringe pattern shifts one complete black to white and back to black fringe. Record this voltage.
4	Excite the test structure at the desired frequency and amplitude. Record the frequency, ω, and amplitude. At this point several clearly identifiable fringes should be present on the computer monitor
5	For the leg that contains the phasor bias, the PZT mounted mirror will need to be excited at, ω, the frequency of the test structure. This can be accomplished by connecting the phasor bias (the PZT mounted mirror) to a function generator and dialing in the desired frequency. Set the amplitude at zero and slowly increase the amplitude of the phasor bias PZT, via the function generator, until the zero order fringe is lost.
6	Leaving the amplitude set, adjust the phase of the phasor bias excitation, via the function generator, until the zero order fringe is regained and its width is maximum. Record the phase, α. Be careful not to increase the amplitude in step 5 past the point at which the zero order fringe is lost. If this point is significantly passed you will not be able to regain the zero order fringe by adjusting the phase.
7	Turn off the test structure's excitation (0 Hz) and reduce the amplitude of the phasor bias (PZT mounted mirror) to zero. DO NOT CHANGE THE PHASE. The structure should appear completely white on the computer monitor.

8	Slowly increase the amplitude of the phasor bias (via the function generator) from zero until the entire structure goes black. Record the amplitude, V_1^{st}. At this point the value of B, from Eq. 2.110, is equal to 2.405, the argument of the first dark fringe of J_0, as shown in Fig. 5.5.
9	The voltage V_1^{st} will need to be reset by a scaling factor. This factor is the desired magnitude of the bias vibration B divided by 2.405. The scaling factor is denoted as V_B, for bias voltage and can be computed by using Eq. 5.1 $$V_B = \frac{B}{2.4045} V_{1^{st}} \qquad (5.1)$$ In Eq. 5.1 the desired value of B for this thesis was $\pi/3$, however any known value can be used, as indicated by Eqs. 2.121 – 2.123. In Chapter 2 it was shown that Eq. 2.120 contained three unknowns, I_a, I_m, and Ω, thus, by adding three known values of B into Eq. 2.120 there will now be three equations and three unknowns, a solvable system of equations. Following this reasoning three sets of images with three different, known phasor bias settings (0, B, and –B) are captured at each of the four phase angles (0°, 90°, 180°, and 270° of Eqs. 2.98 – 2.101). Therefore, Eq. 2.120 can now be solved for the fringe locus as shown in Eqs. 2.120 - 2.133.

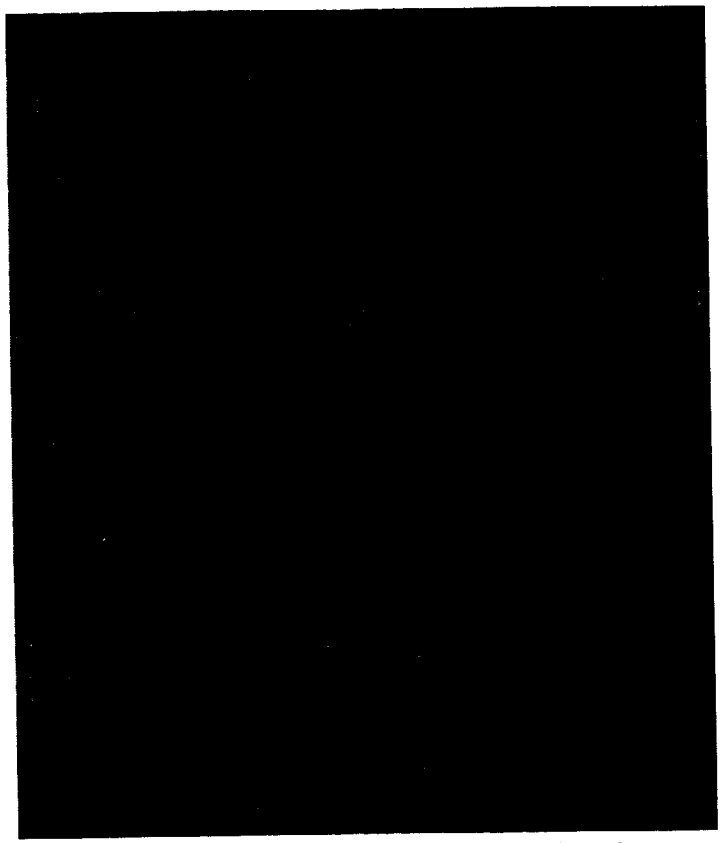

Figure 5.3: Typical EOH image of the cantilever beam in a bending mode.

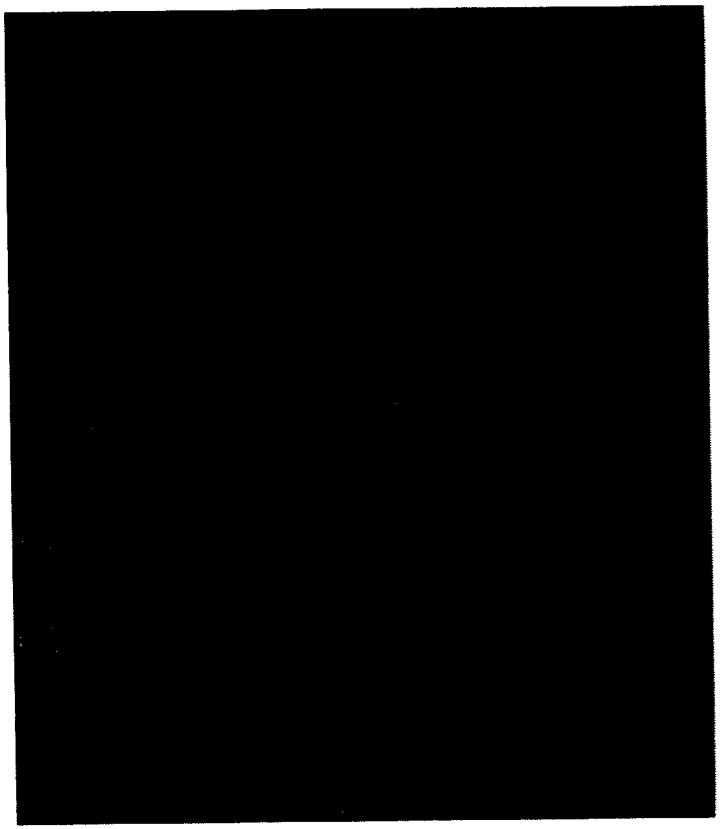

Figure 5.4: FTEOH image using a fifth order modulation. Note how the zero order fringe and the 1st order fringe have been masked

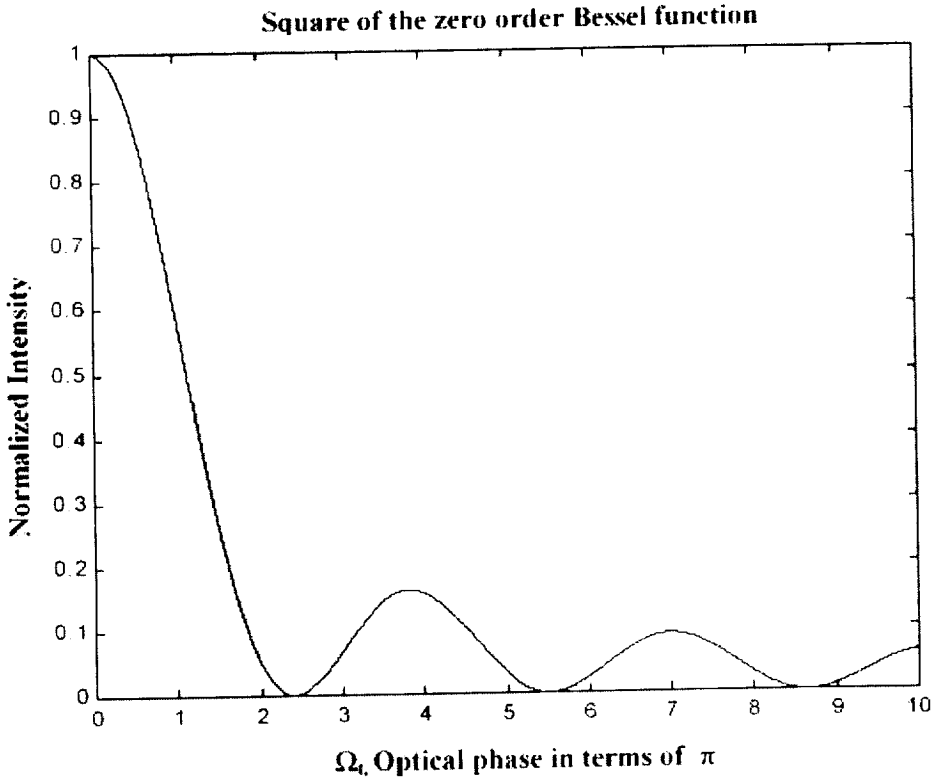

Figure 5.5: Zero order Bessel function.

5.3 FTEOH Data Capture Procedure

When taking FTEOH measurements, the amplitude of the laser diode current modulation must first be calibrated to ensure clear resolution of the individual fringes. This procedure is outlined in Table 5.2. If the amplitude is not set correctly fringe masking will not occur.

Table 5.2: Setting the amplitude of the laser diode current source.

Step	Setting the Amplitude of the Laser Diode Current Modulation
1	Tune the laser diode current modulation and the test structure to the same frequency.
2	Turn the excitation of the test structure off.

3	Starting with the amplitude of the current modulation at zero, slowly increase the amplitude until the image of the test structure goes black. This is the calibrated amplitude for obtaining FTEOH measurements and should be used exclusively throughout the measurement cycle. At the point where the test structure goes black is the first null of the zero order Bessel function.

5.4 DETERMINING DISPLACEMENTS

After data capture the EOH and FTEOH images were phase unwrapped in accordance with the procedure of section 3.3.5. As a part of the unwrapping process the image (EOH and/or FTEOH) is dissected into small columns, where omega is then determined for each column. The three-dimensional plot for both the non-modulated and the modulated case are shown in Fig. 5.6 and Fig. 5.7. The rows of the columns of Fig. 5.6 and Fig. 5.7 are then averaged across the plot. The average value of each row is then divided by the sensitivity vector, Eq. 3.41. The overall result is the plot of average row value versus the displacement of the test structure. Figure 5.8 represents the average row value versus the displacement for both the modulated case and the non-modulated case. Here it can be seen that for the point of interest, which is the base of Fig. 5.3 and Fig. 5.4, on the test structure the overall displacement for both cases will result in the same value.

In Fig. 5.8 the displacement immediately after the dark null does not match with that of the non-modulated case this is most likely a result of the non-linearities of the first bright fringe of the modulated case. The square of the zero order Bessel function can be approximated as a cosine wave where the approximation becomes more exact as the

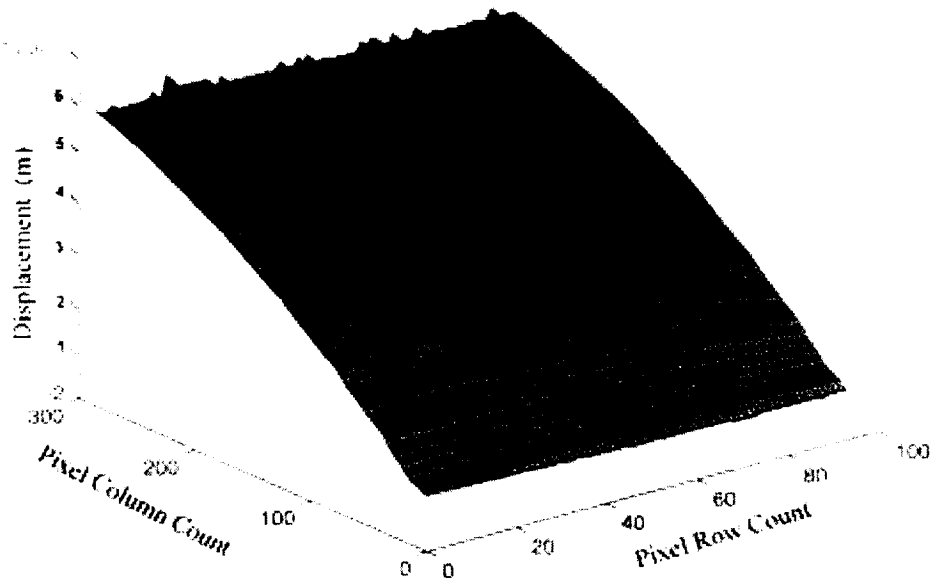

Figure 5.6: 3-D Plot of displacement for the interference pattern of Figure 5.3, i.e. no modulation.

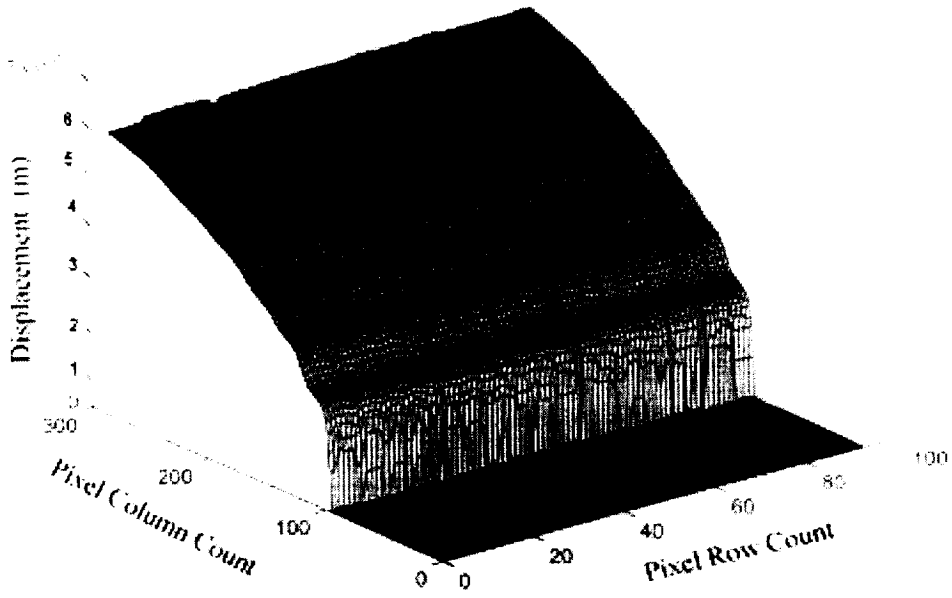

Figure 5.7: 3-D Plot of displacement beam and interference pattern of Figure 5.4.

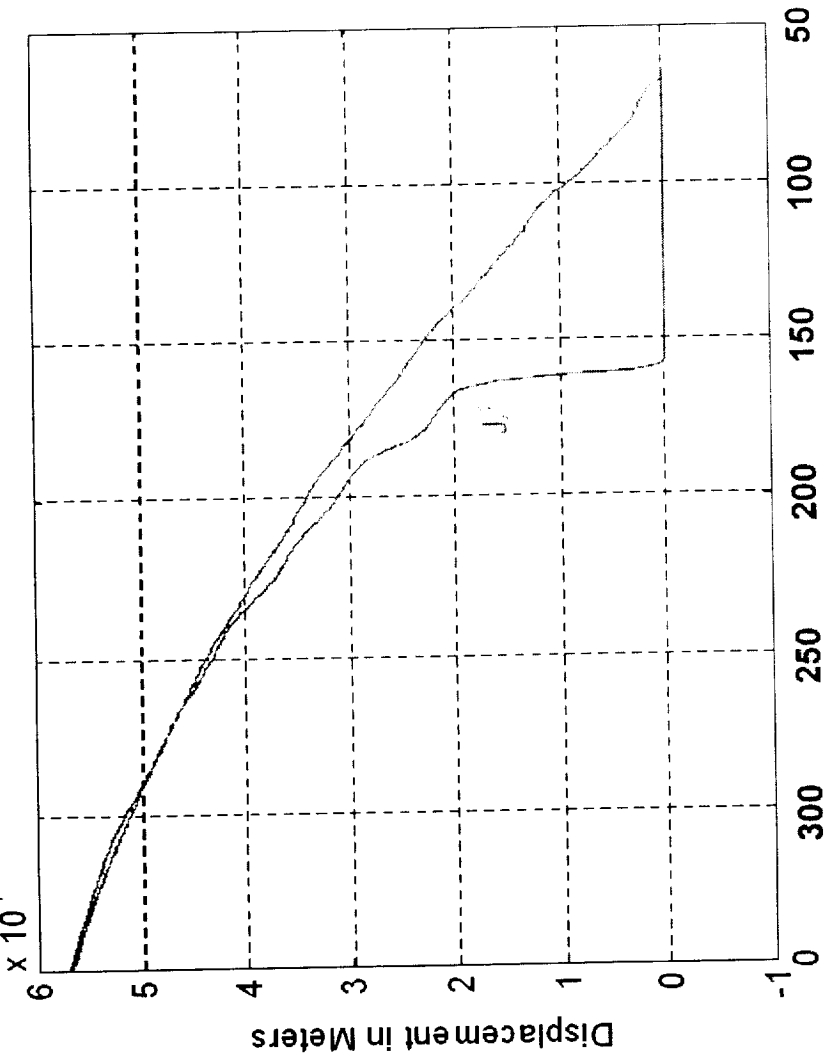

Figure 5.8: Average omega value for each row within the unwrapped omega image vs. the actual displacement of the test structure.

operand of the function increases. The same is true for higher order Bessel functions, the cosinusiodal approximation between the two functions becomes better and better as the operand increases. Initially the approximation does not match well because the width of the first couple waves is wider than that of a cosine wave of the same frequency and thus the cosine approximation used when determining Ω_{unwrap} has a greater error at for those fringes immediately after the null.

Here it can be seen that the overall displacement for the test structure for both the modulated and the non-modulated is case is $5.7x10^{-7}$ m. This displacement can be verified using the displacement equation given by Vest [22], shown in Eq. 5.1

$$L(P) = \xi_n \frac{\lambda}{4\pi} \Big/ 2 . \tag{5.1}$$

In Eq. 5.1 *L(P)* is the displacement of a particular point on the test structure, ξ_n is the n^{th} zero of $J_0^2(\Omega)$, shown in Table 5.3. One could calculated the displacement for the interference pattern of Fig. 5.1 by counting the number of fringes ~5.5, determining the approximate operand just past the 5^{th} zero and using those values in Eq. 5.1.

Table 5.3: Zeros of the Bessel function J_0^2

n	ξ_n	*n*	ξ_n
1	2.2048	11	33.7758
2	5.5200	12	36.9170
3	8.6537	13	40.0584
4	11.7915	14	43.1997
5	14.9309	15	46.3411
6	18.0710	16	49.4826
7	21.2116	17	52.6240
8	24.3524	18	55.7655
9	27.4934	19	58.9069
10	30.6346	20	62.0484

The operand for 5.5 fringes can be determined by averaging the distance between the 5^{th} and the 6^{th} zero ~ 16.50095. Now using these values the displacement can be calculated using Eq. 5.1 as shown below:

$$L(P) = \frac{16.50095\lambda}{8\pi} = 5.587x10^{-7}\,m \tag{5.2}$$

where $\lambda = 851x10^{-9}\,m$. The calculated value of Eq. 5.2 is very close to that of Fig. 5.7, in which case one can conclude that the displacement for Fig. 5.1 and Fig. 5.2 is correct.

5.5 FUTURE WORK

Future work for this project would include the investigation of shutter control. Although discussed in this thesis, shuttering of the CCD camera was not applied to any of the data gathered. It is the belief of this author that if shuttering were applied to FTEOH the appearance of the residual zero order fringe would either be completely masked having no difference in intensity from that of the other masked fringes or have an intensity that is significantly darker than those images shown here.

5.6 CONCLUSION

The primary objective of this study was to show that modulating the frequency of the laser diode current source produced an interference image with masked lower order fringes and the displacement of the modulated image was the same as the non-modulated image. It has been shown that this is indeed the case and although it can be difficult in practice the FTEOH technique can be used to expand the useful measurement range of electro-optic holography.

CHAPTER 6.0

REFERENCES

[1] Erf, R. Holographic Non-Destructive Testing. New York: Academic Press, 1974.

[2] Fleming, Gary. Buehrie, Ralph and Storaasli, Olaf L. "Modal Analysis of an Aircraft Fuselage Panel." Presented at 3rd International Conference on Vibration Measurement by Laser Techniques, Anacona, Italy June 16-19 1998.

[3] Pryputniewicz, Ryszard J. Holographic Numerical Analysis. Worcester: Worcester Polytechnic Institute, 1996.

[4] Fleming, Gary. Letter to author, 30, Oct. 1998.

[5] Aleksoff, C.C. "Temporally Modulated Holography." J. Appl. Opt. 10 (1971): 1329-1342.

[6] Serway, R.A. Principles of Physics. New York: Harcourt Brace College Publishers, 1994.

[7] Pedrotti, F.L. and Pedrotti, L.S. Introduction to Optics. New Jersey: Prentice Hall, 1993.

[8] Fowles, G.R. Introduction to Modern Optics. New York: Dover Publications, 1975.

[9] Hawkings, S. A Brief History of Time. New York: Bantum Books, 1988.

[10] Kasper, J. and Feller, S., The Complete Book of Holograms. New York: John Wiley and Sons Inc., 1987.

[11] Neumann, D.B., Jacobson, C.F. and Brown, G.M. "Holographic Technique for determining the phase of vibrating objects." Appl. Opt. 9 (1970), 1357-1362.

[12] Hariharan, P. Holographic Interferometry. Ed. Rastogi, Pramod K. New York: Springer-Verlag, 1994.

[13] Stetson, K. and Brohinsky, W.R. "Electro-Optic Holography and its Application to Hologram Interferometry," Appl. Opt. 29, (1985) 3631-3637.

[14] Stetson, Karl A. and Brohinsky W.R. "Electro-Optic Holography System for Vibration Analysis and Non-Destructive Testing." Optical Engineering. 26, 1987): 1234-1239.

[15] Breuckmann, B. and Thieme, W. "Computer-aided analysis of holographic interferograms using the phase shift method." Appl. Opt. 24 (1985), 2145-2149.

[16] Davies, J.C., Buckberry, C.H., Jones, J.D.C., and Panell, C.N. "Development of fiber optics electronic speckle pattern interferometer." SPIE, 863 (1987), 194-203.

[17] Ford, H.D., Atcha, H. and Tatam, R.P. "Optical Fiber Technique for the Measurement of Small Frequency Separations: Application to surface Profile Measurement Using Electronic Speckle Pattern Interferometry." Meas. Sci. Tech. 4 (1993), 601-607.

[18] Fleming, G. A. and Blotter, J., "Power Flow Using Electro-Optic Holography Part I: Obtaining the Structural Phase." 5th International Conference on Sound and Vibration, 1998.

[19] Wang, J. and Grant, I. "Electronic Speckle Interferometry, Phase-Mapping, and Nondestructive Testing Techniques Applied to Real-Time, Thermal Loading." Appl. Opt. 34 (1995), 3620-3627.

[20] Pryputniewicz, Ryszard J. "A Hybrid Approach to Deformation Analysis." Photo-mechanics. 2342 (1994): 282-296.

[21] Wykes, Catherine and Jones, Robert. Holographic and Speckle Interferometry. Cambridge: Cambridge University Press, 1989.

[22] Vest, C., Holographic Interferometry. New York: John Wiley and Sons Publishing, 1979.

[23] Imura, Yoshiko. "Electro-Optic Holograph Preliminary Proposal." Presented at ISU graduate committee, May, 1998.

[24] Mercer, C.R. and Beheim, G. "Fiber Optic Phase Stepping System for Interferometry." Appl. Opt. 30. (1991) 729-734.

[25] Atcha, Hashim and Tatam, Ralph P. "Heterodyning of Fiber Optic Electronic Speckle Pattern Interferometers Using Laser Diode Wavelength Modulation." Meas. Sci. Tech. 5, (1994) 704-709.

[26] Huang, J.R., Ford, H.D. and Tatum, R. P. "Heterodyning of speckle shearing interferometers by laser diode wavelength modulation." Meas. Sci. Tech. 7 (1996), 1721-1727.

[27] Yukihiro, J.C. and Murata,K. "Heterodyne Interferometry with a Frequency-Modulated Laser Diode." Appl. Opt. 27 (1988), 124-128.

[28] Aleksoff, C.C. "Time Average Holography Extended," Appl. Phys. Lett. 14 (1969), 23-24.

[29] Lokberg, O. and Hogmoen, K. "Use of Modulated Reference Wave in Electroinc Speckle Pattern Interferometry." J. Phys. E: Sci. Instr. 9 (1976), 847-851.

[30] Hsu, Hwei, P. Fourier Analysis. London: LIFE Books LTD., 1967.

[31] Zambuto, M. H. , Fisher, W. K., "Shifted Reference Holographic Interferometry," Appl. Opt. 12 (1973), 1651-1655.

[32] Wojciechowska, I. and Sliwinski, A. "Examination of Vibration Amplitude Distribution of Ultrasonic Transducers Using Optical Holography with a Modulated Reference Beam," Ultrason. May 1981, 115-119.

[33] Mix, Dwight F. Random Signal Processing. Englewood Cliffs, Prentice Hall, 1995.

[34] New Focus Catalog. New Focus Co., 1997

[35] Valera Robles, J.D., Harvey, D. and Jones, J. D. C., "Automatic Heterodyning in Fiber Optic Speckle Pattern Interferometry Using Laser Velocimetry," Opt. Engr. 31 (1992), 1646-1653.

[36] Takahashi, Y., Yoshino, T. and Ohde, N., "Amplitude-Stabilized Frequency-Modulated Laser Diode and its interferometric Sensing Applications," Appl. Opt. 36 (1997), 5881-5887.

[37] Kubota, T., Nara, M. and Yoshino, T., "Interferometer for Measuring Displacement and Distance," Opt. Soc. Ame. 12 (1987), 310-312.

[38] Melles Griot 1997-98 Catalog. Melles Griot, 1997.

[39] EOT Catalog. EOT Co., 1999.

[40] Petermann, K. Laser Diode Modulation and Noise. Boston: KTK Scientific Publishers, 1991.

[41] Cheo, P.K., Fiber Optics and Optoelectronics, 2nd Ed. New Jersey: Prentice Hall, 1990.

[42] Fleming, G.A. Letter to Author, Sept., 1999.

[43] Rizzoni, G., Principles and Applications of Electrical Engineering. 2nd Ed. Chicago: Irwin 1996.

[44] SLD Product Page, "SLD-5400 series," SLD, Inc. San Jose, CA

[45] Tatsuno, D. and Tsunoda, Y. "Diode Laser Direct Modulation Heterodyne Interferometer," Appl. Opt. 26 (1987), 37-40.